論文 / 著書情報
Article / Book Information

題目(和文)	
Title(English)	EVALUATION METHOD FOR SHEAR CAPACITY OF FIBER REINFORCED CONCRETE BEAMS BASED ON TENSION SOFTENING CURVES
著者(和文)	JongvivatsakulPitcha
Author(English)	Pitcha Jongvivatsakul
出典(和文)	学位:博士(学術), 学位授与機関:東京工業大学, 報告番号:甲第9341号, 授与年月日:2013年9月25日, 学位の種別:課程博士, 審査員:二羽 淳一郎,岩波 光保,竹村 次朗,高橋 章浩,佐々木 栄一
Citation(English)	Degree:Doctor (Academic), Conferring organization: Tokyo Institute of Technology, Report number:甲第9341号, Conferred date:2013/9/25, Degree Type:Course doctor, Examiner:,,,,
学位種別(和文)	博士論文
Type(English)	Doctoral Thesis

EVALUATION METHOD FOR SHEAR CAPACITY OF FIBER REINFORCED CONCRETE BEAMS BASED ON TENSION SOFTENING CURVES

by

Pitcha Jongvivatsakul

Supervisor: Professor Junichiro Niwa

A Dissertation Submitted to Graduate School of Science and Engineering
in Partial Fulfillment of the Requirements for the Degree of
Doctor of Philosophy

Department of Civil Engineering
Tokyo Institute of Technology
Tokyo, Japan

August 2013

ABSTRACT

Fiber reinforced concrete (FRC) beams are superior in shear strength because of high energy absorption of FRC at fracture. The fibers are; therefore, able to replace some of the vertical shear reinforcements in the structures resulting in the time and cost savings over the shear reinforcements. The reduction of stirrups reduces the problems involved with the congestion of shear reinforcements. The Japanese design guidelines for steel fiber reinforced concrete piers have recommended the equation to calculate the shear capacity of FRC beams. The equation proposed in the current guidelines; however, has not considered the post-cracking behavior of fiber reinforced concrete in detail and limited for the steel fiber reinforced concrete members.

A number of investigators have proposed several empirical and semi-empirical equations to predict the shear strength of fiber reinforced concrete beams. The available studies; however, have been performed without providing stirrups and the softening behavior of fiber reinforced concrete has not been intensely discussed. Although the synthetic and hybrid fibers have become more attractive in recent years because of the effectiveness to improve the shear strength and their relatively less costs when compared with that of steel fibers, most of research works in FRC field have focused exclusively on steel fibers. There is a scarcity of study on the shear resisting mechanism of fiber reinforced concrete beams with stirrups and various fibers. In addition, based on the previous research, it was found that the shear resisting mechanism of fiber reinforced concrete beams was affected by width and length of diagonal crack.

The fracture mechanics of concrete was applied for explaining the shear behavior of fiber reinforced concrete in this study. The tension softening curve—one of the parameters in fracture mechanics—was used to explain the post-cracking behavior of FRC beams. The study aims to investigate the shear carried by fibers of FRC beams with stirrups and various fibers by using tension softening curves and to propose the equation of shear capacity for FRC beams.

A total of seventeen FRC beams with various fiber volumes, fiber types, stirrup ratios and specimen sizes were tested. The effects of fiber volumes, fiber types, stirrup ratios and specimen sizes on shear resisting mechanism of FRC beams were examined. The diagonal

crack length and the crack surface displacement, which is the total displacement of the crack in the direction of crack movement, were measured using the image processing. The stress transferred across the diagonal crack of the FRC beams was calculated using the relationship of the tension softening curve. The contribution of fibers to the shear resistance of FRC beams has been investigated based on the fracture mechanics. The method can evaluate the shear carried by fibers with high accuracy even though fiber volumes, fiber types and combinations, stirrup ratios and effective depths were varied.

Furthermore, the simplified equation of shear carried by fibers based on tension softening curves was formulated. It was found that the fracture energy, stirrup ratio and effective depth affected the diagonal cracking behavior (i.e. stress transferred across the crack, diagonal crack length and angle of diagonal crack). Finally, the equation for predicting the shear capacity of FRC beams was proposed. The proposed equation was validated with the test results from this study and results from other investigators. Comparison of the predicted shear capacity versus experimental shear capacity for 43 FRC beams indicated that the proposed equation was capable of predicting the shear capacity of FRC beams. The predictive equations presented in this study will be useful to facilitate the improvement of the design equation for shear capacity of fiber reinforced concrete beams for promoting the wide use of FRC.

ACKNOWLEDGEMENTS

The author would like to express the deeply sincere gratitude to my academic advisor, Professor Junichiro Niwa for his instruction, continuous encouragement, support all through this research and also taking care of me during my stay in Japan. Without his enthusiastic and tireless supervision, this work would be impossible to be accomplished. I am grateful to Professor Nobuaki Otsuki for his valuable suggestion and friendly guidance. Sincere words of thanks also go to the members of the supervising committee: Professor Mitsuyasu Iwanami, Associate Professor Eiichi Sasaki, Associate Professor Jiro Takemura and Associate Professor Akihiro Takahashi for their valuable suggestion and comments that helped improve the quality of this study.

I would like to extend my words of esteem to Assistant Professors, Dr. Koji Matsumoto for his support, advice and kindness throughout this study. I wish to pass my gratitude to Dr. Ken Watanabe for his suggestion, which broadened my attitude and knowledge. Special thanks are to the secretary of the laboratory, Ms. Osami Kumagai and Ms. Noriko Nakajima for their kind helps in administrative matters. I am obliged to the Kajima Technical Research Institute for training me as the researcher during the internship.

I am thankful to all members and staffs of Concrete Laboratory, Professor Niwa's Laboratory, Professor Otsuki's Laboratory and Professor Iwanami's Laboratory for their unforgettable company, encouragement and helping my experiment. Without their helps, this research could not be completed.

I wish to acknowledge the Ministry of Education, Culture, Sports, Science and Technology (MEXT) for opportunity provided and financial support. I would like to express my sincere to the Center of Urban Earthquake Engineering (CUEE) for partially supporting research fund.

For fulfilling my life in Japan, I heartily appreciate my Japanese, international and Thai friends in Tokyo Institute of Technology and the Thai Students' Association in Japan under the Royal Patronage.

Last but not least, I would like to thank my family who were being a part of my support and encouragement so far.

TABLE OF CONTENTS

ABSTRACT i

ACKNOWLEDGEMENTS iii

TABLE OF CONTENTS iv

1 INTRODUCTION 1

1.1 Background 1

1.2 Research Motivation 3

1.3 Hypothesis of the Study 4

1.4 Objectives and Scope of the Study 5

1.5 Content of the Dissertation 5

2 LITERATURE REVIEW 9

2.1 Introduction 9

2.2 Fiber Reinforced Concrete 9

2.3 The Current Design Guidelines for Steel Fiber Reinforced Concrete Members in Shear 11

2.4 Other Studies on the Shear Capacity of FRC Beams 12

2.5 Factors Affecting Shear Strength and Diagonal Cracking Behavior of FRC Members 17

2.5.1 Volume fraction of fibers 17

2.5.2 Stirrup ratio 17

2.5.3 Fiber type 18

2.5.4 Effective depth 18

3 TENSION SOFTENING CURVES OF FIBER REINFORCED CONCRETE (FRC) 19

3.1 Introduction 19

3.2 Significance of Tension Softening Curves and Fracture Energy 19

3.3 The Bending Test of Notched Beams and Results 20

3.3.1 Materials 20

3.3.2 Specimens 21

3.3.3 Test program and measurements 23

3.4 Investigation of Tension Softening Curves 24

3.5 Results of Notched Beam Tests 28
3.6 Results of Tension Softening Curves 33
3.7 Conclusions of Chapter 3 35

4 EXPERIMENTAL PROGRAM OF FIBER REINFORCED CONCRETE BEAMS 37
4.1 Introduction 37
4.2 Experimental Cases 37
4.3 Materials 39
4.3.1 Concrete 39
4.3.2 Fibers 40
4.3.3 Reinforcing steels 41
4.4 Mixing, Casting and Curing of Concrete 44
4.5 Specimens 45
4.6 Test Setup and Instrumentation 48
4.7 Measuring Items 49
4.7.1 General measuring items 49
4.7.2 Crack surface displacement using the image analysis 49
4.7.3 Length and angle of diagonal crack 53

5 SHEAR BEHAVIOR OF FIBER REINFORCED CONCRETE BEAMS 55
5.1 Introduction 55
5.2 Calculation of Shear Forces 55
5.3 General Behavior and Load-Deflection Relationships of FRC Beams 57
5.4 Shear Capacity and Shear Carried by Fibers Observed in the Experiment 59
5.4.1 Effect of fiber volume fraction (Series I) 59
5.4.2 Effect of stirrup ratio (Series II) 63
5.4.3 Effect of fiber types (Series III) 63
5.4.4 Effect of effective depth (Series IV) 64
5.5 Flexure Cracking Behavior 65
5.6 Diagonal Cracking Behavior 66
5.6.1 Crack surface displacement 69
5.6.2 Diagonal crack length 74
5.6.3 Angle of diagonal crack 76
5.6.4 Angle of principal tensile strain 78

5.7 Conclusions of Chapter 5 79

6 EVALUATION METHOD FOR SHEAR CARRIED BY FIBERS OF FRC BEAMS USING TENSION SOFTENING CURVES 81

6.1 Introduction 81

6.2 Specimen Modeling 81

6.3 Evaluation Method Using Tension Softening Curves 83

6.4 Stress Transferred Across the Diagonal Crack in FRC Beams 85

6.5 Calculated Shear Carried by Fibers 88

6.6 Conclusions of Chapter 6 90

7 PROPOSAL OF PREDICTIVE EQUATION FOR SHEAR CAPACITY OF FRC BEAMS 91

7.1 Introduction 91

7.2 Proposal of Predictive Equations for Shear Carried by Fibers 91

7.3 Equations for the Shear Capacity of FRC Beams 98

7.4 Accuracy of the Existing Equations 98

7.5 Accuracy of the Proposed Equations 104

7.6 Conclusions of Chapter 7 109

8 CONCLUSIONS 111

8.1 General Conclusions 111

8.2 Recommendations for the Further Study 113

REFERENCES 115

APPENDIX Pictures of the specimens after loading tests **119**

CHAPTER 1

INTRODUCTION

1.1 Background

Reinforced concrete (RC) is one of the most widely used structures in world's construction. Reinforced concrete consists of two materials that are concrete and reinforcement steel bars. Concrete, which is the main material in RC structures, has the outstanding property because of its high compressive strength and durability; however, it is weak in tension resulting in the developing of cracks when load gives rise to tensile stress excess of the tensile strength of concrete. The plain concrete beams fail suddenly when the first crack forms. To overcome this shortcoming, the steel bars, which are high tensile strength materials, are used together with the concrete in such a way that the tension force needed for moment equilibrium after the concrete cracks.

Among the different types of failure in RC members, the shear failure is well known as a very sudden failure that occurs without a warning and should be prevented. Since the 1995 Hyogoken-Nambu earthquake, the standard specifications of Japan Society of Civil Engineers (JSCE) for seismic design of reinforced concrete structures have been revised. Thus, the current standard specifications of JSCE for seismic design of reinforced concrete structures (2010) have required a large amount of steel bars in structures in order to prevent shear failure from the severe earthquake. This causes the congestion of reinforcing steel bars in the structures and making the difficulty in filling the concrete during the construction.

One way to improve the shear performance without adding more reinforcing steel bars is the use of short discrete fibers as a shear reinforcement because the addition of fibers to concrete can clearly enhance the shear strength of fiber reinforced concrete (FRC) members as reported by a number of researchers (Swamy and Bahia, 1985, Tan et al., 1992 and Kwak et al., 2002). Consequently, the fibers can replace some of the transverse shear reinforcements in the

structures resulting in the time and cost savings over the shear reinforcements and tie bars. The reduction of stirrups reduces the problems involved with the congestion of shear reinforcements. The fibers commonly used in FRC structures are steel fibers; however, recently, synthetic and hybrid fibers have become more attractive than before because of the effectiveness to improve shear strength as published by Li et al. (1992), Nonghabai (2000), Greenough and Nehdi (2008) and Altoubat et al. (2009) and their relatively less costs when compared with that of steel fibers. Adding of fibers to concrete converts its brittle characteristic to ductile one. When concrete cracks, the randomly oriented fibers can resist the formation and growth of crack, thus improving the post cracking behavior.

The shear capacity of steel fiber reinforced concrete members can be predicted by the equation proposed in the design guidelines of JSCE for steel fiber reinforced concrete piers (1999). In the design guidelines, the increment of the shear strength due to steel fibers is expressed as a value κ, which is defined as a ratio of the shear carried by steel fibers to the shear carried by concrete, and κ is proposed to equal to 1.0 for the member with 1.0-1.5 % of steel fiber volume to concrete full volume. The design guidelines (1999); however, have been provided for on steel fibers. Other kinds of fibers have not been included in the recommendation.

Watanabe et al. (2010b) studied the shear capacity of reinforced concrete beams with stirrups and steel fibers. It was concluded that all of the experimental values of κ (κ_{exp}) were more than 1.0 when the volume fraction of steel fibers to full concrete volume was varied from 0.3% to 1.0%. Fiber contribution is underestimated in the design guidelines. In addition, there was a combination effect between steel fibers and stirrups, which would relate with the diagonal crack behaviors that are width and length of diagonal crack. The length and width of the diagonal crack were the important factors to investigate the shear carried by fibers. Nonetheless, Watanabe et al. (2010b) did not measure the values of width and length of diagonal crack quantitatively. In addition, a few numbers of researches have studied on the influences of width and length of diagonal crack on the shear capacity of fiber reinforced concrete beams. Therefore, the relation between the diagonal cracking behavior and the shear capacity of FRC beams has not been clarified.

1.2 Research Motivation

In order to promote the wide use of fiber reinforced concrete structures, the accurately predictive equation for the shear capacity of FRC members is crucial. Nevertheless, the current JSCE equation for steel fiber reinforced concrete members (1999) is conservative and covers only the steel fibers. There is a lack of guidelines for design of FRC beams with various types of fibers. It is because the influences of steel, synthetic and hybrid fibers on the shear resisting mechanism of FRC beams with shear reinforcements have not been completely understood.

Most of research works have focused exclusively on steel fibers. The experimental investigations and proposed equations have been published for the steel fiber reinforced concrete beams and mainly without stirrups (Sharma, 1986, Narayanan and Darwish, 1987, and Khuntia et al., 1999). The available studies; however, have been performed without providing stirrups and the softening behavior of fiber reinforced concrete has not been considered. In addition, the fiber-matrix interfacial bond stress, which has not been satisfactorily quantified yet, is required in the equations proposed in those studies. To overcome this shortcoming, the utilization of tension softening curve is suggested in this study. The tension softening curves can be used to evaluate the tensile stress transferred across the crack without requiring the fiber-matrix interfacial bond stress and the number of fibers per unit area.

In addition, in the past researches, the investigations on shear behavior of FRC beams with synthetic fibers have been conducted. The empirical equations have been proposed by Li et al. (1992) and Greenough and Nehdi (2008). These equations; however, were formulated based on the limited kinds of fibers and without shear reinforcements. Therefore, the above lacks of research should be eliminated and the more precise predictive equation for fiber reinforced concrete should be developed.

1.3 Hypothesis of the Study

As mentioned in Section 1.1, since the length and width of diagonal crack are important for describing the shear behavior of FRC beams (Watanabe et al., 2010b), the fracture mechanics of concrete is taken into account in this study in order to investigate the cracking behavior of fiber reinforced concrete. The fracture mechanics of concrete is well known as one field to explain the cracking in concrete structures. The fracture mechanics of concrete tries to find the quantitative relations between crack length, material's resistance to crack growth and the stress transferred across the crack. The fracture energy (G_F) and the tension softening curves are the parameters in fracture mechanics. The tension softening curves represent the relationship between stress across the diagonal crack and the crack opening displacement as shown in **Fig. 1.1**. Once the width of crack is known, the tensile stress transferred across the crack can be calculated using the curve. Therefore, tension softening curve is used in this study as a tool for converting width of crack to stress. Then, the shear carried by fibers is the summation of the stress multiplied by area that stress transferred, which is calculated from crack length and width of beams.

Not only the knowledge of the fracture mechanics that has been applied for investigating the shear behavior of FRC beams, but also the image analysis system, which is the method for measuring the crack surface displacement developed by Higashi et al. (2009). The crack surface displacement is total crack displacement including the opening and sliding of crack. This system can measure crack surface displacement in the wide region with high accuracy. Therefore, the cracking behavior of FRC beams can be discussed quantitatively.

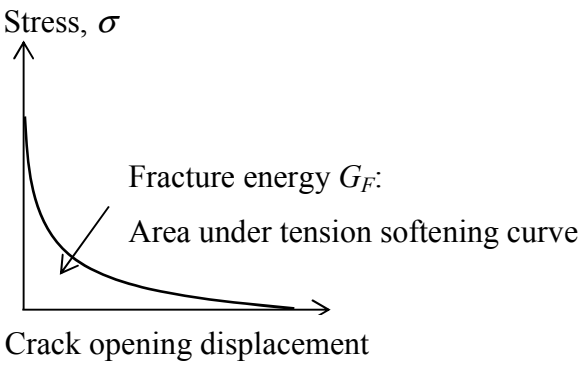

Figure 1.1 Tension softening curve

1.4 Objectives and Scope of the Study

The main objectives of the study are a) to investigate the effects of fiber volume fractions, stirrup ratios, fiber types and sizes of specimens on the shear capacity of fiber reinforced concrete beams, b) to evaluate the shear carried by fibers of FRC beams using the crack surface displacement, diagonal crack length and the tension softening curves and c) to propose the predictive equation for shear capacity of FRC beams.

To achieve these objectives, the experiments of 17 FRC beams were performed. The parameters affecting the shape of diagonal crack, which are fiber contents, stirrup ratios, fiber types and specimen sizes, were considered. The shear carried by fibers was investigated by using tension softening curves. The displacement of crack was measured by the image analysis. The tensile stress transferring along the diagonal crack was converted from the crack surface displacement using the tension softening curve. The shear carried by fibers equals to the stress multiplied by the crack surface area. The validity of the model was verified by comparison with the experimental results. Moreover, the simplified equation of shear carried by fibers based on tension softening curves was formulated. Finally, the equation for predicting the shear capacity of FRC beams was proposed.

The findings in this study provide the understanding of the effectiveness of fibers in the shear resistance mechanism of fiber reinforced concrete members and shall be useful for improvement of the design equation for the shear capacity of FRC beams.

1.5 Content of the Dissertation

The flow of this thesis is presented in the form of flowchart as shown in **Fig. 1.2**. The thesis consists of eight chapters. The contents of this thesis are organized as follows.

Chapter 1 included the background, motivation and hypothesis of this study. The objectives of the study were also provided.

In **Chapter 2**, fiber reinforced concrete, the existing design equation for steel fiber reinforced concrete in the design guidelines and the previous researches on shear behavior of fiber reinforced concrete beams are summarized. The factors affecting shear strength of FRC beams are listed.

Tension softening curves of fiber reinforced concrete are investigated in **Chapter 3**. Significance of tension softening curves for explaining the behavior of FRC is summarized. The bending tests of notched beams are performed. The fracture energy and the tension softening curve of each fiber reinforced concrete are discussed.

Chapter 4 explains the experimental program of FRC beams in detail. The content consists of the materials, experimental cases, manufacture of test specimens, loading methods and measuring items. A method for measuring crack surface displacement by the image analysis and a method for measuring length and angle of diagonal crack are also introduced.

The experimental results of FRC beams are presented in **Chapter 5**. The shear capacity and shear carried by fibers of FRC beams are discussed. The diagonal crack propagation behavior of FRC beams obtained from the image analysis is shown. The effects of fiber volume fractions, stirrup ratios, fiber types and specimen sizes on shear behavior of FRC beams are examined.

Chapter 6 includes the method for evaluating the shear carried by fibers. The shear carried by fibers is evaluated based on the tension softening curves presented in **Chapter 3** and experimental results shown in **Chapter 5**. The validation of the proposal equation is made with the experimental results.

Chapter 7 formulates the simplified predictive equation for shear carried by fibers based on the investigation in **Chapter 6**. Furthermore, the predictive equation for the shear capacity of FRC beams is proposed and validated with a number of FRC beams from other researchers.

Finally, the conclusions obtained in this study and the recommendations for further study are given in **Chapter 8**.

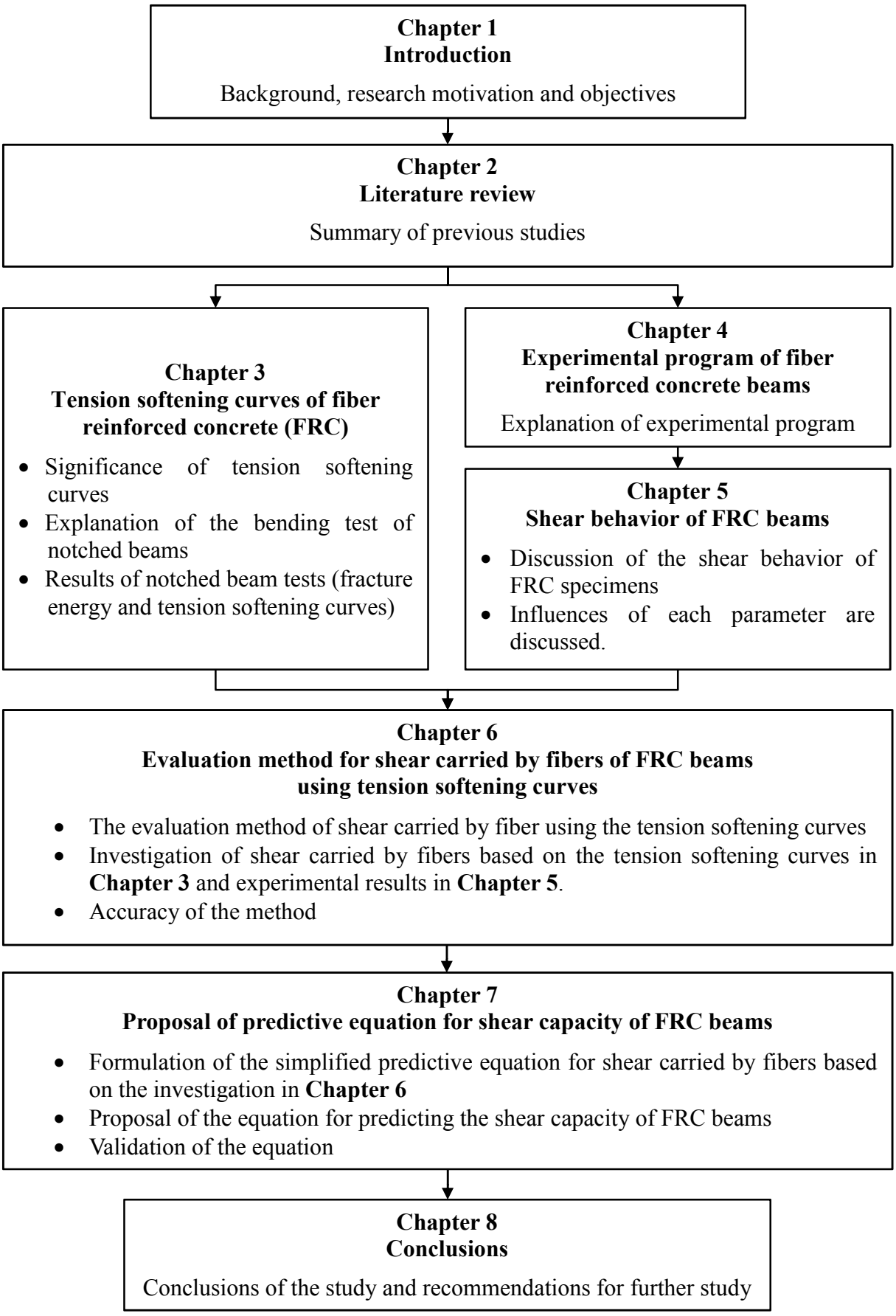

Figure 1.2 Outline of the dissertation

CHAPTER 2

LITERATURE REVIEW

2.1 Introduction

Fiber reinforced concrete and the current equation for predicting the shear capacity of FRC members are introduced in this chapter. Previous investigations on the shear capacity of FRC beams done by other researchers are reviewed. The basic of fracture mechanics is explained. Finally, the factors affecting shear capacity of FRC beams based on the literatures are presented.

2.2 Fiber Reinforced Concrete

Fiber reinforce concrete (FRC) is a composite material between a cement matrix and discrete fibers. Fiber can be made of steel, polymers, carbon, glass or natural materials. Mixtures of different types and/or sizes of fibers can be also used and called hybrid fiber reinforced concrete. Fibers added to the concrete improved the properties of concrete in tension due to the bridging mechanism as shown in **Fig. 2.1**. The mechanism of the fibers involves transfer of stress from the matrix to the fibers by interfacial bonding or by interlock between the fibers and matrix for the deformed fibers. Stress is shared by the fibers and matrix in tension until the matrix cracks. After the matrix cracked, stress transfers over the crack through fibers. Failure modes of FRC are either bond failure between fibers and matrix or material failure. **Figure 2.2** presents the fracture surface of FRC (ACI 544.1R-96, 2002).

The mechanical properties of a cementitious matrix are improved when fibers are added (ACI 544.4R-88, 1999). The compressive strength and elastic properties are not significantly affected by fibers unless a high percentage of fibers is used (Thomas and Ramaswamy, 2007 and Bencardino et al., 2008). The tensile strength increased about 40 percent due to the

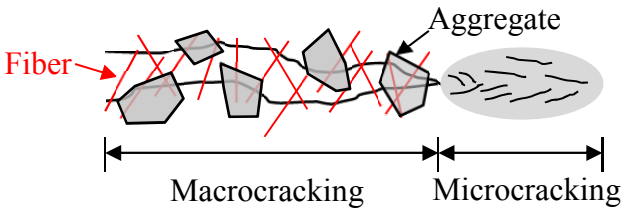

Figure 2.1 Fiber bridging mechanism in cracks

Figure 2.2 Fracture surface of FRC (ACI 544.1R-96, 2002)

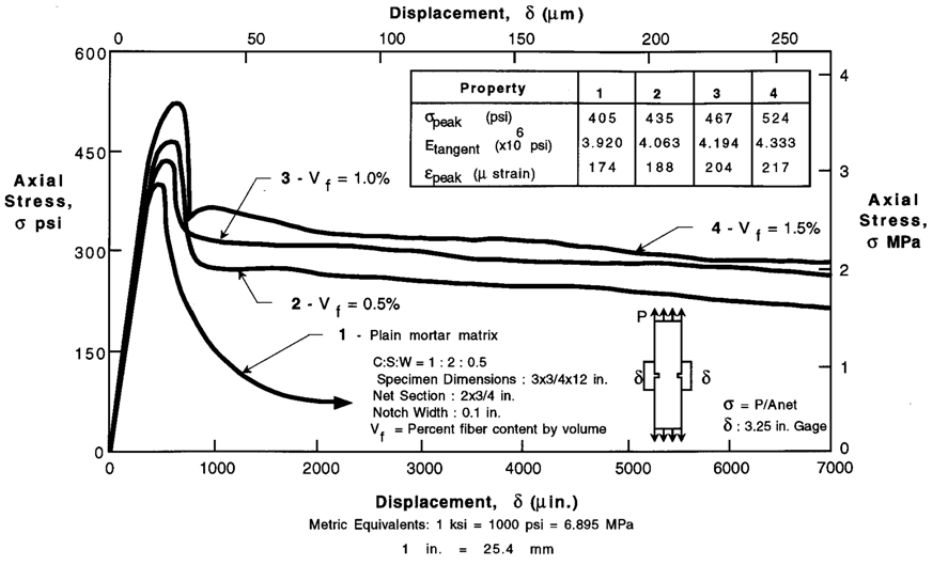

Figure 2.3 Typical results of stress-displacement curves obtained from direct tension tests on plain mortar matrix and SFRC (ACI 544.1R-96, 2002)

addition of fibers (Thomas and Ramaswamy, 2007). The fibers can improve the post-peak behavior and modify the brittle behavior to the ductile behavior. Therefore, the enhancement of the fracture energy and toughness is obtained (Balaguru et al., 1992 and Bischoff, 2003) as

shown in **Fig. 2.3**. The improvement; however, significantly depends on the fiber types and percentage of fibers (ACI 544.1R-96, 2002).

2.3 The Current Design Guidelines for Steel Fiber Reinforced Concrete Members in Shear

The design guidelines of JSCE for steel fiber reinforced concrete (SFRC) piers have been published (1999). The shear capacity of SFRC members can be calculated by Eq. (2.1). The shear capacity of SFRC members (V_{yd}) consists of the shear carried by the linear member without shear reinforcement (V_c), the shear capacity of shear reinforcement (V_s) and the component of effective tensile force in longitudinal tendon parallel to the shear force (V_{pe}). However, V_{pe} is not considered in this study since the axial force and prestressed force are not applied. Therefore, the shear capacity of SFRC member without the axial force can be predicted by the Eqs. (2.2)-(2.8). The shear contribution due to steel fibers is taken into account by the coefficient κ (Eqs. (2.6) and (2.7)), which is the modified factor in V_c.

$$V_{yd} = V_{cd} + V_{sd} + V_{ped} \tag{2.1}$$

$$V_{cd} = \beta_d \cdot \beta_p \cdot \beta_n \cdot f_{vcd} \cdot b_w \cdot d \tag{2.2}$$

$$\beta_d = \sqrt[4]{1/d} \ (d\text{: m}) \tag{2.3}$$

$$\beta_p = \sqrt[3]{100 p_w} \tag{2.4}$$

$$\begin{aligned} \beta_n &= 1 && \text{if } N'_d \geq 0 \\ &= 1 + 2 \cdot M_o / M_d && \text{if } N'_d < 0 \end{aligned} \tag{2.5}$$

$$f_{vcd} = 0.2 \cdot (1 + \kappa) \cdot \sqrt[3]{f'_{cd}} \ \text{(MPa)} \tag{2.6}$$

$$\kappa = 1 \tag{2.7}$$

$$V_{sd} = A_w f_{wy} (z/\text{s}) \tag{2.8}$$

where, b_w is web thickness (mm), d is effective depth (mm), p_w is longitudinal reinforcement ratio, N'_d is design axial compressive force, M_d is design flexural moment, M_o is flexural

moment necessary to cancel stress due to axial force at extreme tension fiber corresponding to design flexural moment M_d, f'_{cd} is the design compressive strength of the concrete (MPa), s is stirrup spacing (mm), A_w is the total cross-sectional area of stirrups provided in the range of s (mm^2), f_{wy} is the yield strength of stirrups (MPa) and z is distance from the location of compressive stress resultant to the centroid of tension steel ($z = 7d/8$) (mm).

The predictive equation for the shear capacity of SFRC members proposed in this design guidelines has been recommended to use the steel fiber volume fraction between 1.0 to 1.5% of concrete full volume. Since there was not enough experimental data, the shear carried by fibers has been proposed to be calculated from V_c and κ. For safety reason, the value of κ has been proposed to be 1.0. This means that the shear carried by steel fibers is considered to be equal to the shear carried by concrete itself. Nevertheless, the current equation gives the conservative values for shear capacity (Watanabe et al., 2010b) and it does not consider the post-cracking behavior of concrete in detail. Therefore, the further study is needed in this area in order to improve the accuracy of the equation.

The design considerations for steel fiber reinforced concrete in ACI were also produced. ACI 544 (1999) and ACI 318 (2008) have proposed the following equation for calculating the shear capacity of SFRC beams based on the test results of Sharma (1986).

$$V_{ACI} = \frac{2}{3} f_t \left(\frac{d}{a}\right)^{0.25} b_w d + \frac{A_w f_{wy} d}{s} \tag{2.9}$$

where f_t is the tensile strength of fiber reinforced concrete obtained from results of indirect tension test of 150×300 mm cylinders and d/a is the effective depth-to-shear-span ratio.

This equation is empirical in nature. The equation was formulated from results of steel fibers with straight, crimped and deformed end. ACI equation considered the influence of fibers (i.e. effects of different end types and volume fractions) by only parameter f_t. The equation is simple but the accuracy is low.

2.4 Other Studies on the Shear Capacity of FRC Beams

A number of researchers have studied on shear behavior of FRC beams especially those of SFRC beams. The studies concluded that the use of steel fibers (Niyogi and Dwarakanath,

Table 2.1 Existing predictive equations for FRC beams proposed by other investigators

Investigators	Predictive equations for the shear strength of FRC beams	Application		No. of equation
		Existing of stirrups	Types of fibers	
Sharma (1986) (Recommended by ACI Committee 544 (1999))	$v_{frc} = k f_t \left(\frac{d}{a}\right)^{0.25}$ k=1 if f_t is obtained by direct tension test; k=2/3 if f_t is obtained by indirect tension test; k=4/9 if f_t is obtained using modulus of rupture; or $f_t = 0.79\sqrt{f'_c}$	With stirrups	Steel	(2.10)
Narayanan and Darwish (1987)	$v_{frc} = e\left(0.24 f_{sp} + 80 p_w \frac{d}{a}\right) + 0.41\tau F$ e=1 for a/d >2.8 e=2.8d/a for other cases	Without stirrups	Steel	(2.11)
Ashour et al. (1992)	$v_{frc} = \left(0.7\sqrt{f'_c} + 7F\right)\frac{d}{a} + 17.2 p_w \frac{d}{a}$	Without stirrups	Steel	(2.12)
Khuntia et al. (1999)	$v_{frc} = (0.167 + 0.25F)\sqrt{f'_c}$	Without stirrups	Steel	(2.13)
Kwak et al. (2002)	$v_{frc} = 2.1 e f_{sp}^{0.7}\left(p_w \frac{d}{a}\right)^{0.22} + 0.8(0.41\tau F)^{0.97}$ e=1 for a/d >3.5 e=3.5d/a for other cases	Without stirrups	Steel	(2.14)
Greenough and Nehdi (2008)	$v_{fr-scc} = 0.167\sqrt{f'_c} + \frac{L_f}{D_f}\rho_f p_w \frac{d}{a} + 0.369\tau \frac{L_f}{D_f}\rho_f$	Without stirrups	Steel and poly-ethylene	(2.15)
Li et al. (1992)	$v_{frc} = 1.25 + 4.68\left[(f_f f_{sp})^{3/4}\left(p_w \frac{d}{a}\right)^{1/3} d^{-1/3}\right]$ for a/d > 2.5 $v_{frc} = 9.16\left[(f_f)^{2/3}(p_w)^{1/3}\frac{d}{a}\right]$ for a/d < 2.5 d in m.	Without stirrups	Steel, aramid, acrylic and poly-ethylene	(2.16)

v_{frc}: shear strength of FRC beams (MPa), f'_c: compressive strength of concrete (MPa), f_{sp}: split cylinder strength of fiber concrete (MPa), f_f: flexural strength of concrete (MPa), d: effective depth (mm), a: shear span (mm), p_w: the amount of tensile reinforcement ($p_w = A_s/bd$), τ: fiber-matrix interfacial bond stress between the fiber and corresponding concrete (τ= 4.15 MPa), F: fiber factor (Eq. (2.17)), L_f: the fiber length (mm), D_f: the fiber diameter (mm) and ρ_f: volume percentage of fibers (%).

1985 and Mansur et al., 1986) and some synthetics fibers (Li et al., 1992 and Nonghabai, 2000) (e.g., acrylic, aramid, polyethylene, polyolefin and carbon) as the shear reinforcement enhanced the shear strength of the beams. Thus, the fibers can substitute the stirrups resulting in the reduction of the amount of stirrups in the beams (Lim and Oh, 1999 and Cucchiara et al., 2004). In addition, the toughness and ductility are improved (Swamy and Bahia, 1985 and El-Niema, 1991).

During the last three decades, wide researches have been performed on the shear strength of FRC beams, both normal and high-strength concrete (Ashour et al., 1992 and Khuntia et al., 1999). A number of investigators have proposed several empirical and semi-empirical equations to predict the shear strength of fiber reinforced concrete beams. **Table 2.1** lists the existing shear strength equations for FRC beams.

Sharma (1986) proposed the empirical equation (Eq. (2.10)) for predicting the shear strength of SFRC beams based on the experimental results. As mentioned before, ACI 544 (1999) recommended this equation in the design considerations for calculating the shear capacity of SFRC beams. The shear strength can be calculated from the tensile strength of concrete (f_t) obtained from results of indirect tension test of 150 × 300 mm cylinders and the effective depth-to-shear-span ratio. The influences of different fiber types and quantities are considered to their influence on parameter f_t. The equation is simple but does not explicitly account for factors that are known to significantly affect the shear strength such as the fiber volume and shape of fibers.

Narayanan and Darwish (1987) suggested that the ultimate shear strength of SFRC beams could be predicted from the split-cylinder strength, the dowel action and the contribution of fibers pullout forces along the inclined crack, which is represented by the fiber-matrix interfacial bond factor (τ) and fiber factor (F). The formulas for shear strength of SFRC beams have been proposed as Eq. (2.11) in **Table 2.1**. The fiber factor can be calculated from Eq. (2.17).

$$F = \left(L_f / D_f\right) \cdot \rho_f \cdot d_f \tag{2.17}$$

where, L_f is the fiber length (mm), D_f is the fiber diameter (mm), ρ_f is volume percentage of fibers (%), d_f is bond factor representing the different bond characteristics of the fiber (d_f equals 0.5 for round fibers, 0.75 for crimped fibers, and 1.0 for indented fiber). The

equation require the fiber factor (F) and the fiber-matrix interfacial bond stress (τ), which have not been satisfactorily determined yet.

Ashour et al. (1992), Khuntia et al. (1999) and Kwak et al. (2002) have proposed the modified equations for predicting shear strength of steel fiber reinforced concrete beams without stirrups (Eqs. (2.12), (2.13), (2.14), respectively) based on the Sharma equation, Narayanan and Darwish equation and their experimental results. Ashour et al. (1992) and Khuntia et al. (1999) recommended using the square root of concrete strength instead of the tensile strength. As well as Narayanan equation, the fiber factor is required in these equations. Khuntia et al. (1999) proposed the values of d_f (in Eq. (2.17)) in their study. d_f is 1 for hooked or crimped steel fibers and 2/3 for round steel fibers.

There were few investigators researched on the shear strength of other fiber types. Greenough and Nehdi (2008) investigated the influence of fiber types on the shear behavior of fiber-reinforced self-consolidating concrete (FR-SCC). The ACI equation was modified based on regression analysis and the modified ACI equation was proposed by Greenough and Nehdi (2008) as Eq. (2.15) in **Table 2.1**. The equation was formulated from FRC beams with steel and polyethylene fibers only.

Li et al. (1992) tested the steel and synthetic fiber reinforced concrete beams and proposed the predictive equations as Eq. (2.16) in **Table 2.1**. Fibers made of steel, aramid, acrylic and polyethylene were used as the shear reinforcement. The equation is based on the product of the flexural strength and splitting cylinder tensile strength of FRC. However, since the behavior of FRC in shear is different from that in flexure, the use of the flexure strength in calculating the shear strength is questionable.

As mentioned in above literatures, most of the researches carried out on FRC; however, were mainly related to steel fibers and without providing the shear reinforcement. In addition, the softening behavior of fiber reinforced concrete has not been considered. The fiber factor and the fiber-matrix interfacial bond stress, which have not been satisfactorily quantified yet, are required in those studies. To overcome these shortcomings, the tension softening curve is suggested in this study. The tension softening curves can be used to evaluate the tensile stress transferred across the crack without requiring the value of fiber-matrix interfacial bond stress.

Watanabe et al. (2010b) reported that a combination of steel fibers and stirrups had a synergetic effect to increase the shear capacity of SFRC beams. The results showed that the

experimental value of κ (κ_{exp}) of SFRC beams with stirrups was higher than κ_{exp} of SFRC beams without stirrups as shown in **Fig. 2.4**. A combination of steel fibers and stirrups had a synergetic effect to increase the shear capacity of SFRC beams. Moreover, there was an optimized combination of steel fibers and stirrups to increase the value of κ_{exp} as shown in **Fig. 2.5**.

The combination would relate with the diagonal crack behavior (i.e. length and width of

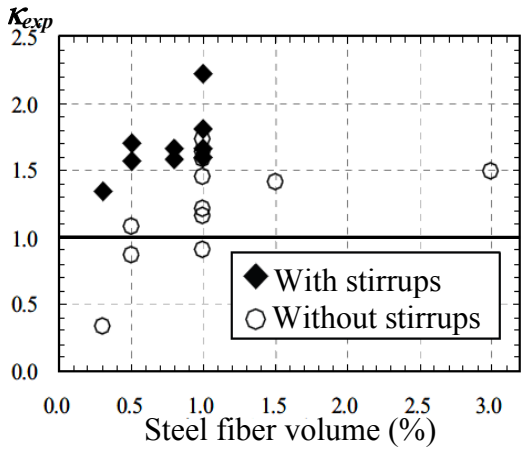

Figure 2.4 Influence of stirrups on the values of κ_{exp} for FRC beams

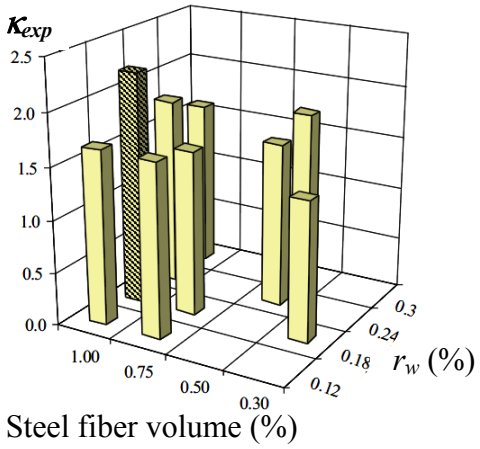

Figure 2.5 κ_{exp} associated with steel fiber volume fraction and r_w

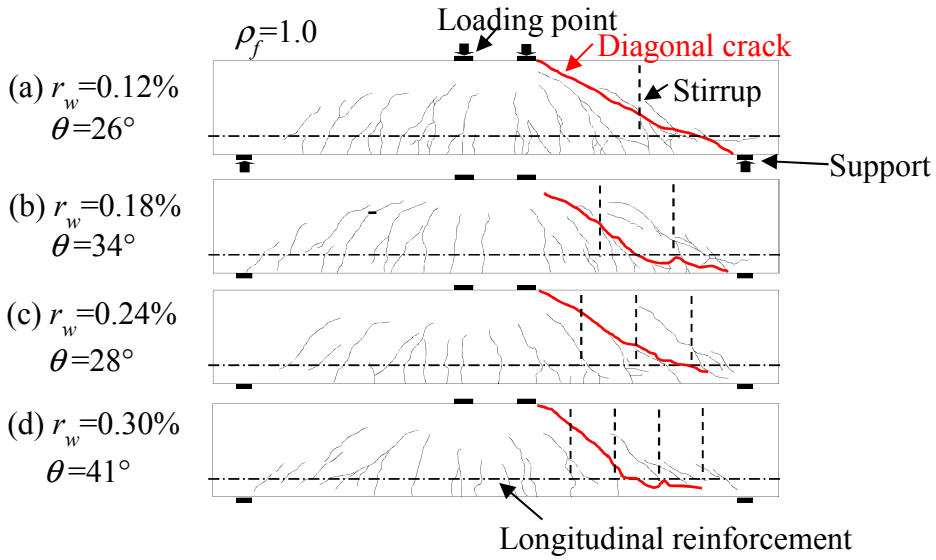

Figure 2.6 Crack pattern (Watanabe et al., 2010b)

diagonal crack). From the test results, the angle of diagonal crack (θ) became steeper as stirrup ratio (r_w) increased and the length of the diagonal crack decreased as shown in **Fig. 2.6**. In addition, the stirrups are effective to prevent a rapid opening of the diagonal crack. By considering the shear force transferred by the bridging effect of the steel fibers, the force transferred along the diagonal crack increased as the length of the diagonal crack increased, and decreased as the width of it increased. The combination of both positive and negative contributions to the shear transfer along the diagonal crack should result in the variation of κ_{exp} as well as the shear carried by the steel fibers. Finally, the authors concluded that the length and width of the diagonal crack was the key to evaluate the optimized combination of steel fibers and stirrups on SFRC beams. However, they did not measure length and width of diagonal crack quantitatively. Thus, the shear carried by fibers has not been investigated.

2.5 Factors Affecting Shear Strength and Diagonal Cracking Behavior of FRC Members

Based on the literature, the factors affecting shear strength of FRC beams and the factors affecting the diagonal crack behavior (i.e. length and width of diagonal crack) were examined in this section. The important factors were selected and were designed as the experimental parameters to investigate the shear resisting mechanism of FRC beams. From the literature, the factors affecting shear strength and diagonal crack behavior of FRC beams can be listed as follows:

2.5.1 Volume fraction of fibers

Six SFRC beams were tested by Narayanan and Darwish (1987) in order to investigate the influence of steel fiber volume fraction on the ultimate shear strength. Steel fiber volume fraction was increased from 0.5% to 3.0%. The results showed that, by increasing the steel fiber volume fraction, the failure mode changed from shear to flexure failure when the volume fraction of fibers was increased beyond an optimum value. In the series test, this value was 1.0%. The tests confirmed that the volume of steel fibers was very effective to increase shear strength of SFRC beams.

2.5.2 Stirrup ratio

Base on the test results of Watanabe et al. (2010b), it was found that the arrangement of stirrups affected the diagonal cracking behavior of SFRC beams. The angle of diagonal crack

became steeper with the increase in stirrup ratio. Therefore, the stirrup ratio significantly affects the shear behavior of FRC beams.

2.5.3 Fiber type

According to the experimental results of Greenough and Nehdi (2008), the types of fiber had a considerable influence on the shear behavior. At the present, there is no equation for shear capacity of FRC beams with other types of fibers except steel fibers. Consequently, the effect of fiber types on shear capacity of FRC should be clarified.

2.5.4 Effective depth

Li et al. (1992) concluded that the shear strength of fiber reinforced mortar beams was found to decrease with the beam size. Plain mortar beams reinforced with 2% of steel fibers showed the decrease in shear strength of 20%, as the beam depth increased from 102 to 204 mm with the shear span to effective depth ratio (a/d) and longitudinal reinforcement ratio (p_w) remaining constant.

In addition, the size of specimen strongly affects the width and length of diagonal crack. In ordinary RC beams, it is well known that the width of crack is wider in the larger specimen. It leads the size effect on shear capacity of RC beams. However, the size effect on shear capacity of FRC beams has not been fully understood.

Four significant factors that are fiber volume fraction, stirrup ratio, fiber types and effective depth were determined as the experimental parameters in this study. The influences of the four parameters are discussed in **Chapter 5**. In this study, the tensile stress along the diagonal crack is evaluated by using the tension softening curve. The shear force transferring due to the bridging effect of steel fibers is investigated. In addition, from the experimental results, the empirical equation is proposed to predict the shear carried by fibers of FRC beams.

CHAPTER 3

TENSION SOFTENING CURVES OF FIBER REINFORCED CONCRETE (FRC)

3.1 Introduction

Fiber reinforced concrete has been used over the last decades with the aim of improving the tensile load-deformation of concrete, which shows the brittle behavior in tension. The parameters proposed to describe the fracture behavior in concrete (i.e. tension softening curves and fracture energy) are used in this study. This chapter explains significance of those parameters, the method of test for fracture energy and tension softening curves by use of notched beam and the results of the notched beam tests. The characteristic of each fiber reinforced concrete is discussed in this chapter.

3.2 Significance of Tension Softening Curves and Fracture Energy

The tension softening curve is one of the fracture mechanics parameters. It is the relationship between tensile stress and crack opening displacement in the fracture zone. The total area under the tension softening curve is defined as the fracture energy (G_F). The fracture energy is the energy necessary for creating a perfect crack of unit area which cannot transfer the normal stress anymore. The tension softening diagram can describe the post-cracking behavior and express the resistance of concrete against crack development. In addition, the tension softening curves can reflect the fracture behavior of each fiber reinforced concrete because the softening behavior after cracking depends on the type, shape, fiber volume fraction and so on (JSCE, 2010). Therefore, it is effective to explain the mechanism of FRC beams. Tension softening curve affects the shear contribution due to the bridging effect from fibers.

In this study, the crack surface displacement is transformed to tensile stress along the diagonal crack by using the relationship of tension softening curve. The using of tension softening curves for investigation of shear carried by fibers will be explained in detail in **Chapter 6**.

3.3 The Bending Test of Notched Beams and Results

The tension softening curve can be measured by the direct tensile test. However, it is difficult to carry out the test because the test requires a highly rigid testing machine completed with the precise displacement control. Instead of the direct tensile test, the tension softening curves can be determined by the poly-linear approximation analysis method. The tension softening curves have been determined from the bending tests of the notched beams. **Figure 3.1** shows the determination procedures of tension softening curves from bending test.

The tension softening curves of fiber reinforced concrete with various types of fibers and fiber volume fraction were determined by notched beam tests following JCI standard (2003a). The experimental cases of the notched beam tests are summarized in **Table 3.1**. The test method and the estimation procedure for tension softening curve are explained in this section.

3.3.1 Materials

The mix proportion of concrete and characteristic of fibers used in the notched beams were the same as those of FRC beams presented in **Chapter 4** and **Chapter 5**.

(1) Concrete

Table 3.2 summarizes the mix proportion of concrete. High-early strength cement, fine

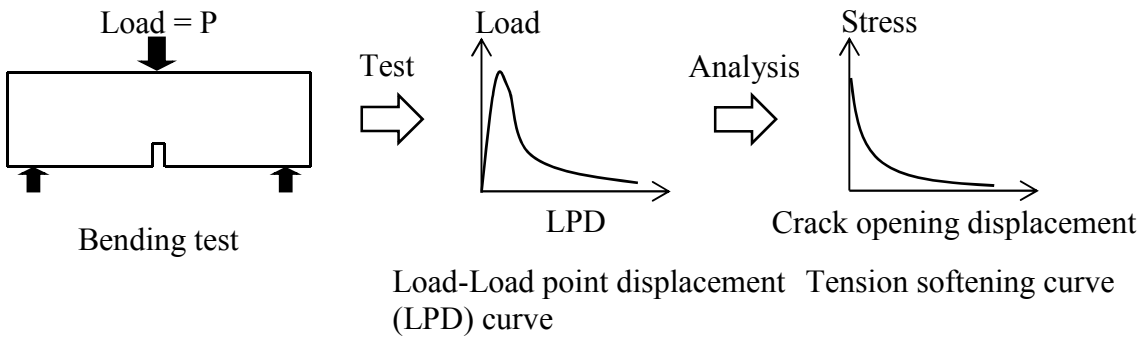

Figure 3.1 Tension softening curve analyzed from bending test

aggregates, coarse aggregates and superplasticizer, which was high-performance air entrained (AE) water reducing agent, were used. The water-to-cement ratio was 0.35. In order to achieve good workability, the superplasticizer (Type: SP8-SBsX2 and SP8SV) was used in the range of 1.1-1.3% to the weight of cement for each concrete mix. The concrete was designed with an average 7-day age concrete strength of 50 MPa.

(2) Fibers

Five fiber types and three combinations of fibers were incorporated into concrete, including steel, synthetic and hybrid fibers. The characteristics of fibers are summarized in **Table 3.3**. Lengths of fibers were 30 and 60 mm. Steel fibers had the highest tensile strength. Pictures of steel and synthetic fibers are shown in **Fig. 3.2**. The enlarged figures in **Fig. 3.2** present the end types and surface of each fiber. Steel fibers had hooked ends with smooth surface. PP had straight ends with rough surface. PVA was straight ends with smooth surface. PET was straight ends with dented surface. The volume fractions of fibers to full concrete volume in this study were 0.5% and 1.0% as shown in **Table 3.1**.

3.3.2 Specimens

Specimens were the rectangular cross section with a notch at the mid-length. The detail of notched beams is illustrated in **Fig. 3.3**. The beams have a dimension of 100×100×400 mm. The notched width was 5 mm and height was 30 mm. The test span was 300 mm. Four notched beams were cast for one test.

During the mixing of the concrete, fibers were added and dispersed uniformly. Superplasticizer was used to improve workability of fresh concrete. The amount of superplasticizer was slightly different depending on the types of fibers. For the mixes of 60-mm steel fibers and polypropylene fiber, the additional superplasticizer (i.e. total superplasticizer = 1.3%) was added to obtain the similar slump of concrete with other fibers. Satisfactory workability was achieved in all specimens. There was no significant difference of workability among all specimens. The distribution of fibers was found to be uniform and fiber randomly oriented in the concrete. Also, no fiber balling was observed. After mixing, concrete was cast in the steel molds and compacted with an electrical vibrator. The curing process for

Table 3.1 Experimental cases of notched beams

Specimen	Material type of fibers	Fiber length (L_f) (mm)	Fiber volume (ρ_f) (%)
SF30-05-N	Steel (SF30)	30	0.5
SF30-10-N	Steel (SF30)	30	1.0
SF60-10-N	Steel (SF60)	60	
PP-10-N	Polypropylene (PP)	30	
PVA-10-N	Polyvinyl alcohol (PVA)	30	
PET-10-N	Polyethylene terephthalate (PET)	30	
30&PP-10-N	Hybrid (SF 30mm+PP)	-	0.5%+0.5%
60&PP-10-N	Hybrid (SF 60mm+PP)	-	
30&60-10-N	Hybrid (SF30+SF60)	-	

Note: The specimens were named following the system of "fiber type-ρ_f-Notch".

Table 3.2 Mix proportion of concrete

G_{max} (mm)	W/C	Slump (cm)	s/a (%)	Unit weight (kg/m^3)				Super plasticizer (%)
				W	C	S	G	
20	0.35	18±2.5	53.1	165	471	917	790	1.0-1.3

G_{max}: maximum size of coarse aggregate, W: water, C: high early strength cement, s/a: volume ratio of sand to aggregate, S: fine aggregate, G: coarse aggregate and Super plasticizer: percentage of cement weight.

Table 3.3 Fibers properties

Material type of fibers	Length L_f (mm)	Diameter D_f (mm)	Density (kg/m^3)	Strength (MPa)	Elastic modulus (GPa)	Shape of cross section	Surface	Shape of the end
Steel	30	0.62	7850	1050	210	Round	Smooth	Hooked
Steel	60	0.90	7850	1050	210	Round	Smooth	Hooked
Polypropylene	30	1.6×0.6	910	470	15	Rectangle	Rough	Straight
Polyvinyl alcohol	30	0.66	1300	960	23	Round	Smooth	Straight
Polyethylene terephthalate	30	0.70	1370	460	5.8	Round	Smooth	Straight

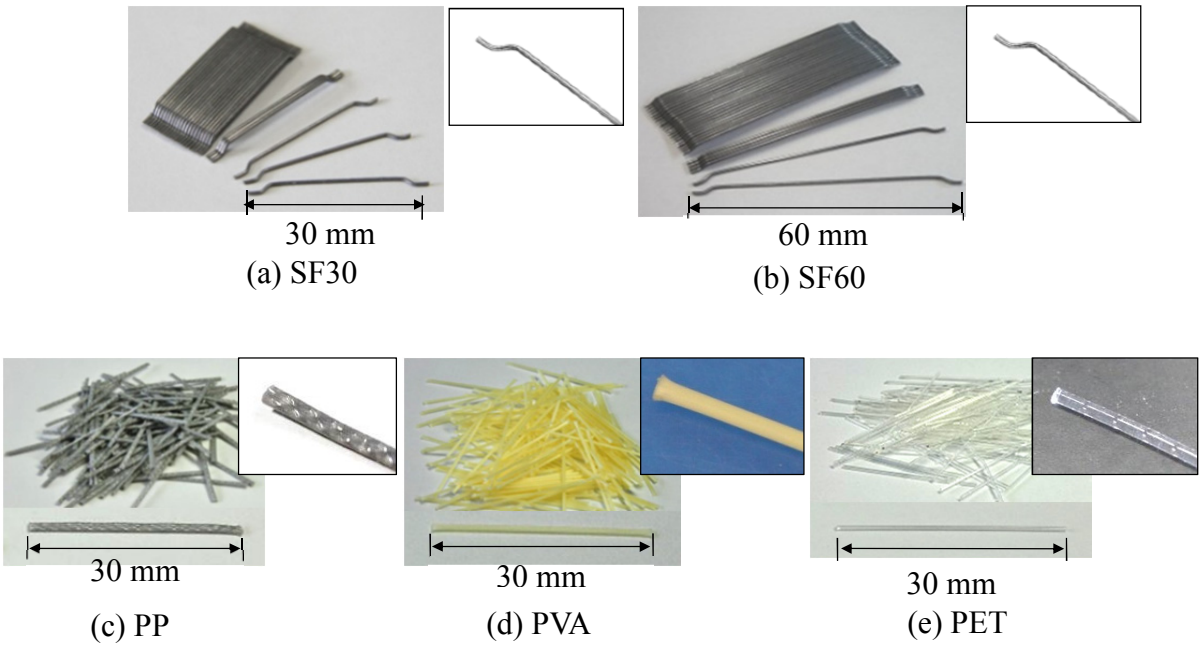

Figure 3.2 Fibers

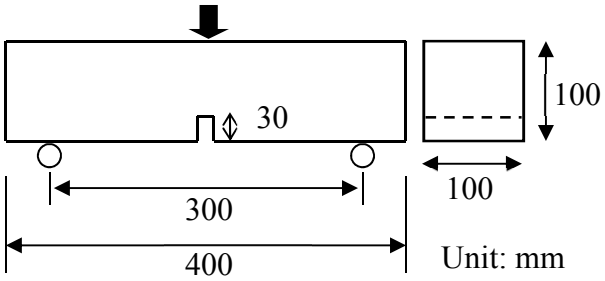

Figure 3.3 Outline of notched beam specimen

specimens was done by spraying water to cloths and covering with polyethylene sheets for seven days. For each test, three cylinders with ∅100×200 mm and three cylinders with ∅150×300 mm were cast and cured with the same condition as the notched specimens in order to determine the compressive strength and split tensile strength of concrete, respectively.

3.3.3 Test program and measurements

Three point loading tests of notched beams were conducted according to JCI-S-002-2003 (2003b). Both supports were hinged supports having rollers. The supports were horizontally movable to avoid any restraint on the deformation until the specimen completely ruptures. Four notched beams were tested for estimation of one tension softening curve following JCI-

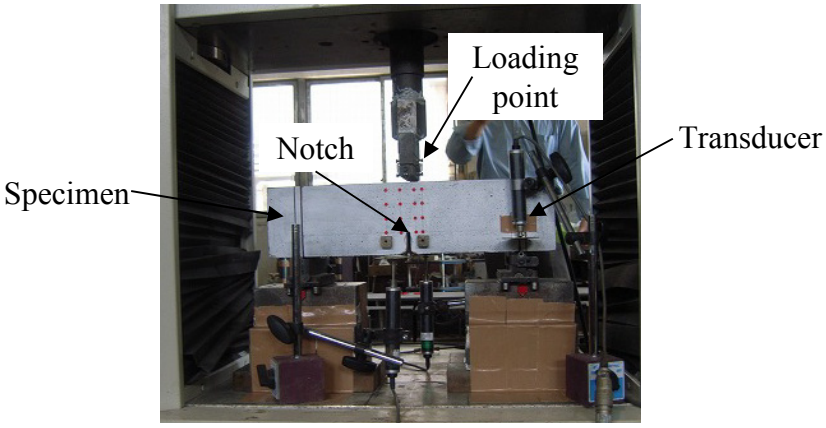

Figure 3.4 A notched specimen under loading

S-001-2003 (2003a). **Figure 3.4** shows a notched beam under loading. Four displacement transducers were installed to measure the load point displacement (LPD) of beams during loading.

3.4 Investigation of Tension Softening Curves

The fracture behavior of concrete is strongly related to the behavior of the fracture process zone. Fracture process zone consists of bridging zone and microcracking zone (**Fig. 3.5**). The bridging zone is a part of macrocrack, which stress transfers across the crack by partial matrix or fibers. The microcracking zone is a zone where the initiation of microcracks and their growth are dominant.

Tension softening curve is the material property related to the bridging effect of fibers in fiber reinforced concrete. The curve represents relationship between transmitted tensile stress across the crack surface and the crack opening displacement, as shown in **Fig 3.6**. The stress transferred across the crack is determined from a tension softening curve corresponding to the post peak stress-displacement relationship obtained from the direct tension test. However, as mentioned before, the direct tension test is difficult to perform because the behavior after the peak is unstable unless a very stiff machine is used. The test requires a special testing machine and it is very difficult to obtain a stable loading condition during the test. To avoid the difficulties in the direct tension test, the indirect testing methods for investigating the tension softening curves have been proposed (Kitsutaka, 1997, Kurihara et al., 1996 and Nanakorn and Horii, 1996).

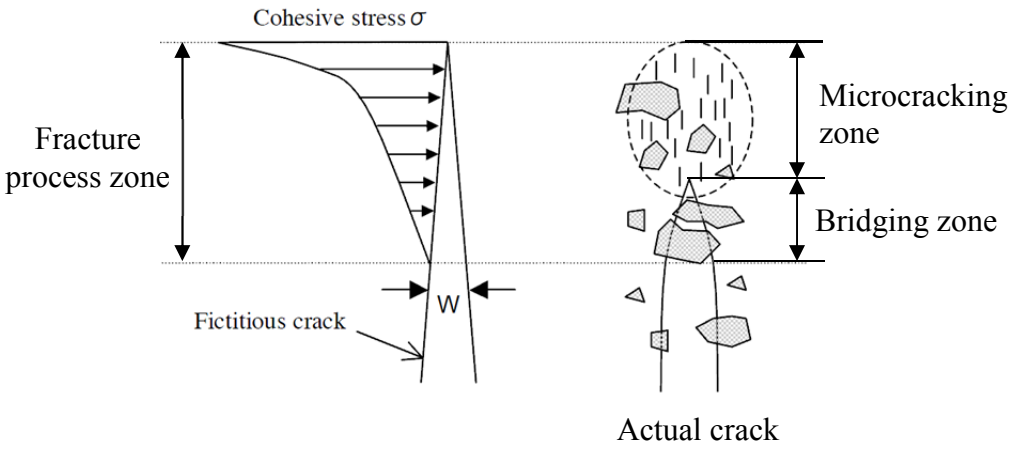

Figure 3.5 Fracture process zone (JCI-S-001-2003, 2003a)

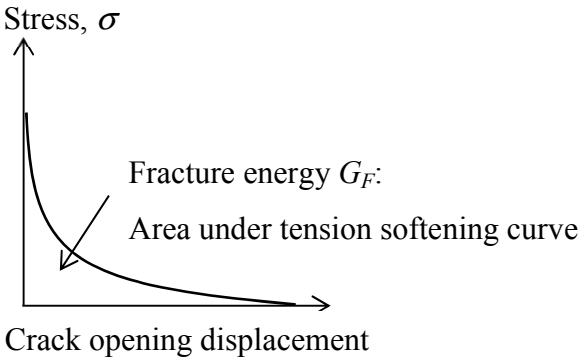

Figure 3.6 Tension softening curve

According to the Japan Concrete Institute (JCI) standard (2003a), the tension softening curves can be investigated from poly-linear approximation using the data of load-displacement curves obtained from mode I stable failure testing on notched specimens. The tension softening curves determined by this method are the curves expressed the relationship between the tensile stress (σ) and the crack opening displacement (w). The crack just ahead of the notched tip is considered. The test method is three-point bending test of notched beams. The requirements of the test are that there should be only a single propagating crack and the starting point of the crack propagation should be known. Another requirement is that the crack opening displacement at the starting point of the crack propagation must always be the maximum when compared with other locations.

The JCI standard (2003a) has recommended the program with confirmed reliability for the analysis of tension softening curves. In this study, the tension softening curves were estimated by using the program proposed by JCI (2003a), which has been developed by Prof. Uchida

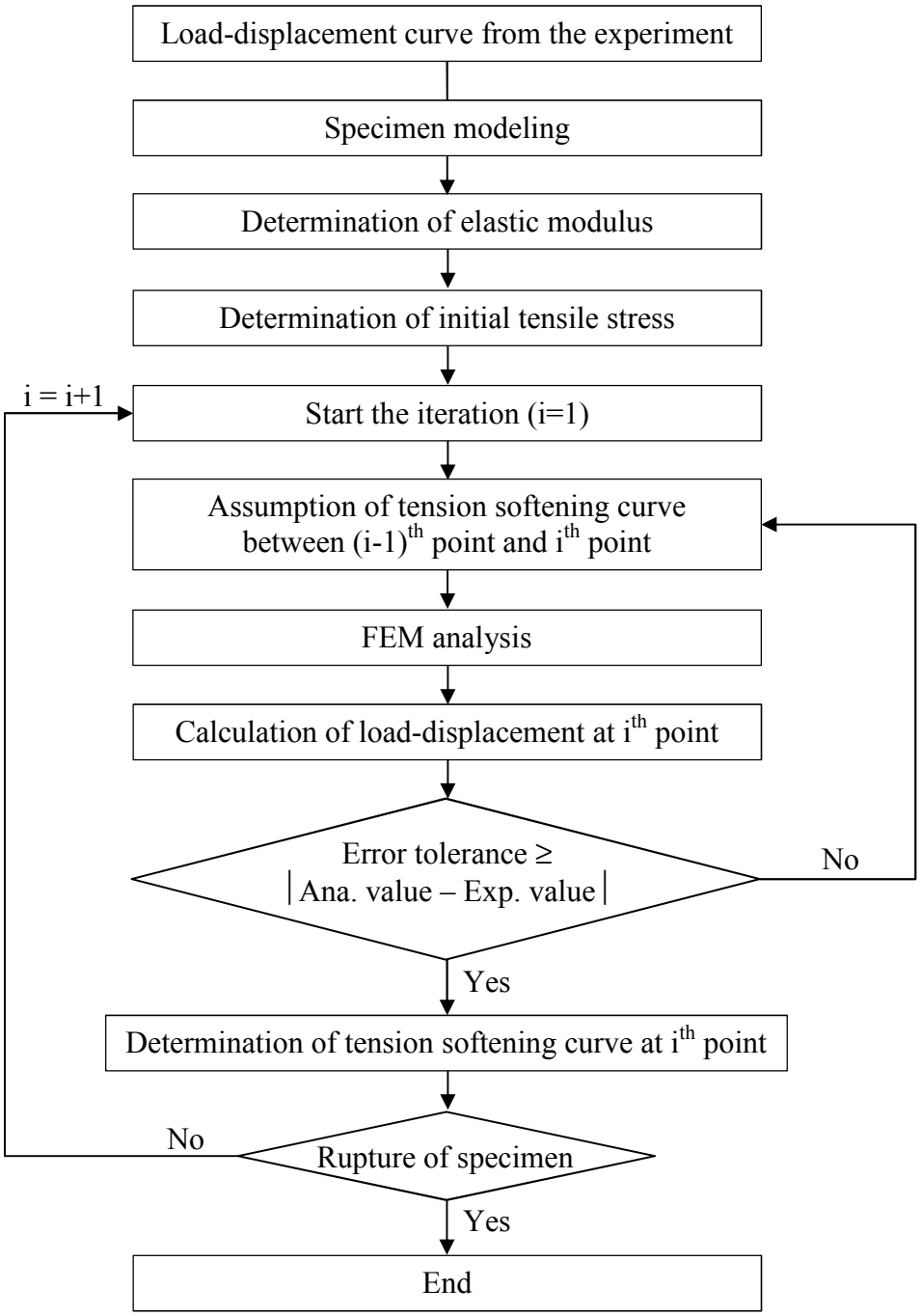

Figure 3.7 Flow chart of the poly-linear approximation method (FEM FT method)

(published as Kurihara et al, 1996). The program is denoted as FEM FT method. The FEM FT method has been written in the FORTRAN programing language and it is available to the public. The tension softening curves were estimated by poly-linear approximation using the average data of load-displacement curves obtained from four notched specimens. **Figure 3.7** presents the analysis flow of poly-linear approximation. The nonlinear finite element method (FEM) analysis was performed and obtained the analytical results. The specimens were

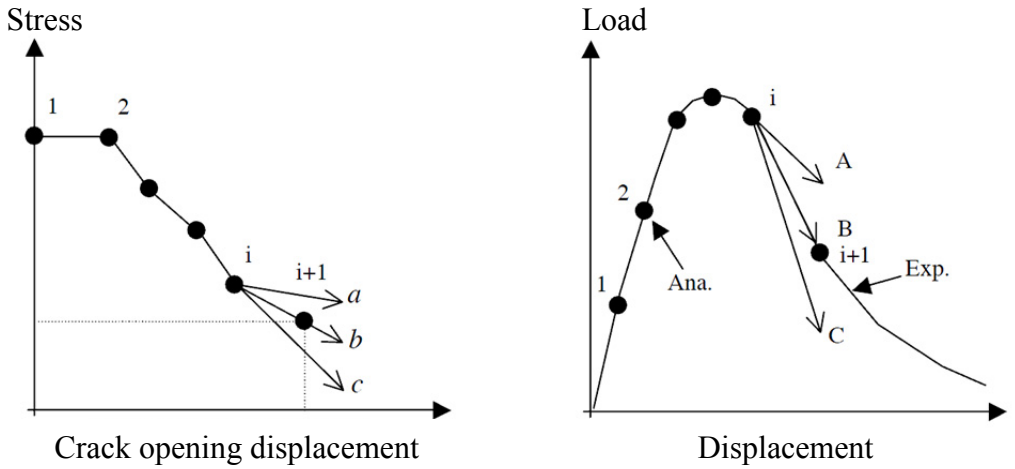

(a) Assumption of tension softening curve (b) Comparing of load-displacement curve

Figure 3.8 Poly-linear approximation method (JCI-S-001-2003, 2003a)

modeled. The elastic modulus of concrete was calculated from the initial slope of load-displacement obtained from the test results. The initial tensile stress was assumed and the FEM analysis was carried out. The tensile stress that made the analytical load-displacement curve agree with the experimental load-displacement curve was determined as the initial tensile stress, which is the initial point in the tension softening curve. Next, the latter parts of tension softening curve were investigated. The slope of the tip of tension softening curve, which was used as the constitute model in the FEM analysis, was assumed and changed in order to determine the optimum slope. The optimum slope was the slope of tension softening curve that offered the agreement between the analytical load-displacement and the experimental one. For example, by assuming slope *b* (line *b* in **Fig. 3.8(a)**), the analytical result provided line B in **Fig. 3.8(b)**. Since line B (**Fig. 3.8(b)**) agreed with the load-displacement from the experiment, line *b* (**Fig. 3.8(a)**) was determined as the point on tension softening curve. The analyzing was iterated until the analytical results agreed with the experimental results of load-displacement curves within the specified tolerance. This process was sequentially repeated to determine the overall shape of tension softening curve. During the analysis, the tension softening curve that has been already determined was used as a constitute model for subsequent calculation steps. The tension softening curves was extended step by step as shown in **Fig. 3.8**.

Tension softening curves obtained from the FEM FT method represent the relationship between crack opening displacement (w) and tensile stress (σ). However, in FRC, since the

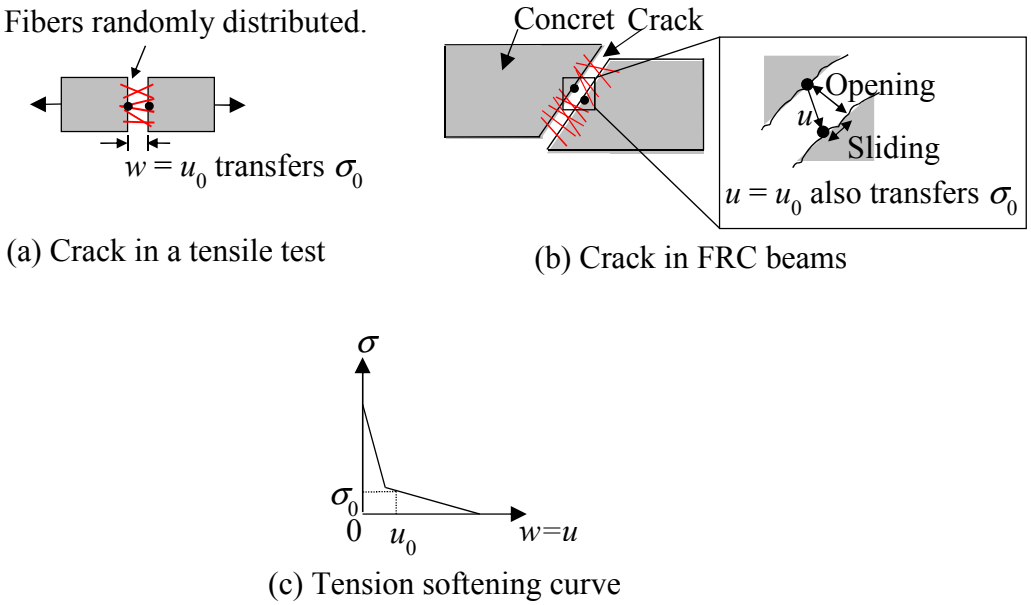

Figure 3.9 Relationship between crack opening displacement and crack surface displacement

fibers are randomly distributed in the concrete, the pullout forces arise in any directions. In the case that the opening displacement is dominant, the total displacement of crack surface in a tensile test (**Fig. 3.9(a)**) is equal to the total displacement of crack surface (u) in FRC beams, which is the displacement between the black dots as presented in **Fig. 3.9(b)**, (i.e. $w = u = u_0$). In this case, w and u transfer the same amount of stress σ. Thus, u is equivalent to w and is used for calculating the stress from the relationship of tension softening curves (**Fig. 3.9(c)**). The dominance of the opening displacement will be confirmed later in **Chapter 5** (Section 5.6.4). It is noted that this assumption may not be applicable in the case of major sliding displacement such as mortar.

3.5 Results of Notched Beam Tests

Nine bending tests of notched beams were conducted including eight fiber types and two fiber volume contents (ρ_f=0.5% and 1.0%) as summarized in **Table 3.1**. During the notched beam tests of FRC, the crack initiated from edge of the notch and propagated to the loading point. **Figure 3.10** presents notched beam under loading. Only one crack was observed in each notched FRC beam. The crack became wider with the increase in displacement and the softening behavior of FRC was observed. **Table 3.4** lists the compressive strength, tensile strength and fracture energy of the concrete measured by notched beam tests. Fracture energy

Table 3.4 Properties and expression of tension softening curves

Specimen	f'_c (MPa)	f_t (MPa)	G_F (N/mm)	Expression
SF30-05-N	59.6	2.7	2.71	$\sigma = \begin{cases} 4.5 - 58.6u & \text{for } u < 0.06 \text{ mm} \\ 1.0 - 0.24u & \text{for } u \geq 0.06 \text{ mm} \end{cases}$
SF30-10-N	56.6	3.6	4.24	$\sigma = \begin{cases} 7.0 - 40.2u & \text{for } u < 0.13 \text{ mm} \\ 1.85 - 0.55u & \text{for } u \geq 0.13 \text{ mm} \end{cases}$
SF60-10-N	55.9	3.4	8.82	$\sigma = \begin{cases} 4.3 - 50.5u & \text{for } u < 0.04 \text{ mm} \\ 2.3 - 0.31u & \text{for } u \geq 0.04 \text{ mm} \end{cases}$
PP-10-N	58.8	3.9	3.02	$\sigma = \begin{cases} 3.9 - 23.5u & \text{for } u < 0.12 \text{ mm} \\ 1.1 - 0.18u & \text{for } u \geq 0.12 \text{ mm} \end{cases}$
PVA-10-N	59.9	3.6	2.34	$\sigma = \begin{cases} 3.6 - 18.2u & \text{for } u < 0.16 \text{ mm} \\ 0.7 - 0.09u & \text{for } u \geq 0.16 \text{ mm} \end{cases}$
PET-10-N	61.5	3.3	2.89	$\sigma = \begin{cases} 3.4 - 25.2u & \text{for } u < 0.10 \text{ mm} \\ 0.9 - 0.25u & \text{for } u \geq 0.10 \text{ mm} \end{cases}$
30&PP-10-N	48.0	2.6	3.27	$\sigma = \begin{cases} 4.4 - 51.7u & \text{for } u < 0.06 \text{ mm} \\ 1.32 - 0.38u & \text{for } u \geq 0.06 \text{ mm} \end{cases}$
60&PP-10-N	44.5	2.6	7.49	$\sigma = \begin{cases} 3.7 - 17.4u & \text{for } u < 0.11 \text{ mm} \\ 1.82 - 0.26u & \text{for } u \geq 0.11 \text{ mm} \end{cases}$
30&60-10-N	44.9	2.4	7.50	$\sigma = \begin{cases} 5.3 - 41.2u & \text{for } u < 0.08 \text{ mm} \\ 2.03 - 0.35u & \text{for } u \geq 0.08 \text{ mm} \end{cases}$

f'_c: compressive strength, f_t: tensile strength from split tensile test, G_F: fracture energy and expression: formulated from the results of tension softening curves obtained following the JCI standards (JCI-S-001-2003, 2003a).

(G_F) was calculated from area under the load – load point displacement (LPD) curves of notched beams (shown in **Fig. 3.11**) using Eq. (3.1).

$$G_F = \frac{W_0 + W_1}{A_{lig}} \tag{3.1}$$

$$W_1 = \left(\frac{S}{L} m_1 + 2m_2 \right) g \cdot LPD_c \tag{3.2}$$

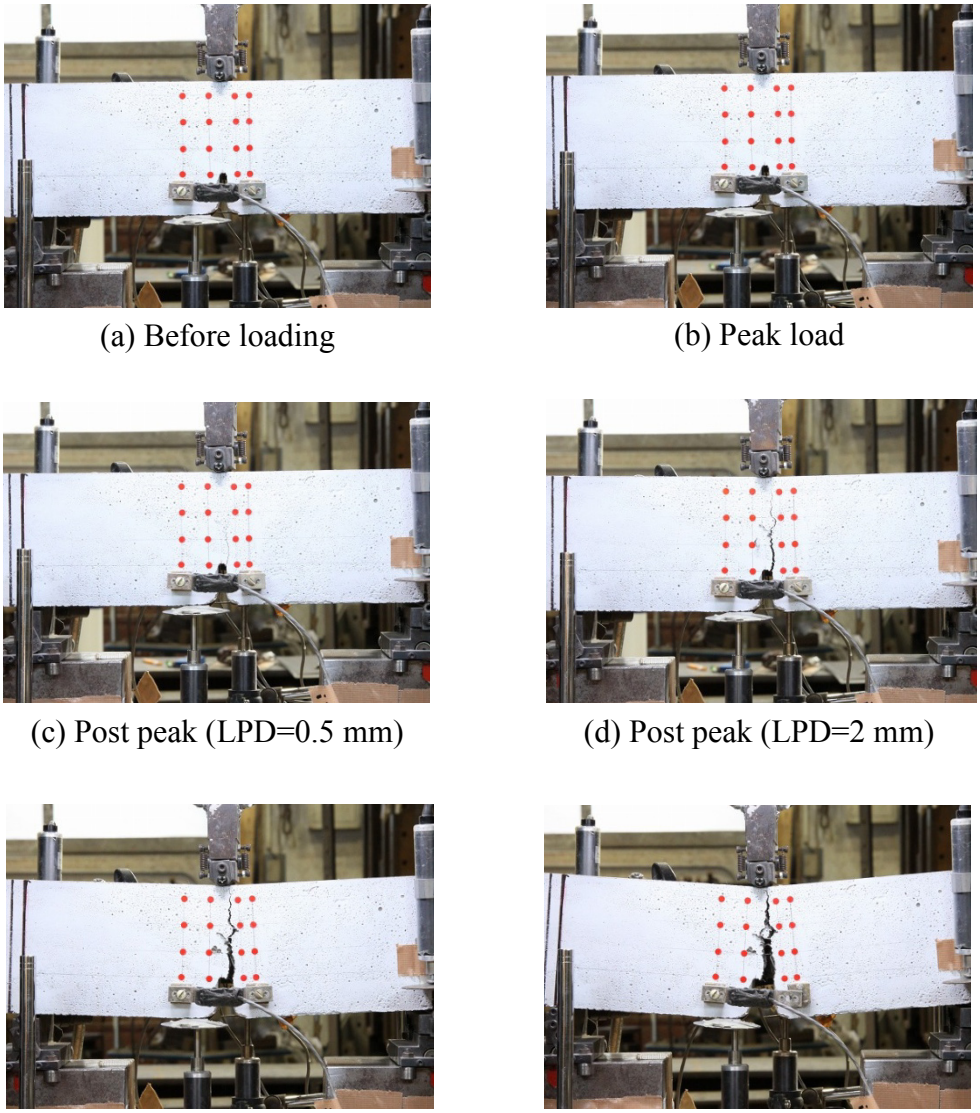

(a) Before loading (b) Peak load

(c) Post peak (LPD=0.5 mm) (d) Post peak (LPD=2 mm)

(e) Post peak (LPD=5 mm) (f) Post peak (LPD=10 mm)

Figure 3.10 A notched beam under loading (SF30-10-N)

where, G_F: fracture energy (N/mm), W_0: area below the load-load point displacement (LPD) curve up to the rupture of specimen (N·mm), W_1: work done by deadweight of specimen and equipments attached to a specimen (N·mm), S: loading span (mm), L: total length of specimen (mm), m_1: mass of a specimen (kg), m_2: mass of equipments attached to a specimen (kg), A_{lig}: area of broken ligament (mm^2), g: gravitational acceleration (9.807 m/s^2) and LPD_c: load point displacement at the time of rupture (mm). Since it is difficult to continue testing of fiber reinforced concrete until the specimen completely ruptures, the JCI standard (2003b) allows stopping the test after LPD reaches 3 mm or more depending on the purpose of testing. In this study, the test was continued until LPD reached 15 mm.

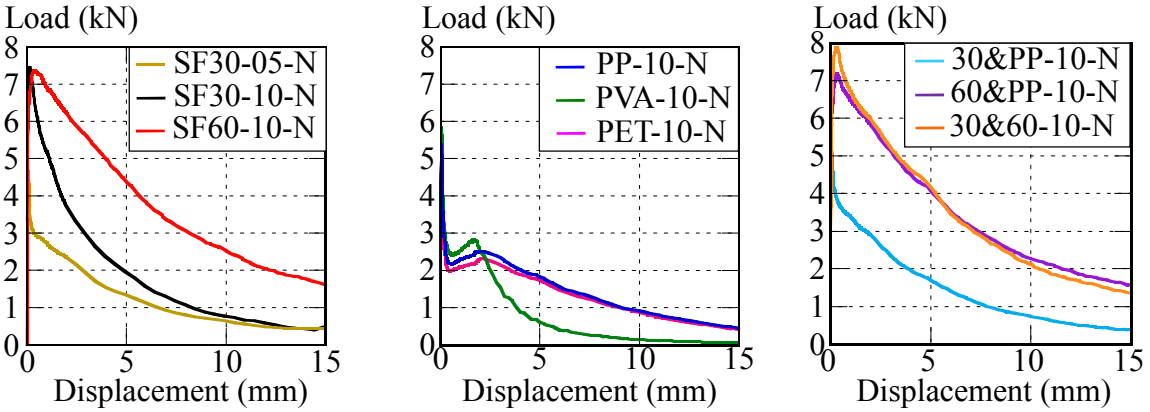

Figure 3.11 Load-LPD curves

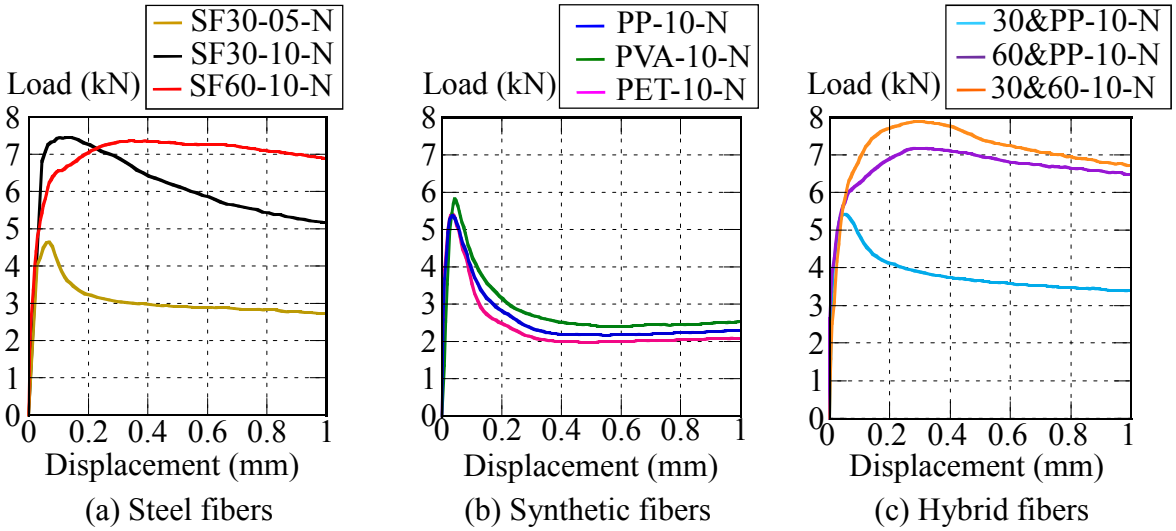

Figure 3.12 Initial part of load-LPD curves

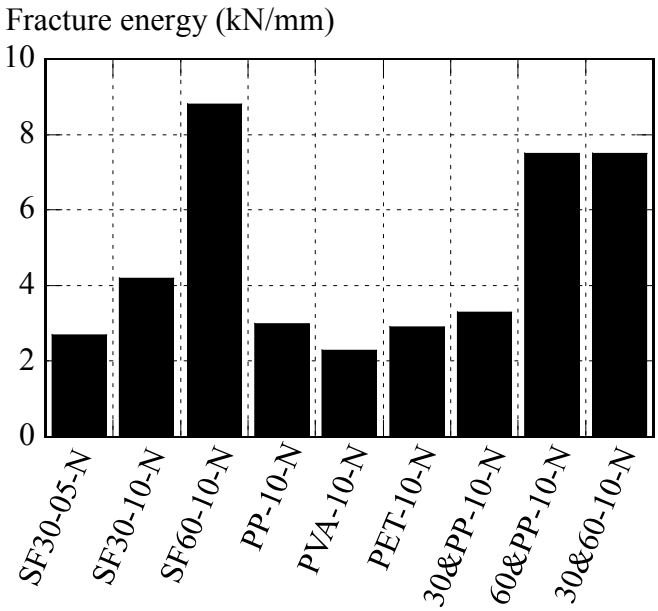

Figure 3.13 Fracture energy of fiber reinforced concrete

Following the JCI standard (2003a), the fracture energy and the tension softening curve can be calculated and analyzed from the average load–load point displacement (LPD) curves of at least four notched specimens. The average load–LPD curves of four notched specimens are shown in **Fig. 3.11**. **Figure 3.12** demonstrates the initial part of load-LPD curves.

Firstly, the curve exhibits linear relation. In this region, the load is carried by the matrix behaving elastically. At this stage, there is no crack in the matrix. After that, the curve is non-linear due to the presence of fibers. In this region, the load is transferred between the matrix and fibers (Suwantnodom, 2008). Load still increases until the matrix cracks (macrocracking). From this stage, the load cannot transfer between the matrix and fibers anymore. This leads to the peak load. **Figure 3.12(a)** presents that the maximum load increases with the increase in fiber volume fraction. In addition, comparing the same fiber volume fraction (ρ_f=1.0%), the fiber types influenced the maximum load. It is because the maximum bridging force that can be reached before initiation of the macrocrack in the matrix depends on the elastic modulus, fiber geometry, end types and number of fibers (ACI 544.4R-88, 1999). After the peak load, the matrix is no longer contributing the load capacity. The load is carried by only the fibers that are gradually pulled out or cut off. For specimen with ρ_f=1.0%, the load–LDP curves show either a gradual decrease in the load after the peak for fibers with hooked-end (i.e., steel fibers) or a sudden decrease in load for straight fibers without improving end anchorage (i.e., synthetic fibers). In notched beams with 0.5% of steel fibers (SF30-05-N), the small drop occurs because of the less number of fibers at crack section. After this stage, load decreases with the further displacement development. The load-LPD curves of specimens having steel fibers (**Fig. 3.11(a)** and **(c)**) demonstrate similar behavior. The load gradually decreases with the increase in LPD. On the other hand, the transfer of load to synthetic fibers shows a small increase in load due to the interfacial bonding from fiber surface until fibers begin to break or pull-out (**Fig. 3.11(b)**). Considering the post peak region, the specimens having steel fibers (**Fig. 3.11(a)** and **(c)**) resisted higher load than specimens with synthetic fibers at the same displacement.

The fracture energy of each fiber reinforced concrete was calculated from the load-displacement curves shown in **Fig. 3.11** following Eq. (3.1). The fracture energy is listed in **Table 3.4** and plotted in **Fig. 3.13**. The value of G_F calculated from Eq. (3.1) was compared with G_F calculated from the area under tension softening curve to confirm that the difference was slight. Although the remaining load of SF60-10-N was highest at LDP =15 mm when

compared with other specimens, the difference between G_F calculated from Eq. (3.1) and calculated from area under tension softening curve of SF60-10-N was only 3%, which was negligible. Therefore, the load-LPD curves until 15 mm was acceptable for the calculation of G_F. It is noted that the results of tension softening curves will be discussed in Section 3.6.

By comparing SF30-05-N with SF30-10-N, which are the specimens having ρ_f=0.5% and 1.0%, respectively, the fracture energy increased with the increase in fiber volume fraction. Furthermore, the fracture energy of steel fibers (SF30-10-N and SF60-10-N) was higher than that of the synthetic fibers (PP-10-N, PVA-10-N and PET- 10-N). More energy is needed for creating the crack in steel fiber reinforced concrete. Since the hybrid fibers contained the steel fibers, the fracture energy was moderate. G_F of SF60-10-N was the highest among the all fiber types. This means length of fiber enhances the fracture energy.

3.6 Results of Tension Softening Curves

The tension softening diagrams of nine cases of fiber reinforced concrete are shown in **Fig. 3.14**. The tension softening curves can be divided into two zones. First zone is immediately after cracking, where the stress abruptly decreases. Second zone is where the stress decreases slowly as the increase in crack opening displacement and this zone is important for discussing the shear resisting mechanism of FRC beams because the crack surface displacement at the peak load is in the range of the second zone.

The results showed that SF30-10-N showed the highest peak stress. The fiber reinforced concrete with 1.0% of steel fibers can resist higher tensile stress across the crack more than 0.5% of steel fibers. Regard to the influence of fiber types, SF60-10-N resisted the highest stress across the crack after $u \geq 0.12$ mm. It is because fiber length increased; thus, the bonding improved. At the identical crack opening displacement, steel fibers (SF30-10-N and SF60-10-N) transferred higher stress than that by synthetic fibers (PP-10-N, PVA-10-N and PET-10-N) due to their high tensile strength and anchorage, while hybrid fibers showed the moderate stress. There were two mechanisms in which the stress transferred between crack surfaces was lost. SF30-05-N, SF30-10-N, SF60-10-N, PP-10-N, 30&PP-10-N, 60&PP-10-N and 30&60-10-N failed in the pull-out mechanism, whereas PVA-10-N and PET-10-N exhibited both pull-out and cut-off mechanisms. Because the tensile strength of fibers was comparatively greater than their bond strength, pull-out failure occurred.

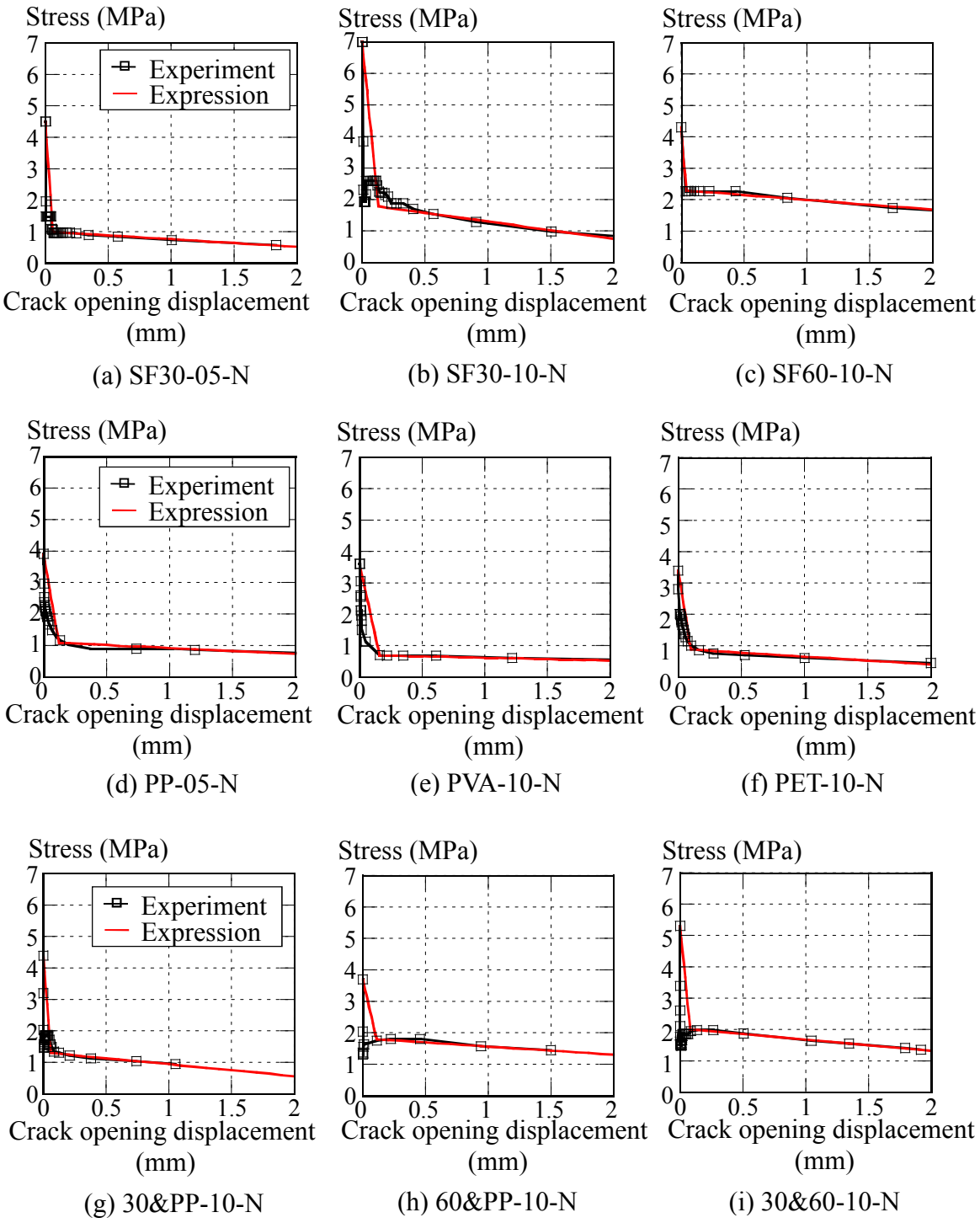

Figure 3.14 Experimental results and expression of tension softening curves

Using a least-squares data-fitting procedure, the shape of bilinear curves of the tension softening diagram can be obtained as shown in **Table 3.4**. As explained in section 3.4, when the opening displacement is dominant, the crack surface displacement (u) is equivalent to crack opening displacement (w) in the fiber reinforced concrete. Hence, the crack surface displacement (u) is used for calculating the stress from the relationship of tension softening

curves. The beginning of tension softening curve (first linear line) is sometimes difficult to fit curve. However, the equation of the second linear line can be fitted well with the experimental results. Only the second linear line was used for the calculation in this study because the crack surface displacement at the peak load was about 1 mm, which was in the second linear line of bilinear tension softening curves. The equations will be used for converting crack surface displacement to stress in **Chapter 6**.

3.7 Conclusions of Chapter 3

The bending tests of notched beams and the investigation of tension softening curves were described. The effects of fiber volume fractions and fiber types on the fracture behavior of fiber reinforced concrete were discussed. The effect of fiber volume fractions was investigated by comparing the specimen having 0.5% of 30-mm steel fibers with specimen having 1.0% of 30-mm steel fibers. The influence of fiber types was discussed by varying the fiber types without changing the fiber volume fraction. Based on the experimental results of notched beam test and the analyzed tension softening curves, the following conclusions can be drawn.

(1) With the increase in fiber volume fraction from 0.5% to 1.0% of concrete full volume, the fracture energy and the maximum load from the bending test increased. In addition, the tension softening curve showed better peak stress and better post peak behavior with the increase of fiber content.

(2) Among the nine types of fiber reinforced concrete (i.e., two types of steel fibers, three types of synthetic fibers and three types of hybrid fibers), the steel fibers with 60 mm length revealed the highest fracture energy. In addition, 60-mm steel fibers gave the best post peak behavior in tension since it resisted the highest stress across the crack after the crack opening displacement reached 0.12 mm. It is because the fiber length increased; hence, the bonding improved. From these results, the long fibers were effective for improving fracture behavior; however, the length of fibers also affected the slump of concrete. Therefore, the proper length of fibers should be used.

(3) Based on the tensions softening curves, steel fibers could transfer more stress than synthetic fibers when there were enough fiber length and bonding strength.

CHAPTER 4

EXPERIMENTAL PROGRAM OF FIBER REINFORCED CONCRETE BEAMS

4.1 Introduction

This chapter summarizes the outline of the experimental program of fiber reinforced concrete (FRC) beams. The test program consists of 17 FRC beams. The parameters in this study were selected from the factors affecting shear strength of FRC beams presented in **Chapter 2**. The content of this chapter presents the experimental cases, the materials used in the experiment, specimen fabrication, test procedure and the measurement items. To measure the diagonal cracking behavior, the image analysis was performed. The crack surface displacement, crack length and angle of diagonal crack were measured from the image processing programs.

4.2 Experimental Cases

In this research, four parameters were selected to investigate the influences of each parameter on the shear capacity and investigate the shear carried by fibers to develop the predictive equation for the shear capacity of FRC beams. The summary of test variables and names of specimens are presented in **Table 4.1**. One FRC beam was prepared for each experimental case. The experimental cases can be classified into four series as the following:

Series I: Fiber volume fraction (ρ_f)

In this series, the effect of fiber volume fraction was investigated. Two fiber volume fractions were tested. There were 0.5% and 1.0% to concrete full volume. The constant variables of Series I were the fiber type and size of specimens. Steel fibers with 30 mm were tested. The effective depth (d) and web thickness (b_w) were 250 mm and 150 mm, respectively.

Table 4.1 Experimental cases

Specimen	Series	Fiber volume (%)	Stirrup ratio (%)	Fiber type	Fiber length (mm)	Effective depth (mm)
SF30-05-r00	I and II	0.5	0.00	Steel	30	250.0
SF30-05-r18			0.18			
SF30-05-r30			0.30			
SF30-10-r00		1.0	0.00			
SF30-10-r12			0.12			
SF30-10-r18			0.18			
SF30-10-r24			0.24			
SF30-10-r30	I, II, III, IV		0.30			
SF60-10-r30	III			Steel	60	
PP-10-r30				Polypropylene (PP)	30	
PVA-10-r30				Polyvinyl alcohol (PVA)		
PET-10-r30				Polyethylene terephthalate (PET)		
30&PP-10-r30				Hybrid (SF 30mm+PP)	-	
60&PP-10-r30				Hybrid (SF 60mm+PP)	-	
30&60-10-r30				Hybrid (SF 30+60 mm)	-	
SF30-10-r32-S	IV		0.32	Steel	30	187.5
SF30-10-r30-L			0.30			375

Note: The specimens were named following the system of "fiber type-fiber volume-stirrup ratio-size".

Series II: Stirrup ratio (r_w)

In order to examine the effect of stirrup ratio, the stirrup ratio in test span was varied from 0.0%-0.3%. There were 0.0, 0.12, 0.18, 0.24 and 0.30% as shown in **Table 4.1**. The number of stirrups used in each specimen was changed corresponding to the stirrup ratio. As well as Series I, the constant variables of Series II were the fiber type and size of specimens.

Series III: Types of fibers

Eight FRC beams were tested to investigate the influences of fiber types, length of fibers and the combinations. There were four fiber types those made of steel, polypropylene (PP), polyvinyl alcohol (PVA) and polyethylene terephthalate (PET). The lengths of fibers were 30 and 60 mm. In addition, there were three combinations of fibers between steel fibers with 30 mm length and polypropylene fibers (30&PP-10-r30), steel fibers with 60 mm length and polypropylene fibers (60&PP-10-r30) and steel fibers with 30 mm length and 60 mm length (30&60-10-r30). In order to eliminate the effect of ρ_f, r_w and effective depth, ρ_f was 1.0% and r_w was 0.30% and d was 250 mm in all specimens.

Series IV: Effective depth (d)

In this series, the influence of effective depth (or size effect) was investigated. The constant variables of Series IV were fiber volume fraction, stirrup ratio and fiber type. In Series IV, fiber volume fraction was 1.0%, stirrup ratio was 0.3% and steel fibers with 30 mm length were used. The series consisted of three specimens with different sizes. The beams were geometrically similar in three-dimensional. The original specimen was SF30-10-r30. The size of SF30-10-r32-S and SF30-10-r30-L was reduced to 0.75 times and enlarged to 1.5 times of the original size in SF30-10-r30, respectively. The results of SF30-10-r32-S and SF30-10-r30-L are compared and discussed with SF30-10-r30.

Specimens were named according to fiber types, fiber volume fraction, stirrup ratio and size of specimens; e.g., SF30-10-r30-L corresponded to the specimen with 30-mm steel fibers, 1.0% of fiber volume, 0.30% of stirrup ratio and large size.

4.3 Materials

4.3.1 Concrete

The concrete was designed with an average 7-day age concrete strength (f'_c) of 50 MPa. The medium compressive strength of concrete (f'_c = 50 MPa) was used in this study because the number of test results of FRC beams using medium compressive strength of concrete that has been published up to date is limited. In addition, 50 MPa is general strength of FRC. The materials used in the concrete mixes were high-early strength cement, fine aggregates, coarse

Table 4.2 Mix proportion of concrete

G_{max} (mm)	*W/C*	Slump (cm)	*s/a* (%)	Unit weight (kg/m^3)				Super plasticizer (%)
				W	*C*	*S*	*G*	
20	0.35	18±2.5	53.1	165	471	917	790	1.0-1.3

G_{max}: maximum size of coarse aggregate, *W*: water, *C*: high early strength cement, *s/a*: volume ratio of sand to aggregate, *S*: fine aggregate, *G*: coarse aggregate and Super plasticizer: percentage of cement weight.

Table 4.3 Fibers properties

Material type of fibers	Length L_f (mm)	Diameter D_f (mm)	Density (kg/m^3)	Strength (MPa)	Elastic modulus (GPa)	Shape of cross section	Surface	Shape of the end
Steel	30	0.62	7850	1050	210	Round	Smooth	Hooked
Steel	60	0.90	7850	1050	210	Round	Smooth	Hooked
Polypropylene	30	1.6×0.6	910	470	15	Rectangle	Rough	Straight
Polyvinyl alcohol	30	0.66	1300	960	23	Round	Smooth	Straight
Polyethylene terephthalate	30	0.70	1370	460	5.8	Round	Smooth	Straight

aggregates and superplasticizer. The detail of mix proportion is summarized in **Table 4.2**. The water-to-cement ratio was 0.35. In order to achieve good workability, the superplasticizer, which was high-performance air entrained (AE) water reducing agent (Type: SP8-SBsX2 and SP8SV), was used in the range of 1.1-1.3% to the weight of cement for each concrete mix. The mix proportion of concrete used in FRC beams was the same with those in the notched beams discussed in **Chapter 3**.

4.3.2 Fibers

Five fiber types and three combinations of fibers were incorporated into concrete, including steel, synthetic and hybrid fibers. The characteristics of fibers are summarized in **Table 4.3**. Pictures of fibers, their end types and surfaces are shown in **Fig. 4.1**. The volume fractions of fibers to full concrete volume in this study were 0.5% and 1.0%. The fibers are the same types with fibers used for the notched beam tests.

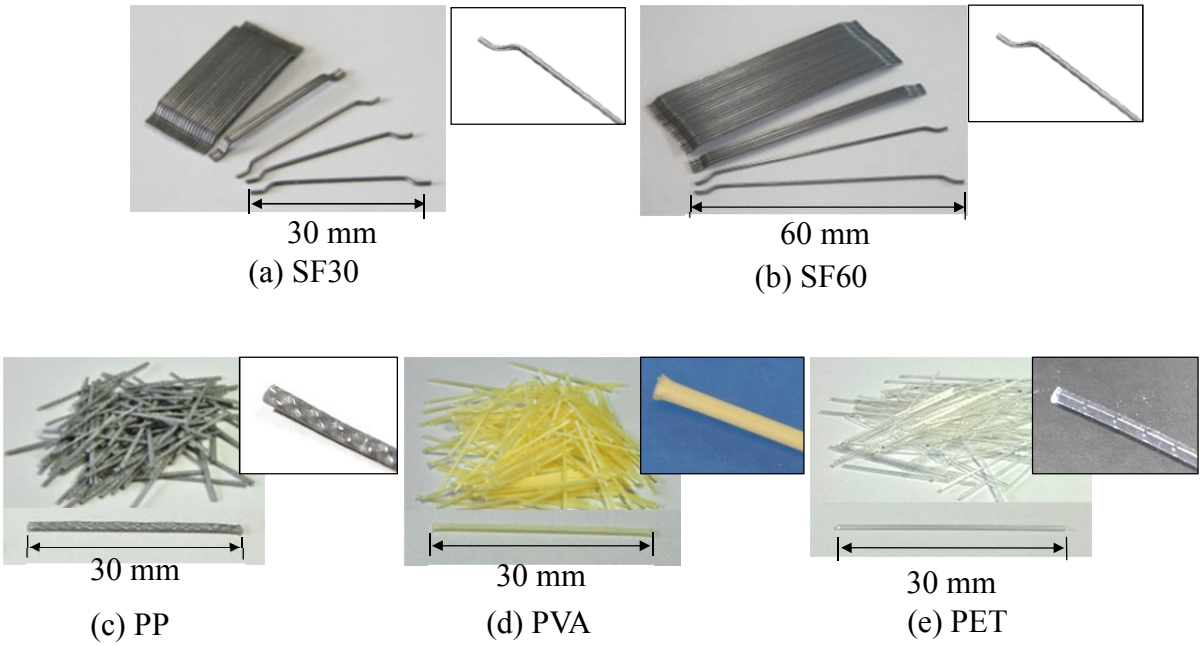

Figure 4.1 Steel and synthetic fibers

4.3.3 Reinforcing steels

The details of reinforcements are summarized in **Table 4.4**. For Series I, II and III, the tensile reinforcing bars used in this research were deformed steel with 25.4 mm nominal diameter (D25 SPBD930). The yield strengths of the reinforcing bars are summarized in **Table 4.5**. The yield strength was 1006-1022 MPa. The stirrups with deformed steels of 6.35 mm in nominal diameter were arranged as shear reinforcement. The yield strength was 315-336 MPa as shown in **Table 4.5**. The compression bars were round bars of 6 mm in diameter. The yield strength was 293-304 MPa.

However, for Series IV, the sizes of tensile reinforcing bars, stirrups and compression reinforcements were changed as follows. For SF30-10-r32-S, the deformed steel bars with 19.1 mm nominal diameter (D19 USD685A) were used as the tensile reinforcements. In addition, the stirrups were D6 SD295A. The round bars with 6 mm in diameter were used as compression bars. For SF30-10-r30-L, the tensile reinforcements used were D36 SPBD930. The stirrups were D10 SD295A. The compression bars were round bar with 9 mm in diameter. The yield strengths of longitudinal reinforcements and stirrups are shown in **Table 4.5**. The specifications for the stirrups are according to JIS Z 2241.

Table 4.4 Details of reinforcements

Specimen	Effective depth (mm)	Reinforcement	Type
Series I, II and III	250.0	Longitudinal reinforcement	D25 SPBD930
		Stirrups	D6 SD295A
		Compression bar	∅6 SR235
SF30-10-r32-S (Series IV)	187.5	Longitudinal reinforcement	D19 USD685A
		Stirrups	D6 SD295A
		Compression bar	∅6 SR235
SF30-10-r30-L (Series IV)	375.0	Longitudinal reinforcement	D36 SPBD930
		Stirrups	D10 SD295A
		Compression bar	∅9 SR235

Table 4.5 Details of test specimens

Series	Specimen	Fibers		Stirrups			Tensile bars			Dimension of specimens					
		Type	ρ_f (%)	r_w (%)	s (mm)	f_{wy} (MPa)	A_s (mm^2)	p_w (%)	f_y (MPa)	b_w (mm)	d (mm)	a (mm)	a/d	h (mm)	Length (mm)
I and II	SF30-05-r00	30mm-Steel	0.5	0.00	700	336	1013	2.7	1022	150	250	700	2.8	300	1800
	SF30-05-r18			0.18	233										
	SF30-05-r30			0.30	140										
	SF30-10-r00		1.0	0.00	700	325			1016						
	SF30-10-r12			0.12	350										
	SF30-10-r18			0.18	233										
	SF30-10-r24			0.24	175										
I-IV	SF30-10-r30			0.30	140										
III	SF60-10-r30	60mm-Steel				315			1006						
	PP-10-r30	Polypropylene (PP)													
	PVA-10-r30	Polyvinyl alcohol (PVA)													
	PET-10-r30	Polyethylene terephthalate (PET)													
	30&PP-10-r30	Hybrid (SF 30mm+PP)				328									
	60&PP-10-r30	Hybrid (SF 60mm+PP)													
	30&60-10-r30	Hybrid (SF 30+60 mm)													
IV	SF30-10-r32-S	30mm-Steel		0.32	175	336	573		732	112.5	187.5	525		225	1350
	SF30-10-r30-L			0.30	210	389	2036	2.4	990	225	375	1050		450	2700

ρ_f: fiber volume fraction, r_w: stirrup ratio, s: spacing of stirrups in test shear span, f_{wy}: yield strength of stirrups, A_s: cross section area of longitudinal reinforcement, p_w: longitudinal reinforcement ratio,f_y: yield strength of longitudinal reinforcement, b_w: web thickness, d: effective depth, a: shear span, a/d: shear span to effective depth ratio and h: height of specimen.

4.4 Mixing, Casting and Curing of Concrete

50-liter capacity of mixing machine was used for mixing the concrete. First, cement and fine aggregate were mixed for 30 seconds and then all of water, which included the superplasticizer, was inserted within 30 seconds and continued mixing for 1 minute. The amount of superplasticizer was slightly different depending on the types of fibers. For the mixes of 60-mm steel fibers and polypropylene fiber, the additional superplasticizer (i.e. total

Figure 4.2 Adding fiber (Hybrid fibers between 60-mm steel and polypropylene)

(a) Concrete just after mixing (b) Concrete slump (PVA-10-r30)

Figure 4.3 Fresh concrete

Figure 4.4 Moist-curing

superplasticizer = 1.3%) was added to obtain the similar slump of concrete with other fibers. Next, fibers were added to mixer and mixed for another 1 minute to ensure that the fibers were dispersed properly as presented in **Fig. 4.2**. After that, coarse aggregate was inserted and mixed for 2 minutes. **Figure 4.3** shows the fresh concrete and slump. Satisfactory workability was achieved in all specimens. There was no significant difference of workability among all specimens. From the observation, the distribution of fibers was found to be uniform and fiber randomly oriented in the concrete. No fiber balling was observed. To ensure the random orientation of fibers, concrete was carefully cast into formwork by move-filling method. In this move-filling method, concrete was filled continuously in the longitudinal direction along the axis of the formwork. Zhou and Uchida (2013) confirmed that, by using move-filling method, fibers were randomly oriented.

After the casting, the beams were covered with moistened cloths and polyethylene sheets and cured for 24 hours. After 24 hours, the formwork was removed and the beam was covered again by moistened cloths and polyethylene sheets as shown in **Fig. 4.4**. Moist-curing was continued until the 6^{th} day after the casting. For each specimen, three cylinders with dimension of ∅100×200 mm and three cylinders with dimension of ∅150×300 mm were cast and cured with the same condition as the specimens to determine the compressive strength and tensile strength of concrete, respectively.

4.5 Specimens

The test program consisted of 17 FRC beams with different fiber volume fraction, stirrup ratio, fiber types and specimen size. The details of tested FRC beams are illustrated in **Fig. 4.5**. All beams were rectangular cross sectional beams designed to fail in shear. **Table 4.5** lists the detail of tested specimens. The ratio of shear span to the effective depth (a/d) was 2.8. The longitudinal reinforcement ratio (p_w) was 2.7%. All specimens were controlled such that they would fail in the left shear span by providing fewer stirrups in the left shear span, which was considered as the test shear span. For example, in **Fig. 4.5(a)**, the left side was the test shear span.

Specimens in Series I, II and III had the same specimen size. The dimension, reinforcing bar arrangement, loading and supporting points, and location of the strain gauges and transducers of specimens in Series I, II and III are illustrated in **Fig. 4.5(b)**. Fifteen beams were tested

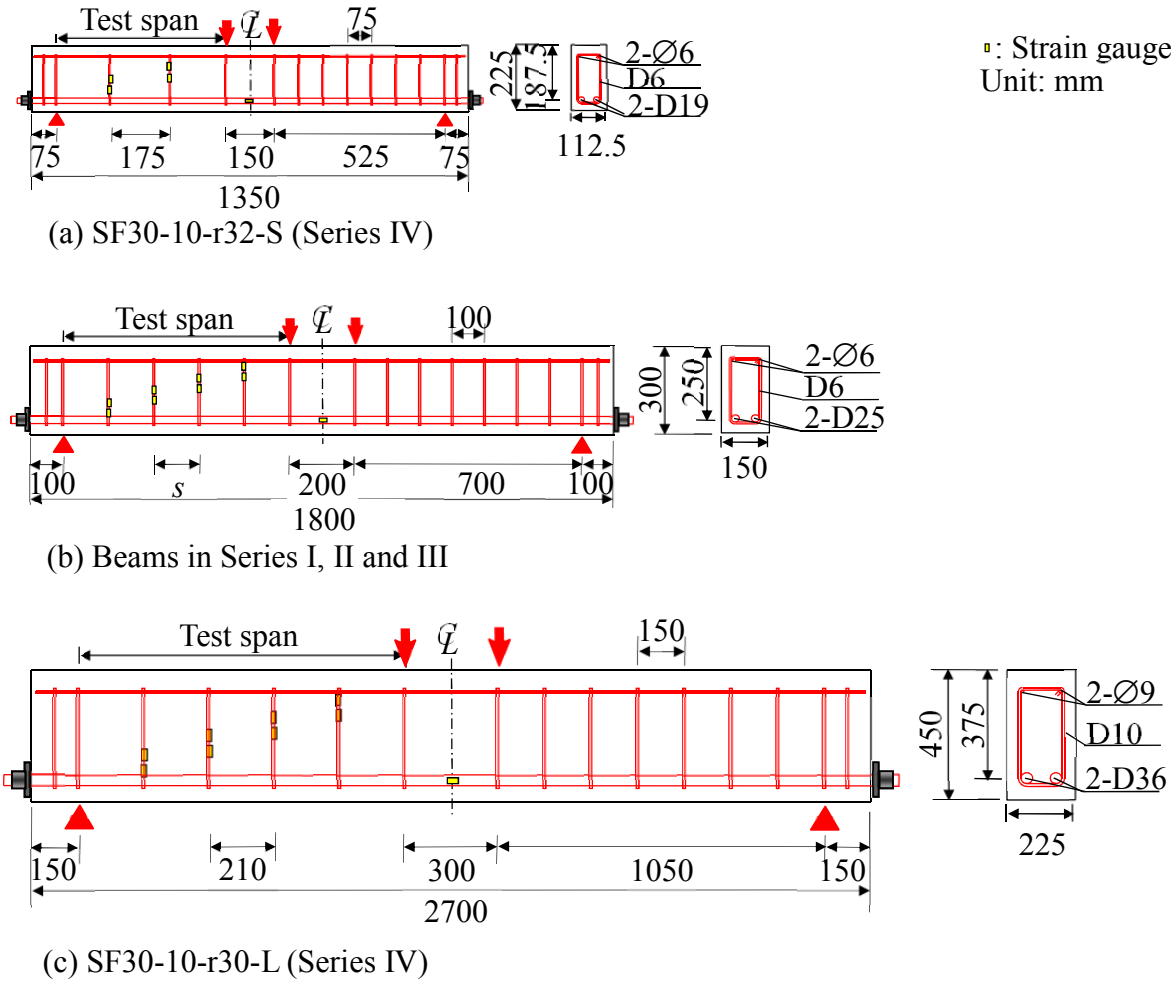

Figure 4.5 Detailed diagram of a FRC beam

following this design. The shear span (a) was 700 mm and the effective depth (d) was 250 mm. The width of beams was 150 mm. Length of specimens was 1800 mm. Two steel bars were arranged as the longitudinal reinforcement of specimens. The longitudinal reinforcement ratio (p_w) was 2.7%.

Since Series II was aimed to investigate the shear carried by fibers of FRC beams with different stirrup ratio, stirrup ratio was varied (i.e. r_w=0.00, 0.12, 0.18, 0.24, and 0.30%). The spacing of stirrups in test shear span was changed corresponding to the stirrup ratio. There were five intervals of stirrup spacing (s) in the test shear span that were 140, 175, 233, 350, and 700 mm as shown in **Table 4.5**. The spacing was controlled by the limitation of diameter of stirrups and specimen size. The use of stirrups, which are smaller than D6, is not preferred. Nonetheless, with this spacing, the stirrups still functioned as the shear reinforcement because

(a) Formwork for Series I, II and III

(b) Formwork for SF30-10-r32-S

(c) Formwork for SF30-10-r30-L

Figure 4.6 Formworks of the specimens

the diagonal crack passed through the stirrups in web concrete in the test shear span as will be explained in **Chapter 5**. On the other hand, stirrups by the interval of 100 mm (stirrup ratio 0.42%) were provided in another shear span.

The size of the specimens was proportionally enlarged for three-dimensional similarity (width, height and length) in Series IV. Beam lengths of 1350, and 2700 mm, beams widths of 112.5, 225 mm, and the effective depths of 187.5 and 375 mm were used as shown in **Table 4.5**. The longitudinal reinforcement ratio (p_w), a/d, stirrup ratio (r_w), fiber content (ρ_f) and fiber types were the same. The main reinforcement consisted of one layer of two steel bars. Along the top of the beams, two compression bars were placed. The stirrup ratio in Series IV was 0.32% and 0.30% for the test shear span. The smaller stirrup spacing was provided in another shear span as shown in **Figs. 4.5(a)** and **4.5(c)** in order to control the failure side. **Figure 4.6** shows formworks of the specimens.

4.6 Test Setup and Instrumentation

Figure 4.7 presents the specimen under loading. Specimens were subjected to a four-point bending. Specimens were placed on the roller supports. Teflon sheets and grease were inserted between a specimen and supports in order to prevent the horizontal friction. The locations of loading and supporting points are illustrated in **Fig. 4.5**. The loads were applied to the beams by steel plates to decrease stress concentration. The steel plates with 65 mm width and 150 mm long were used at loading points, and the steel plates with 50 mm width were placed at the supports. Plates with the same size were used in all specimens in Series I, II and III. However, the size of the steel plates varied in Series IV corresponding to the length of beams. For SF30-10-r32-S, the steel plates with 48 mm width and 112.5 mm long were used as loading plates and the steel plates with 37.5 mm width and 115 mm long were used as

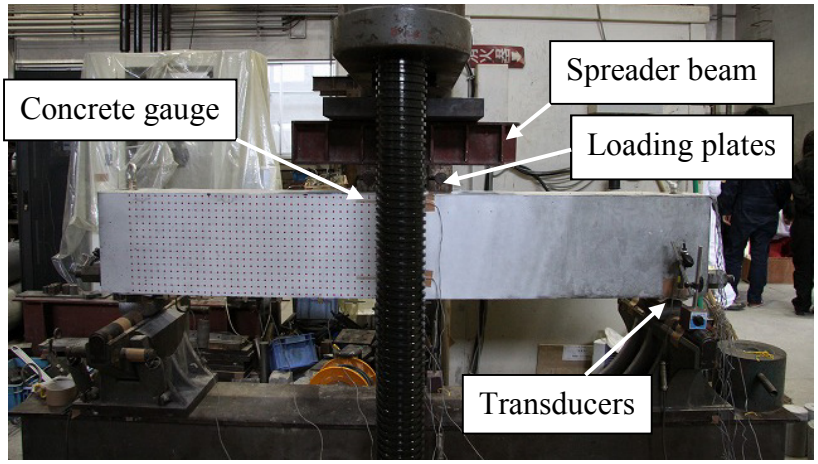

Figure 4.7 Specimen setup

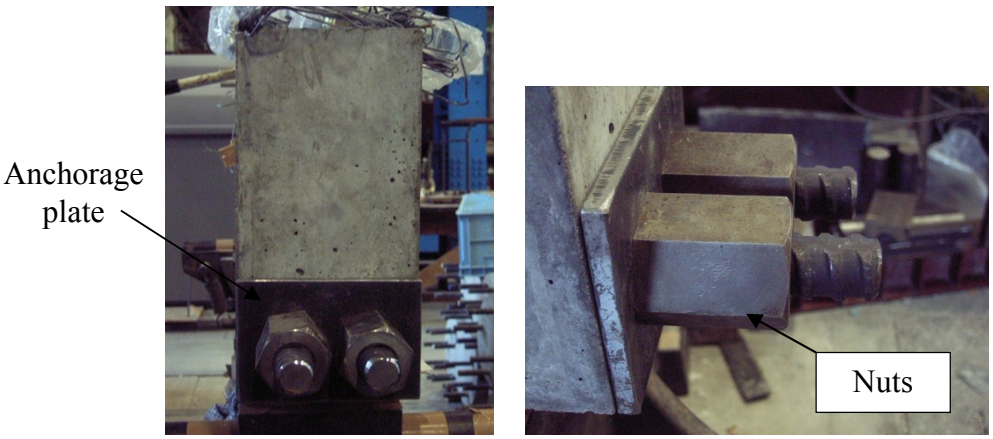

Figure 4.8 Prevention of anchorage failure

supporting plates. For larger specimen (SF30-10-r30-L), the steel plates with 96 mm width and 225 mm long were used as loading plates and the steel plates with 75 mm width and 225 mm long were used as supporting plates. The thickness of all steel plates was 30 mm. Moreover, anchor plates and nuts were used to ensure the sufficient anchorage of the tensile bars and prevent anchorage failure as shown in **Fig. 4.8**.

Displacement transducers and strain gauges were installed to record the deformation and strains of specimens. The locations of transducers were at the supporting points and mid-span. The electrical strain gauge was attached on concrete surface at the depth of longitudinal compression bar. One strain gauge was placed on longitudinal tensile bar at mid-span. The strain of stirrups was measured at the region where the diagonal crack was expected to occur as shown in **Fig. 4.5**.

4.7 Measuring Items

4.7.1 General measuring items

During the loading test, the test specimen was monitored by measuring the applied load. Mid-span deflection was measured by using the transducers. The strain of longitudinal reinforcement bars and stirrups were recorded.

4.7.2 Crack surface displacement using the image analysis

This research focuses on the tensile force transferring across the diagonal crack. The tensile force will decrease with the increase in width of the crack. Therefore, the results of crack surface displacement are needed. In order to measure crack surface displacement of specimens, the image analysis was conducted. Higashi et al. (2009) have developed the real-time image analyzing system for measuring deformation, crack surface displacement and strain generated on the surface of specimens. The procedures of image analysis and calculation method of crack surface displacement are explained in this section.

(1) The procedure of the image analysis

In order to conduct the image analysis, three cameras were setup for taking photos of specimens as presented in **Fig. 4.9(a)**. White color was sprayed on the surface of specimens. Red targets with diameter of 5-mm were attached on the specimen surface with an interval of

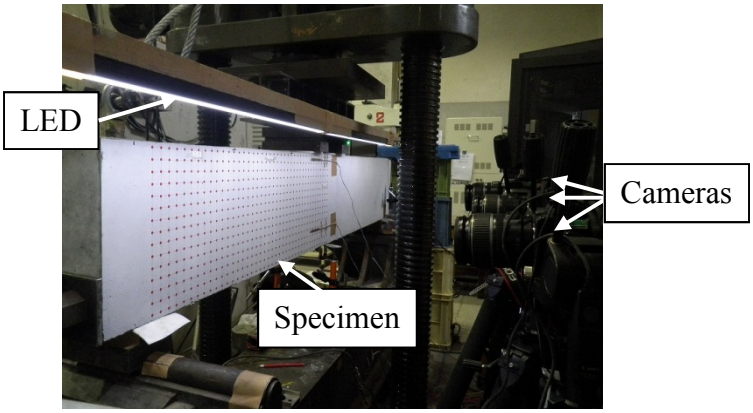

(a) Cameras and LED setups

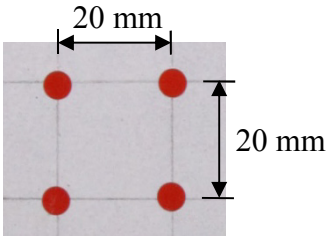

(b) Targets arrangement

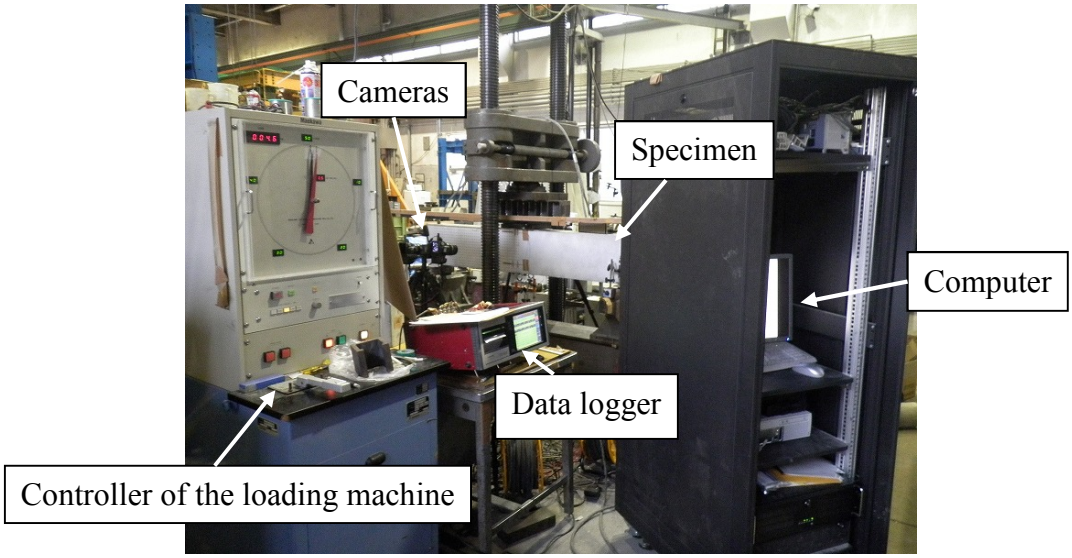

(c) Loading test of specimen with image analysis

Figure 4.9 Preparation for the image analysis

20 mm as shown in **Fig. 4.9(b)**. The purpose of these procedures was to distinguish targets from concrete surface. In order to remove the distortion of images and increase the accuracy of image analysis, the calibration process was conducted before starting the loading test. During the loading test, photos of the specimen were taken by every 5 kN of the shear force by using the digital cameras fixed on tripods. The white light-emitting diodes (LED) were also used for increasing the accuracy of image analysis. A picture of loading test is shown in **Fig. 4.9(c)**. The coordinates of targets were investigated by the image analysis. In addition, nearly the peak load, the photographs were captured with short time intervals to capture the exact behavior at the peak. The image analysis system can investigate the coordinates of the red targets throughout the test span.

(2) Calculation of the crack surface displacement and the angle of principal tensile strain

Crack surface displacement (u) and the angle of principal tensile strain (β) were calculated by using the displacements of targets obtained from the image analysis system developed by Higashi et al. (2009). Crack surface displacement (u) is defined as the total displacement of cracks in the direction of principal tensile strain (β), which is the direction of the crack's movement as shown in **Fig. 4.10**. The crack surface displacement consists of the displacements from opening and sliding (**Fig. 4.10**). The crack opening displacement is the crack width perpendicular to crack surface, while sliding displacement is the displacement in the tangential direction.

The calculation procedure of u is shown in **Fig. 4.11**. First, the displacements of the targets in x and y directions are examined. The displacements of targets are the difference of coordinate of targets between first photo and latter photos. Second, the relative displacement between two targets that the crack passed (Δx, Δy) (**Fig. 4.11(a)**) is calculated by using Eq. (4.1) and Eq. (4.2).

$$\Delta x = \Delta x_1 - \Delta x_2 \tag{4.1}$$

$$\Delta y = \Delta y_1 - \Delta y_2 \tag{4.2}$$

where, Δx is the relative displacement in x direction, Δy is the relative displacement in y direction, (Δx_1, Δx_2) is the displacement of targets in x direction and (Δy_1, Δy_2) is the displacement of targets in y direction.

Third, the angle of principal tensile strain (β) is calculated at the center of square that the crack passed (**Fig. 4.11(b)**) by using Eq. (4.3).

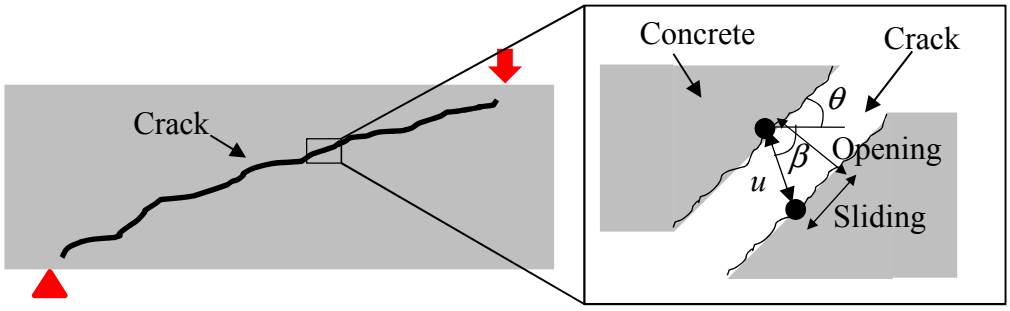

Figure 4.10 Definition of crack surface displacement (u)

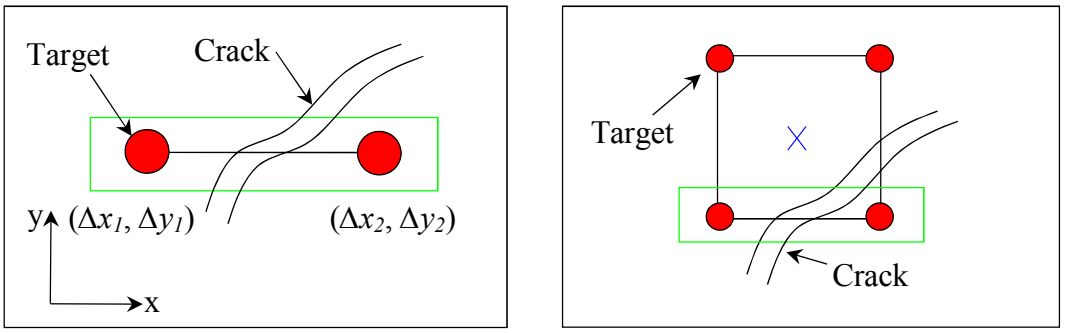

(a) Two targets that crack passed

(b) The square that crack passed

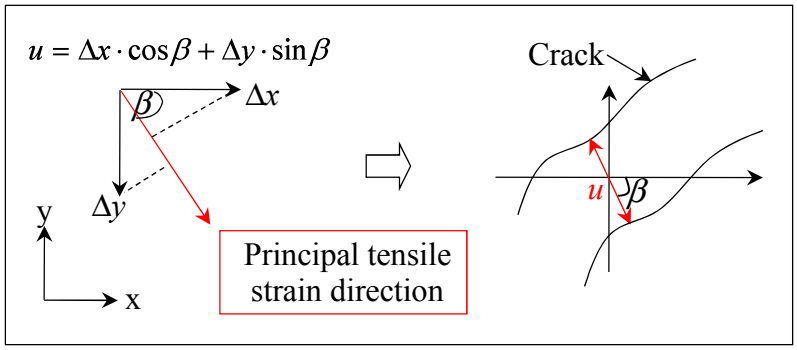

(c) Crack surface displacement (u)

Figure 4.11 Calculation of crack surface displacement

$$\beta = 0.5\tan^{-1}\left\{\frac{\gamma_{xy}}{(\varepsilon_x - \varepsilon_y)}\right\} \tag{4.3}$$

where, β is the angle of principal tensile strain, γ_{xy} is the shear strain, ε_x is the strain of x-axis and ε_y is the strain of y-axis.

Meshing geometry is given based on the targets and displacements of the targets are transformed to the strain of the layer by using the shape function of finite element method. The values of ε_x, ε_y and γ_{xy} in Eq. (4.3) are measured by the image analysis. Finally, the crack surface displacements on the direction of principal tensile strain, u, are determined by Eq. (4.4) as shown in **Fig. 4.11(c)**.

$$u = \Delta x \cdot \cos\beta + \Delta y \cdot \sin\beta \tag{4.4}$$

where, u is crack surface displacement (mm)

Watanabe et al. (2010a) concluded that there was less than 0.03 mm in gap between the displacement measured from π gauge and from the image analysis. This variation was insignificant. Furthermore, β was calculated from the displacement of nodal points of which error was slight; therefore, the variation of β was negligible.

4.7.3 Length and angle of diagonal crack

The length (L) and angle of diagonal crack (θ) were measured from the visible diagonal crack at the peak load by using the image processing system software. The image processing system software supports the analytical functions from image measurement to statistical data processing. The calibration process was conducted to define the length of one pixel in the image for the purpose that the measurement data (in pixel) can be converted to the actual length. Therefore, the program can measure the length and angle of crack from the pictures. The images taken for the image analysis for measuring the crack surface displacements were also used to measure the diagonal crack length and angle of diagonal crack at the peak load. **Figure 4.12** presents measurement of length and angle of diagonal crack of one layer using the program.

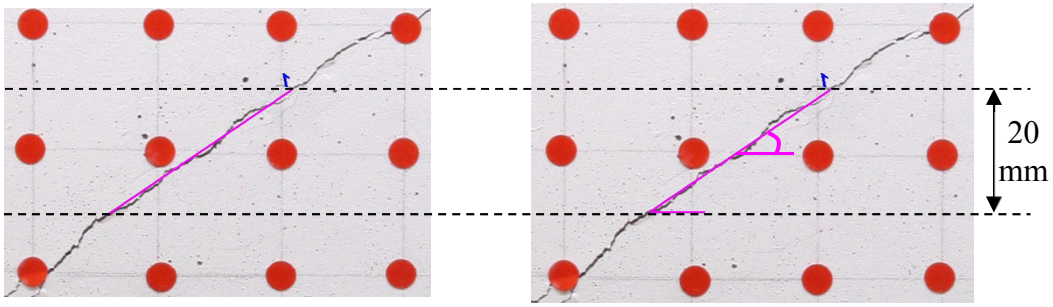

(a) Length (b) Angle

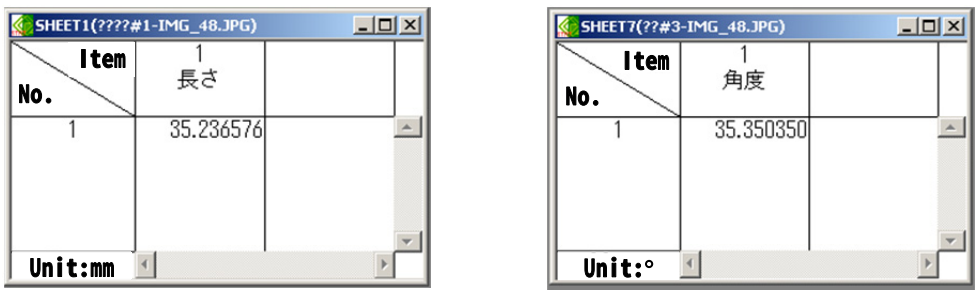

(c) Result of length (d) Result of angle

Figure 4.12 Measurement of length and angle of diagonal crack

CHAPTER 5

SHEAR BEHAVIOR OF FIBER REINFORCED CONCRETE BEAMS

5.1 Introduction

Seventeen FRC beams with different fiber volume fractions, stirrup ratios, types of fibers and specimen sizes were tested following the outline of experiment described in **Chapter 4**. The experimental results of all specimens and the calculation procedures of the shear forces are presented in this chapter. The experimental value of shear carried by fibers (V_f) was calculated based on the principle of superposition. The effects of volume fraction of fibers, stirrup ratios, types of fibers and sizes of specimen on shear capacity and shear carried by fibers of FRC beams are discussed. To clarify the failure mechanism of FRC beams, the image analysis was performed. Influence of the four parameters on diagonal cracking behavior of FRC beams is examined in terms of crack length, crack surface displacement and angle of diagonal crack.

5.2 Calculation of Shear Forces

Considering the free body diagram of a part of the shear span of a FRC beam subjected to point load (**Fig. 5.1**), the equilibrium in the vertical and horizontal directions can be expressed respectively as follows:

$$V = V_c + V_s + V_f \tag{5.1}$$

$$T + H_f = C' \tag{5.2}$$

where, V is the shear capacity of FRC beams, V_c is the shear capacity of members without shear reinforcement, V_s is the shear carried by stirrups, V_f is the shear carried by fibers, T is

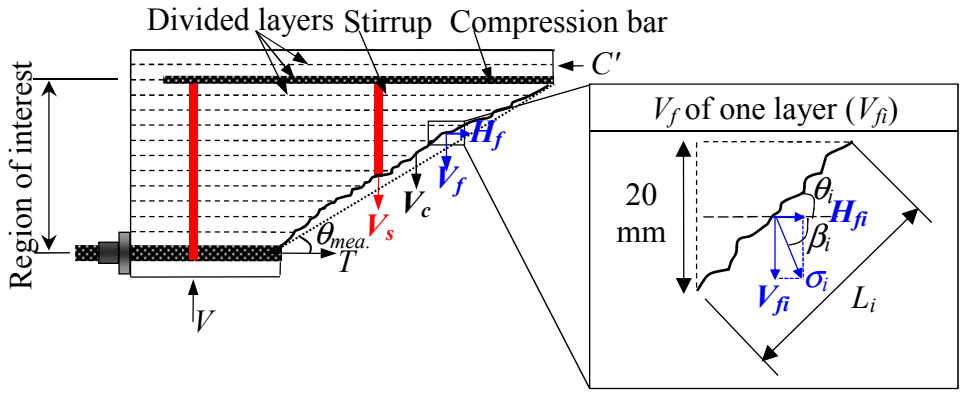

Figure 5.1 Free body diagram of a FRC beam

the horizontal tension, H_f is the horizontal component of force carried by fibers and C' is the horizontal compression.

The equilibrium in vertical direction is discussed from this section. The value of V_c was calculated from Eq. (5.3) following the JSCE design guidelines (1999). The shear carried by stirrups (V_s) was calculated from the modified truss analogy as shown in Eq. (5.4).

$$V_c = 0.2 \cdot \sqrt[3]{f_c'} \cdot \sqrt[4]{1000 / d} \cdot \sqrt[3]{100\, p_w} \cdot b_w \cdot d \tag{5.3}$$

$$V_s = A_w f_{wy} \left(z \cot \theta / s \right) \tag{5.4}$$

where, f'_c is the compressive strength of the concrete (MPa), d is effective depth (mm), p_w is longitudinal reinforcement ratio ($=A_s/b_w d$), b_w is web thickness (mm), s is stirrup spacing (mm), A_w is the total cross-sectional area of stirrups provided in the range of s (mm^2), f_{wy} is the yield strength of stirrups (MPa), z is distance from the location of compressive stress resultant to the centroid of tension steel ($z = 7d/8$) (mm) and θ is angle between the diagonal crack and horizontal line measured from the observed diagonal crack ($=\theta_{mea.}$) (degree).

The equation of V_c was originally formulated from RC beams without shear reinforcements. Nonetheless, as well as the modified truss analogy, Eq. (5.3) was applied for investigating the shear capacity of FRC beams with stirrups. The crack surface displacement of FRC beams with stirrups is in the applicable range of Eq. (5.3) because the crack surface displacements of FRC beams with stirrups are smaller than those of ordinary RC beams without any shear reinforcement.

The definition of V_f in this study is the shear capacity subtracting by V_c (Eq. (5.3)) and V_s (Eq. (5.4)). The experimental value of shear carried by fibers (V_{fexp}) can be obtained from Eq. (5.5).

$$V_{fexp} = V_{exp} - V_c - V_s \tag{5.5}$$

where, V_{exp} is the shear capacity from the experiment.

According to the JSCE design guidelines (1999), the shear capacity of FRC members can be predicted by using Eq. (5.6). The experimental value of κ(= κ_{exp}) can be calculated by Eq. (5.7). Nevertheless, Eq. (5.6) was proposed only for steel fiber reinforced concrete members having 1.0–1.5% fiber out of full concrete volume.

$$V_{JSCE} = (1 + \kappa) \cdot V_c + V_s \tag{5.6}$$

$$\kappa_{exp} = \frac{V_{exp} - V_c - V_s}{V_c} = \frac{V_{fexp}}{V_c} \tag{5.7}$$

where, V_{JSCE} is the predicted shear capacity from the JSCE equation and κ is the coefficient representing the effect of fibers (κ= 1.0) (JSCE design guidelines, 1999).

5.3 General Behavior and Load-Deflection Relationships of FRC Beams

The shear behavior of seventeen FRC specimens is discussed from this section. **Figure 5.2** presents the load-mid span deflection relationships of FRC beams obtained from the experiment. These diagrams show clearly that shape of the load-deflection curves of the corresponding beams is basically similar in all specimens. The load-versus-deflection response exhibited the linear relation up to the first flexural crack. After the first flexural crack, the curve still increased linearly until the initiation of the diagonal crack occurred in a shear span. The formation of the diagonal crack; however, did not mark the failure of FRC beams. The diagonal crack was observed around the middle height of the specimens. After the initiation of the diagonal crack, the diagonal crack propagated to supports and to the top of specimens. The appearance of the diagonal crack reduced the slope of load-deflection curves of FRC beams. Most of the stirrups, which the diagonal crack passed, showed the yielding strain in this stage. The propagation of the diagonal crack length was slow and stopped when the diagonal crack reached the compression zone, where was the position of neutral axis.

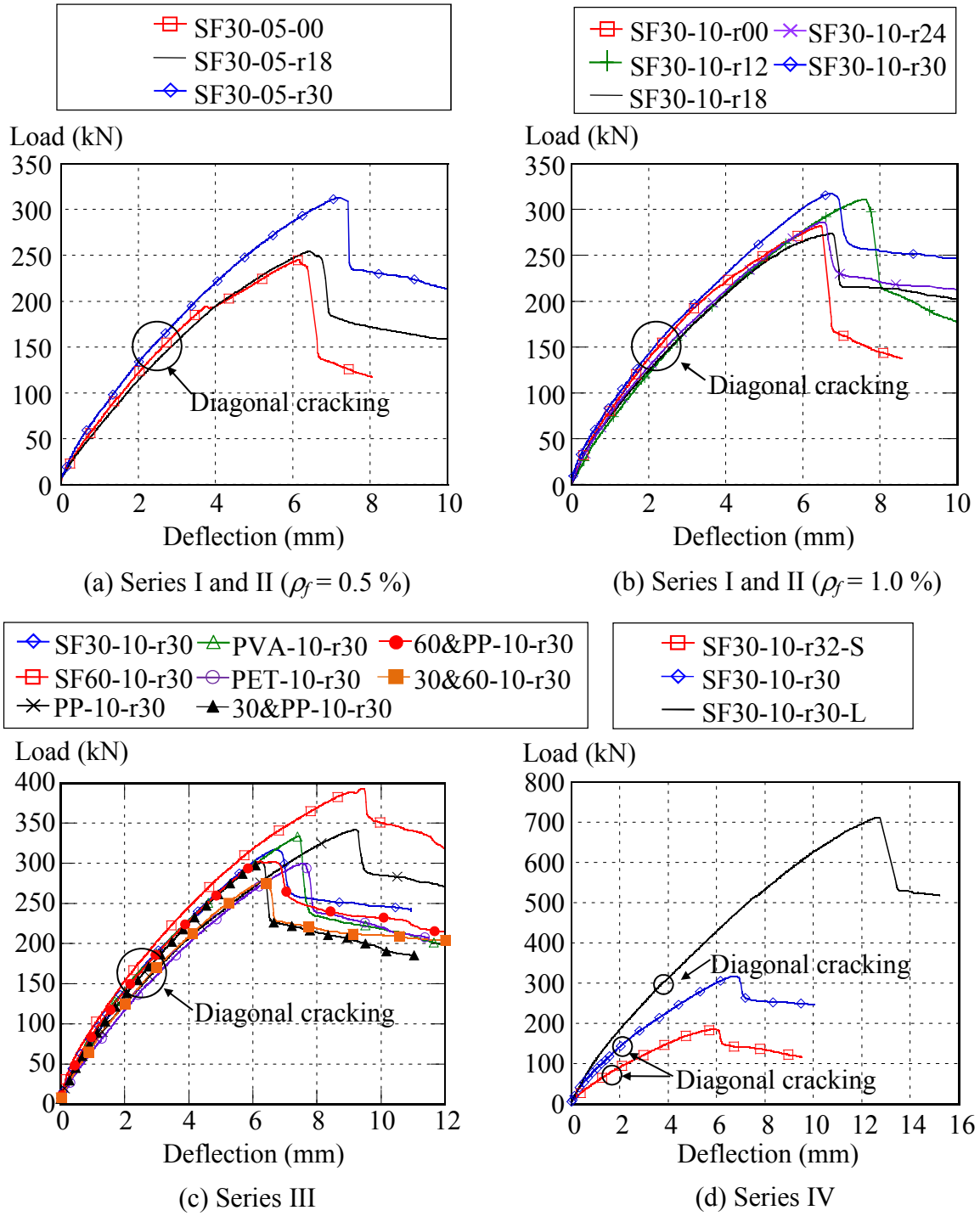

Figure 5.2 Load-deflection curves of FRC beams

From this stage, the rate of load increment became slight and the load-deflection curves showed nonlinear behavior. The stirrups and fibers continued to carry the load until the crushing of concrete, which was the ultimate stage. Crushing was observed above the location of compression bars, where was compression zone. All tested beams failed in shear as

indicated by the sudden drop in the load-deflection curves followed by a complete loss of load carrying capacity.

5.4 Shear Capacity and Shear Carried by Fibers Observed in the Experiment

The concrete properties, information regarding diagonal cracks and experimental results of shear forces are summarized in **Table 5.1**. The values of V_c, V_s, V_{fexp} and κ_{exp} were calculated from Eqs. (5.3), (5.4), (5.5) and (5.7). In most of specimens with steel fibers, the shear capacity of FRC beams from the experiment (V_{exp}) was higher than the calculated value obtained from Eq. (5.6), which is the existing equation for predicting the shear capacity of FRC beams proposed by JSCE design guidelines (1999). As a result, κ_{exp} was more than 1.00 except in SF30-05-r18 and SF30-05-r30. However, κ_{exp} of specimens with synthetic fibers did not reach 1.00. κ_{exp} was varied from 0.78 to 1.68.

The values of V_c for specimens in Series I-III were slightly different because of the difference of compressive strength of concrete. On the other hand, V_s showed the variation due to the deviation from the angle between the diagonal crack and horizontal line ($\theta_{mea.}$). $\theta_{mea.}$ was measured as the angle between horizontal line and the linear line that connected the points that the diagonal crack passed the locations of longitudinal bar and compression bar as shown in **Fig. 5.1**. The values of $\theta_{mea.}$ are given in **Table 5.1**. The specimens consisting of steel fibers (i.e. steel fibers and hybrid fibers) and high stirrup ratio provided steep $\theta_{mea.}$. As a result, V_s of those specimens was lower when compared with the specimens with synthetic fibers or no stirrups. Stirrups that the diagonal crack passed were yielded before the ultimate load. **Figure 5.3** shows the average strain of stirrups in the test span.

5.4.1 Effect of fiber volume fraction (Series I)

Eight FRC beams (Series I and II) were tested with a viewing of investigating the influences of fiber volume fraction (ρ_f) and stirrup ratio (r_w). **Figure 5.4** shows the effects of ρ_f and r_w on the shear capacity (V_{exp}). The shear capacity consists of V_c, V_s and V_{fexp}. **Figure 5.5** illustrates the shear contributions of specimens in Series I and II. **Figure 5.6** presents the effects of ρ_f and r_w on the shear carried by fibers of FRC beams (V_{fexp}).

Table 5.1 Summary of the calculation and experimental results of FRC beams

Specimen	Concrete properties			Results of diagonal crack					Experimental results				
	f'_c (MPa)	f_t (MPa)	G_F (N/mm)	u (mm)	L (mm)	β (°)	θ (°)	$\theta_{mea.}$ (°)	V_{exp} (kN)	V_c (kN)	V_s (kN)	V_{fexp} (kN)	κ_{exp}
SF30-05-r00	54.1	2.8	2.71	1.40	660	64.4	29.7	23.5	122.4	55.9	0.00	66.5	1.19
SF30-05-r18	45.0	2.6	2.71	0.69	488	63.2	35.8	39.8	126.9	52.6	24.0	50.4	0.96
SF30-05-r30	59.3	3.2	2.71	1.25	582	63.9	33.0	37.9	156.5	57.6	42.8	56.2	0.98
SF30-10-r00	64.9	3.9	4.24	1.54	539	66.9	27.9	22.2	141.1	59.4	0.00	81.7	1.38
SF30-10-r12	53.0	3.9	4.24	1.12	493	62.5	33.4	31.5	155.5	55.5	21.0	79.1	1.43
SF30-10-r18	46.6	3.5	4.24	1.10	422	62.4	35.1	36.0	136.8	53.2	26.6	57.0	1.07
SF30-10-r24	48.3	3.3	4.24	0.94	439	63.1	34.0	39.1	143.1	53.8	31.7	57.6	1.07
SF30-10-r30	55.3	3.0	4.24	0.67	387	63.3	34.0	36.8	158.8	56.3	43.0	59.5	1.06
SF60-10-r30	61.9	3.7	8.82	1.08	378	64.6	41.6	38.2	196.3	58.4	39.6	98.3	1.68
PP-10-r30	57.0	3.1	3.02	0.94	428	69.2	32.2	27.5	170.8	56.9	59.8	54.1	0.95
PVA-10-r30	65.4	3.0	2.34	0.69	491	63.7	27.8	27.0	166.8	59.5	61.1	46.1	0.78
PET-10-r30	51.8	3.0	2.89	0.62	427	64.8	26.5	31.0	149.9	55.1	51.9	43.0	0.78
30&PP-10-r30	52.2	2.7	3.27	0.59	388	61.9	34.8	33.0	151.2	55.2	50.0	46.1	0.83
60&PP-10-r30	49.2	3.4	7.49	0.55	333	57.3	42.1	39.0	151.3	54.1	40.1	57.2	1.06
30&60-10-r30	40.2	2.3	7.50	0.65	354	56.8	46.9	45.7	138.7	50.6	31.7	56.4	1.11
SF30-10-r32-S	52.0	3.4	4.24	0.62	293	61.8	35.5	38.7	92.4	33.4	24.9	34.1	1.02
SF30-10-r30-L	55.9	3.0	4.24	1.56	670	64.2	40.1	38.8	356.0	110.6	107.9	137.6	1.24

f'_c and f_t were measured from specimens prepared together with FRC beams, G_F: fracture energy from notched beam tests, u: average crack surface displacement at the peak, L: total crack length at the peak, β: average angle of principal tensile strain at the peak, θ: average angle of diagonal crack at the peak and $\theta_{mea.}$: measured angle between the diagonal crack and horizontal line.

Among the specimens in Series I and II, V_{exp} showed the maximum value in SF30-10-r30 (**Fig. 5.4**), while the maximum value of V_{fexp} was observed in SF30-10-r00 (**Fig. 5.6**). The influence of fiber volume fraction can be investigated by comparing V_{exp} and V_{fexp} of specimens with various ρ_f but same r_w. **Figures 5.5(a)**, **(b)** and **(c)** present the shear contributions of specimens having different ρ_f. The stirrup ratios in **Fig. 5.5** are 0.0%, 0.18% and 0.3%, respectively. Even though compressive strength of concrete was slightly different due to the variation of the tests, the difference in V_c was insignificant when compared the effect of fiber volume in each case of r_w as seen in **Figs. 5.5(a)**, **(b)** and **(c)**. It was found that the increase in

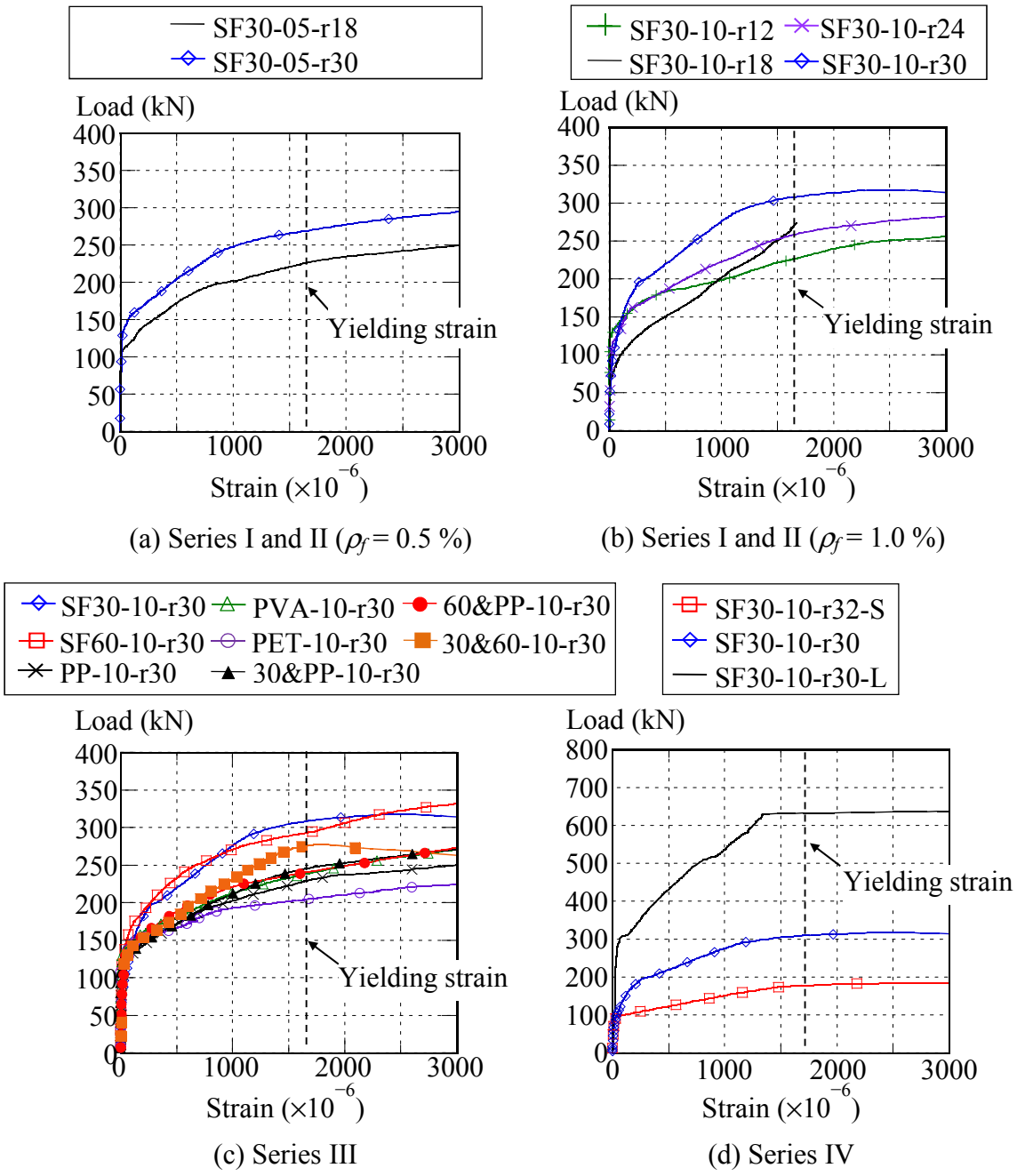

Figure 5.3 Stirrup strain

ρ_f from 0.5 to 1.0% enhanced the values of V_{exp} and V_{fexp}. V_{exp} increased 15, 8, 1% in the beams which r_w = 0.0, 0.18, 0.30%, respectively. Besides, the increase in V_{fexp} was 23, 13, 6% in specimens having r_w = 0.0, 0.18, 0.30% as observed in **Fig. 5.6**. The increase of V_{fexp} is because the more stress can transfer across diagonal crack when fiber volume fraction increased. The increase of V_{exp} and V_{fexp} due to the effect of ρ_f, however, became less significant with the increase in r_w. This implies that the effect of fibers as shear reinforcement is dominant in case of smaller r_w.

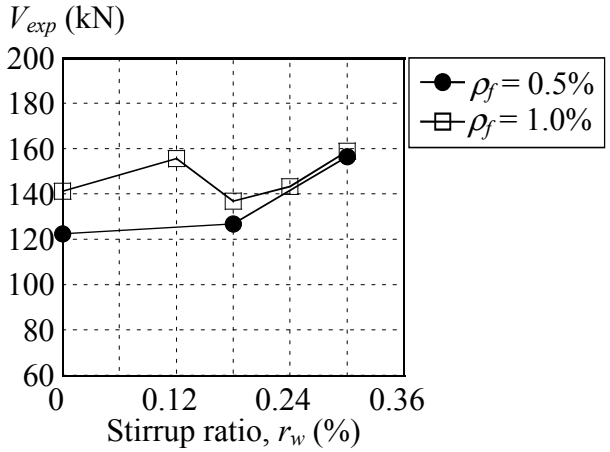

Figure 5.4 Effect of ρ_f and r_w on V_{exp}

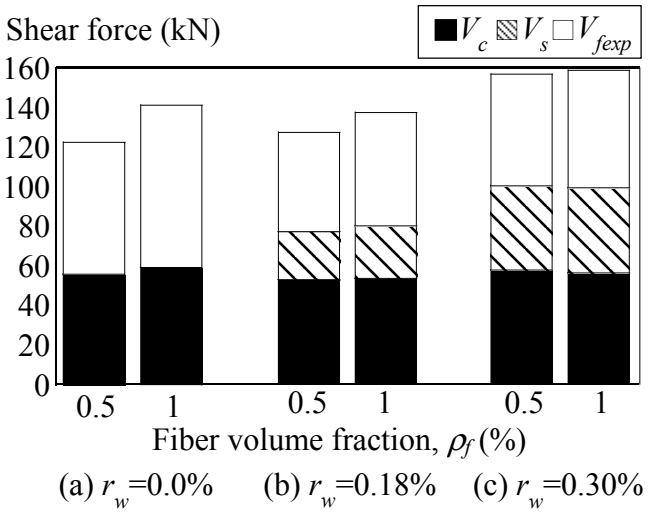

Figure 5.5 Shear contributions in FRC beams (Series I and II)

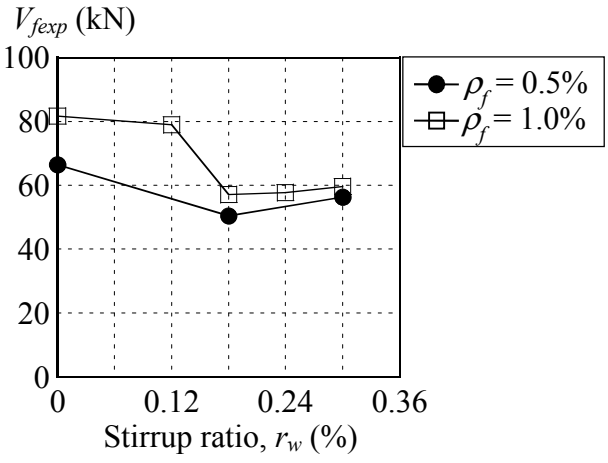

Figure 5.6 Effect of ρ_f and r_w on V_{fexp}

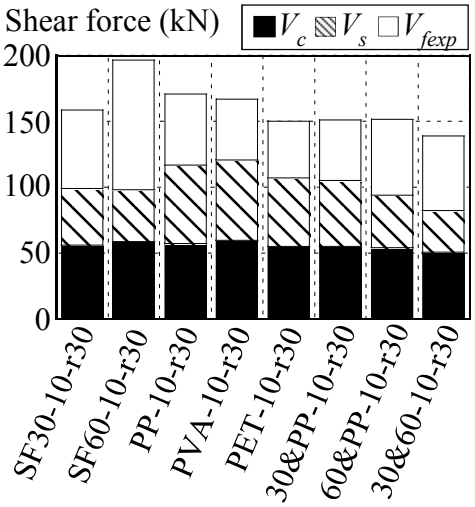

Figure 5.7 Shear contributions in FRC beams (Series III)

5.4.2 Effect of stirrup ratio (Series II)

Influence of stirrup ratio can be discussed from **Figs. 5.4**, **5.5** and **5.6**. In contrast with the effect of volume fraction of fibers, beams with the same ρ_f but different r_w showed another tendency. The value of V_{exp} in FRC beams did not necessarily increase with the increase in r_w as shown in **Fig. 5.4**. Although V_s increased with the increase in r_w (**Fig. 5.5**), V_{fexp} tended to reduce (**Fig. 5.6**). The effect of fibers to increase the shear carried by fibers was dominant in case of low stirrup ratio. Because of the opposite tendency, the shear capacity of FRC beams with stirrups did not monotonically increase with the increase in stirrup ratio. This confirmed that there was an optimized combination of fiber volume fraction and stirrup ratio to increase the shear capacity of FRC beams.

With the increase in r_w, the shear carried by fibers decreased because the diagonal crack length became shorter. Thus, the stress-transferred area reduced. Nonetheless, the increasing of r_w led the smaller crack surface displacement. Therefore, more stress transferred across the crack. This behavior improved V_{fexp}. Due to these positive and negative effects, among the specimens having ρ_f =1.0% but various r_w, the value of V_{fexp} showed the maximum value in SF30-10-r00 and the minimum value in SF30-10-r18. It is noted that the results of diagonal crack length and crack surface displacement will be shown and discussed later.

5.4.3 Effect of fiber types (Series III)

Among all specimens in Series III, the FRC beam with 60-mm steel fibers (SF60-10-r30) revealed the highest shear capacity (V_{exp}). By considering specimens with synthetic fibers, PP-10-r30 provided the highest V_{exp} than PVA-10-r30 and PET-10-r30. Nevertheless, V_{exp} of hybrid specimens was relatively low. It is because the low f'_c in those beams. The shear contributions of concrete, stirrups and fibers are plotted in **Fig. 5.7**. The experimental result of shear carried by fibers (V_{fexp}) of SF60-10-r30 was the greatest as observed in **Fig. 5.7**, thereby resulting in the largest shear capacity. The specimens including steel fibers showed higher V_{fexp} than synthetic fibers except 30&PP-10-r30. In addition, V_{fexp} increased with the increase in fiber length from 30 to 60 mm. In case that enough anchorage and bond are provided, steel fibers are the most effective to enhance the shear carried by fibers. It is because steel fibers have high tensile strength and elastic modulus. Furthermore, based on the experimental results, steel fibers with 60 mm length showed the best performance among all fiber types. The

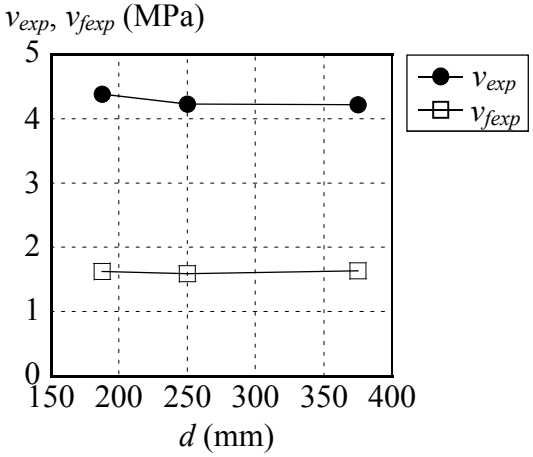

Figure 5.8 Size effect

superior performance of 60-mm steel fibers came from the best post peak behavior in tension (explained in **Chapter 3**).

5.4.4 Effect of effective depth (Series IV)

The influence of specimen size is discussed based on the results of specimens in Series IV. The shear strength of FRC beams (v_{exp}) and the contribution of shear stress due to fibers (v_{fexp}) are given by Eqs. (5.8) and (5.9), respectively.

$$v_{exp} = \frac{V_{exp}}{b_w \cdot d} \tag{5.8}$$

$$v_{fexp} = \frac{V_{fexp}}{b_w \cdot d} = \frac{V_{exp} - V_c - V_s}{b_w \cdot d} \tag{5.9}$$

Figure 5.8 shows results of v_{exp} and v_{fexp}. Although V_{exp} increased with the increase in the specimen size, v_{exp} slightly decreased. It can be concluded that the size effect in FRC beams was very slight when effective depth (d) was in the range from 187.5 to 375 mm. Furthermore, the difference in the shear stress carried by fibers (v_{fexp}) was insignificant as presented in **Fig. 5.8**; hence, there was no size effect on the shear carried by fibers in case of $187.5 \leq d \leq 375$ mm. The reason why the average shear stress transferred across the crack did not decrease in the larger specimen is that the ratio of diagonal crack length to effective depth also increased in the larger specimen (discussed later). This provides the larger crack surface area that the stress can transfer.

5.5 Flexure Cracking Behavior

For all of beams, the flexural cracks were observed in early stage of loading. For all investigated beams in Series I, II and III, the first flexural crack appeared at the similar load level. However, with the difference in the specimen size, the first flexural crack occurred earlier in smaller specimen (SF30-10-r32-S) and later in specimen with larger size (SF30-10-r30-L). Then, cracks propagated to the top of specimens with the increase in the load. **Figure 5.9** presents crack patterns after loading test of the specimens in Series IV. Pictures of the specimens after loading tests are shown in **Appendix**.

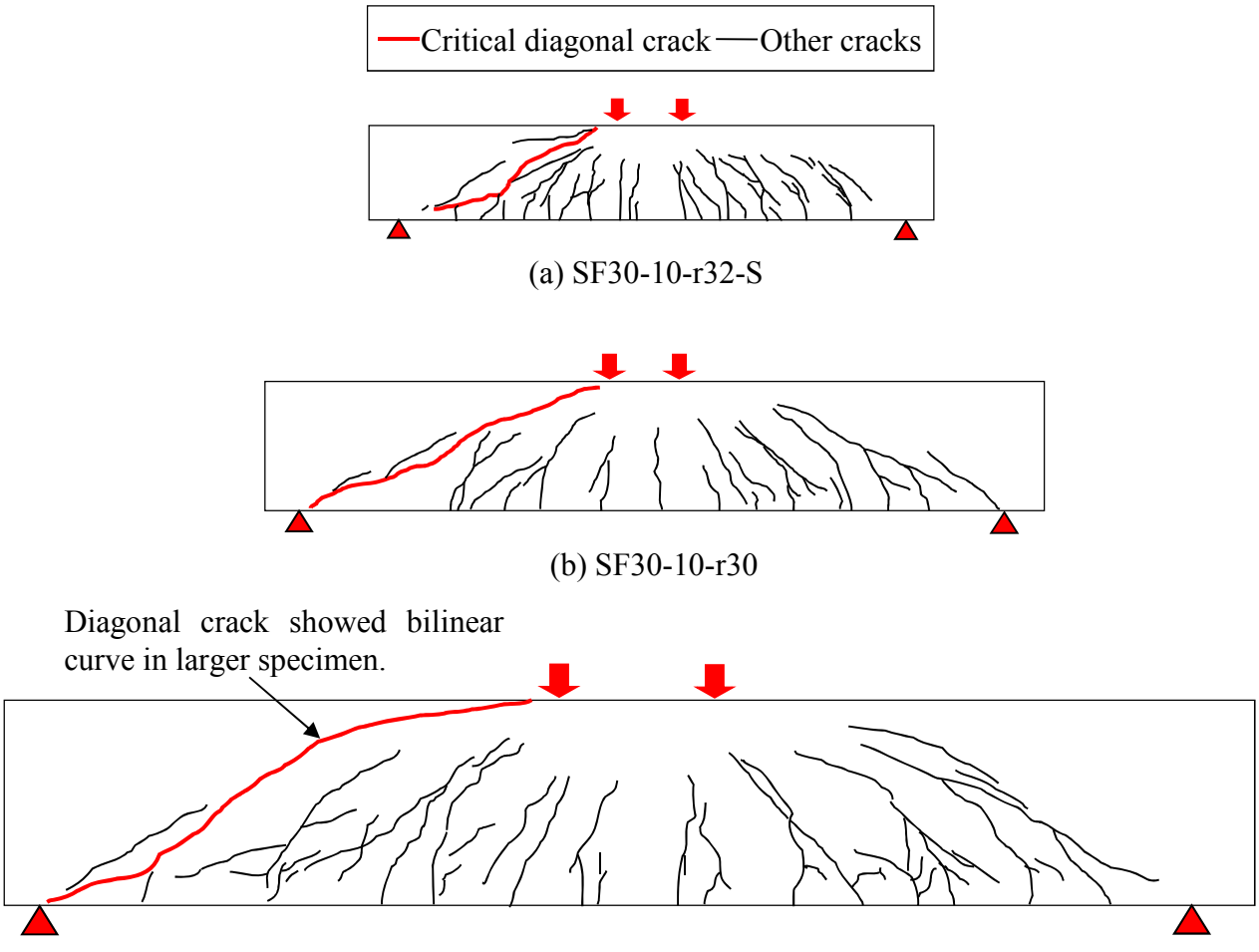

Figure 5.9 Crack patterns after failure

5.6 Diagonal Cracking Behavior

This research focuses on the diagonal crack behavior to explain the shear resistance mechanism of FRC beams. **Figures 5.10-5.12** present the diagonal crack at the peak load corresponding to the image analysis side of specimens in Series I, II, III and IV, respectively. It is obvious that only one critical diagonal crack was remarkable in each specimen. The diagonal crack was not observed near the top and bottom fibers. This study focuses on the tensile force along this diagonal crack.

The image analysis was performed. The specimens were divided as many layers with a height of 20 mm corresponding to the interval of targets of the image analysis. The number of layers of the specimens in Series I, II and III was 15. In addition, there were 11 layers in SF30-10-r32-S and 21 layers in SF30-10-r30-L. However, the region of interest for calculating the shear carried by fibers is only some part as shown in **Fig. 5.10**. The region of interest for investigation of the shear carried by fibers is the part where fibers show their tensile performance. It is from the part below the compression zone to the tip of the diagonal crack in the tension zone. For the specimens in Series I to IV, the region of interest is the part between location of compression bars and tensile reinforcing bars. However, in the specimens with 0.5% of fibers, the diagonal crack propagated into the concrete cover zone and stopped at 30 mm from the bottom of specimen because of the less shear reinforcement. The region of interest of each series is shown in **Figs. 5.10-5.12**. The number of layers in the region of interest was 13 for specimens with 0.5% of fibers, 11 layers for specimens with 1.0% of fibers, 7 layers for SF30-10-r32-S and 16 layers for SF30-10-r30-L. The part above the region of interest is considered as the compression dominant zone. The shear carried by compression dominant zone is taken into account as a part of V_c. The pictures of specimens at the peak load were used to measure the diagonal cracking behavior of each layer (i.e. crack surface displacement (u_i), length of diagonal crack (L_i), angle of principal tensile strain (β_i) and angle of diagonal crack (θ_i)) (see **Fig. 5.1**). The results of these values are discussed in this section.

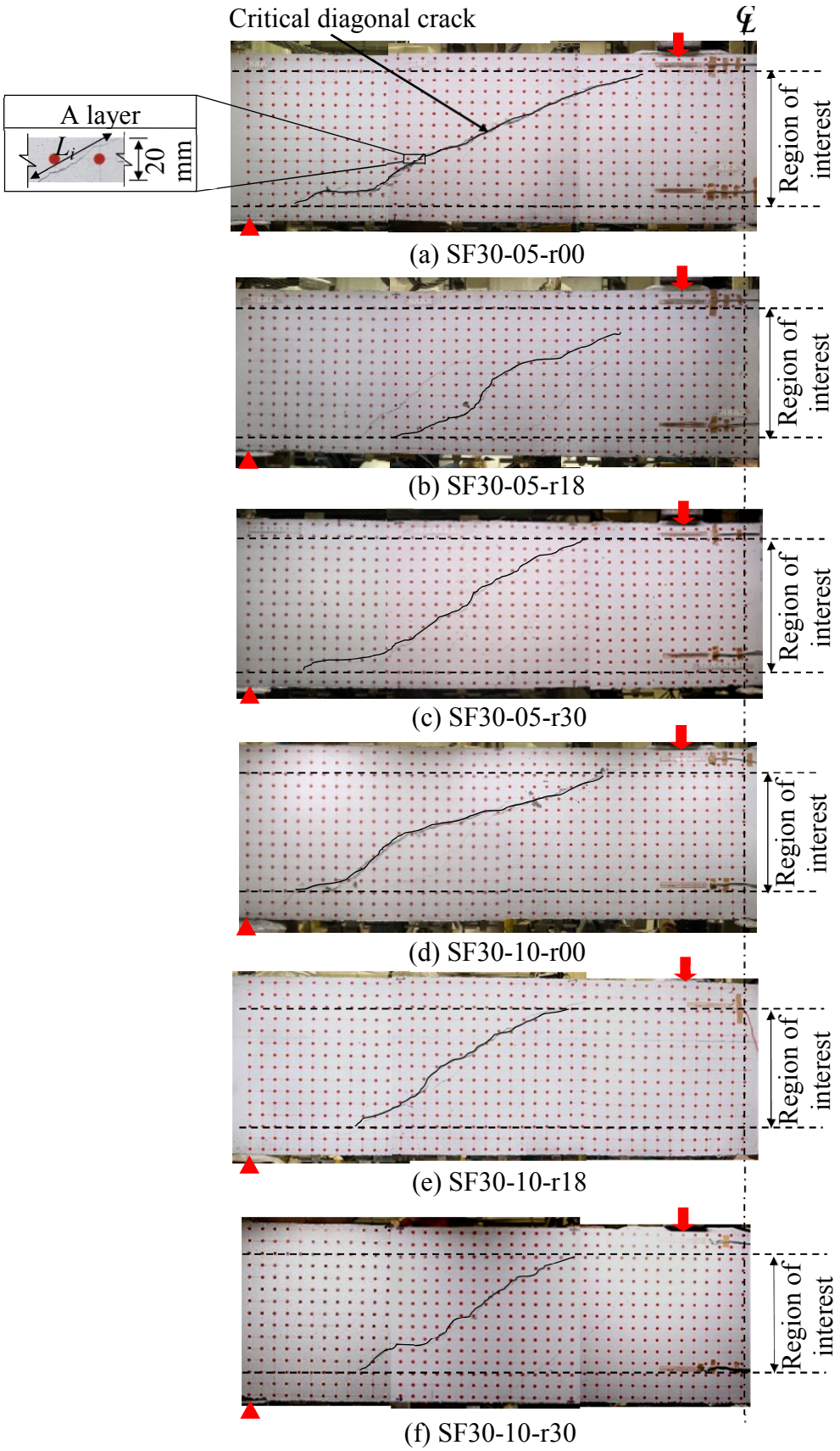

Figure 5.10 Critical diagonal crack at peak load of specimens in Series I and II

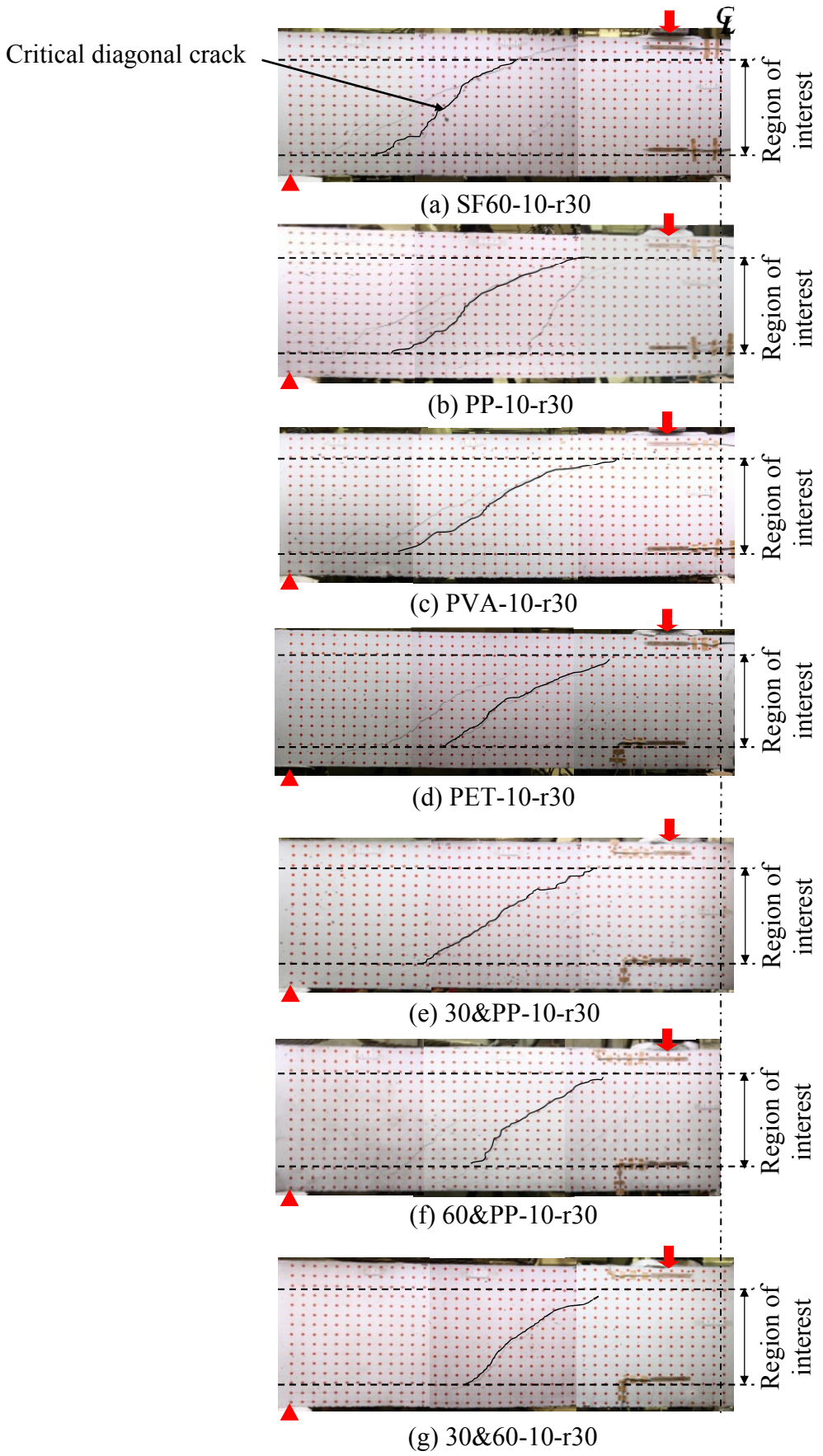

Figure 5.11 Critical diagonal crack at peak load of specimens in Series III

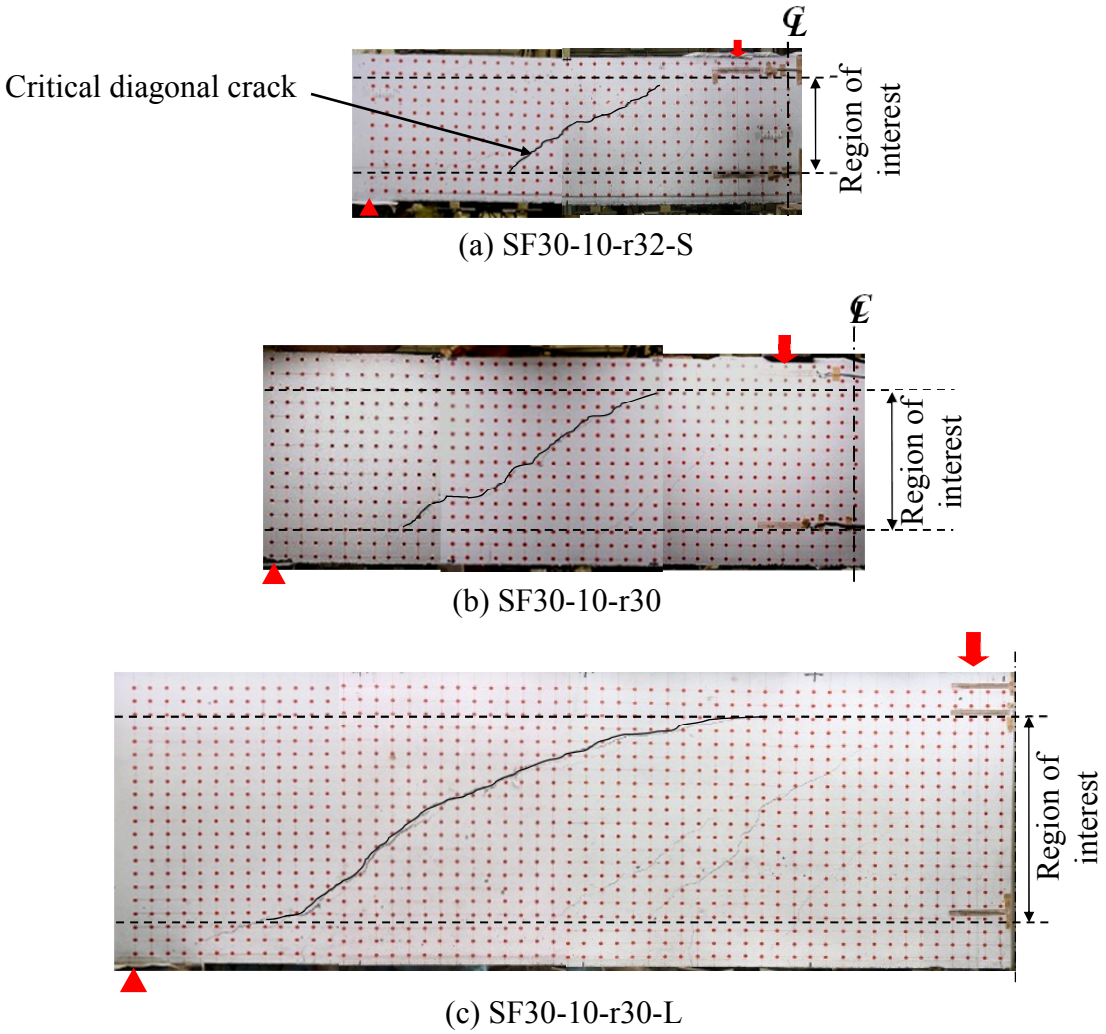

Figure 5.12 Critical diagonal crack at peak load of specimens in Series IV

5.6.1 Crack surface displacement

(1) Crack distribution along the beam depth

The definition of crack surface displacement was explained in Section 4.7.2. Crack surface displacement (u) is defined as the total displacement of cracks in the direction of principal tensile strain (β), which is the direction of the crack's movement. The crack surface displacement consists of the displacements from crack opening and crack sliding. The value of crack surface displacement of each layer (u_i) along the height of the diagonal crack at the peak load is shown in **Fig. 5.13**. Unlike flexure cracks, the diagonal crack displacement (u_i) was greater at approximately the middle height of specimens when compared with u_i at the top and the bottom of specimens because of the compression zone at the top of specimens and

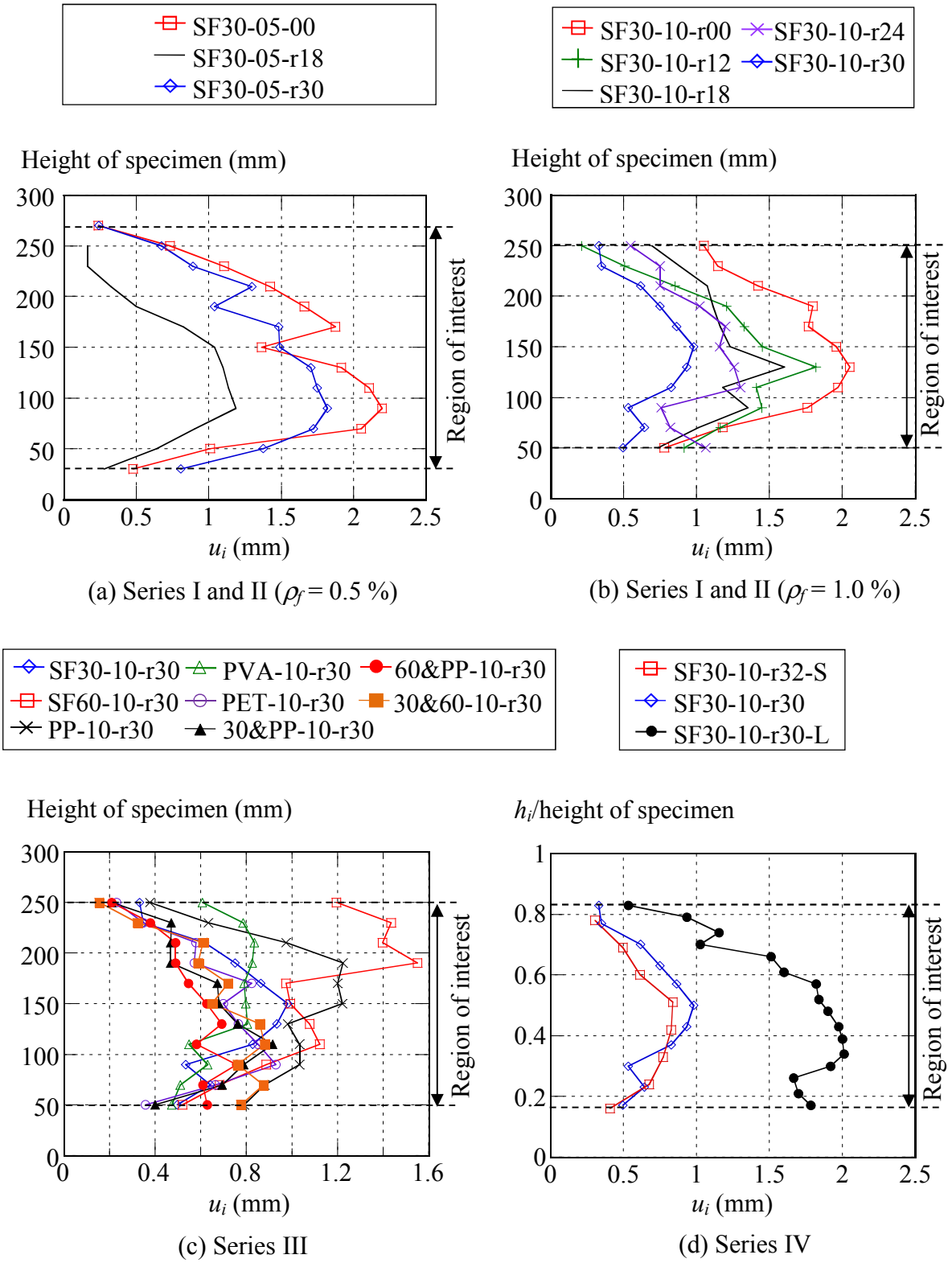

Figure 5.13 Distribution of crack surface displacement along the height of specimens at the peak load

restraint by longitudinal reinforcing bars at the bottom part of the specimens. u_i at the peak load was in the parabolic shape as observed in **Fig. 5.13**. The average values of u_i in the region of interest (u) are listed in **Table 5.1**.

Based on the experimental results of Series I and II, u tended to increase with the increase in ρ_f. On the other hand, u_{avg} tended to decrease with the increase in r_w. However, SF30-05-r30 showed different tendency. This tendency may come from the orientation of steel fibers in the specimen. Considering various types of fibers in Series III, u_i differed depending on the types of fibers. Clear tendency could not be observed. SF60-10-r30 revealed the widest u among all specimens. In order to consider effect of specimen size (Series IV) on crack surface displacement, the crack surface displacement distribution of the specimens in Series IV is plotted in **Fig. 5.13(d)**. The height of each layer (h_i) was normalized by the specimen's height and expressed as a ratio in Y-axis. The crack surface displacement was greater in the larger specimen. Nonetheless, the parabolic shape of distribution of u was also observed though the size of specimens was changed.

(2) Growth of crack surface displacement by loading

Figures 5.14 and **5.15** plot the crack surface displacement measured at the middle height of the specimens (u_{mid}) in the top horizontal axis, together with load-deflection curve. In addition, the values of $2V_c$ and $2(V_c + V_s)$ were indicated in the graphs. The diagonal crack was generated near the load corresponding to $2V_c$. After the initiation of the diagonal crack, the values of u_{mid} linearly increased with the load. Then, u_{mid} increased drastically before the peak load. This increase corresponded to the load when the load-deflection curve started exhibiting a nonlinear behavior. Therefore, the sudden increment in u_{mid} related to the peak and it led to the failure of FRC beams. The crack surface displacement at other heights also showed the same behavior. All fiber types show this behavior.

Since u at the peak load is a key to investigate the shear carried by fibers in this research, it is important to measure u at the peak load. Nevertheless, u increased drastically just before the peak load. Thus, some pictures were taken near the peak load with short time interval in order to capture behavior at the peak exactly. The picture at the peak load was compared with other pictures around the peak to confirm that the differences between the pictures were insignificant. As a result, the deviation from the difference of taken-time of the picture at the peak does not affect the discussion in this study.

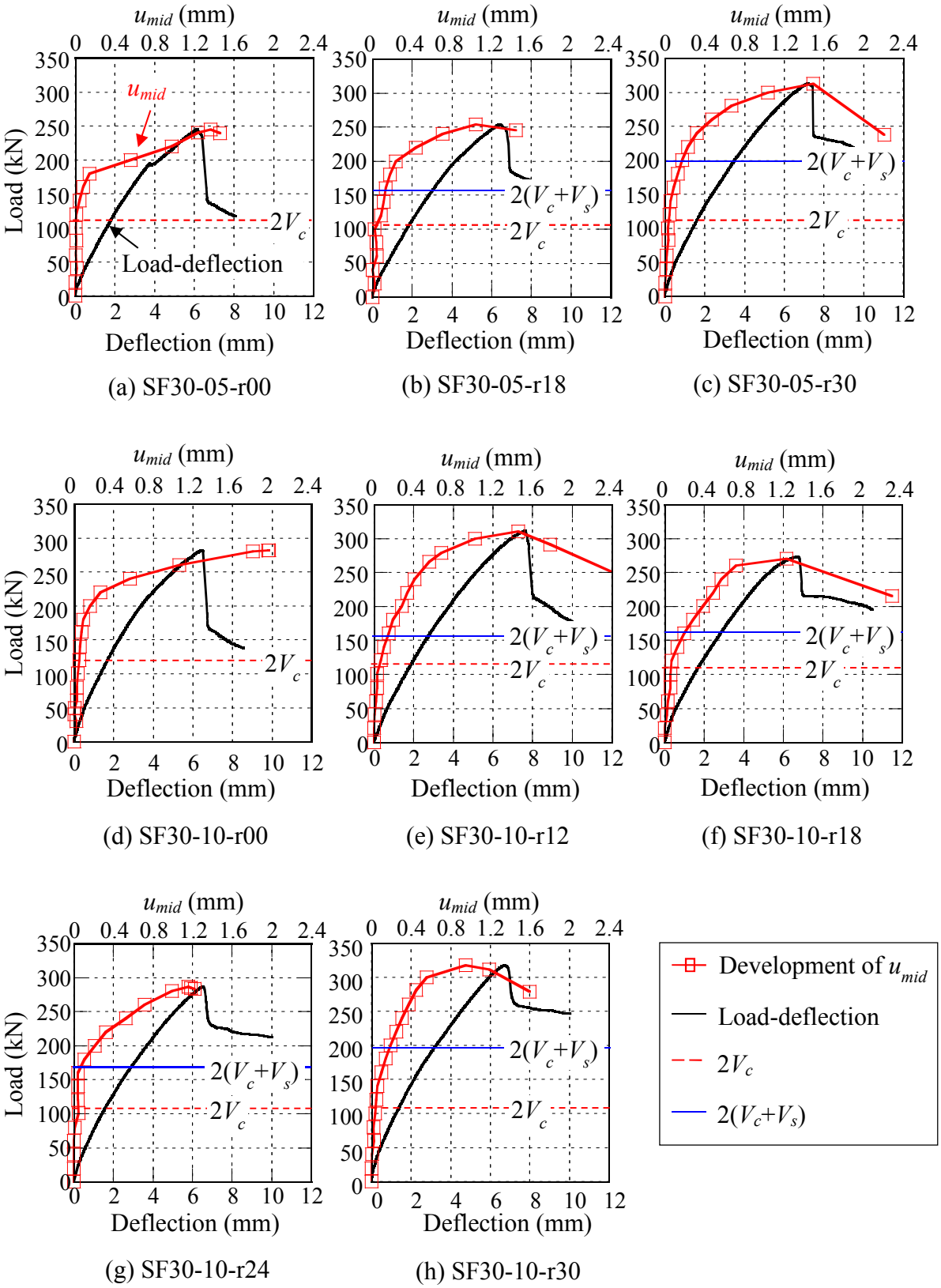

Figure 5.14 Development of crack surface displacement and deflection (Series I and II)

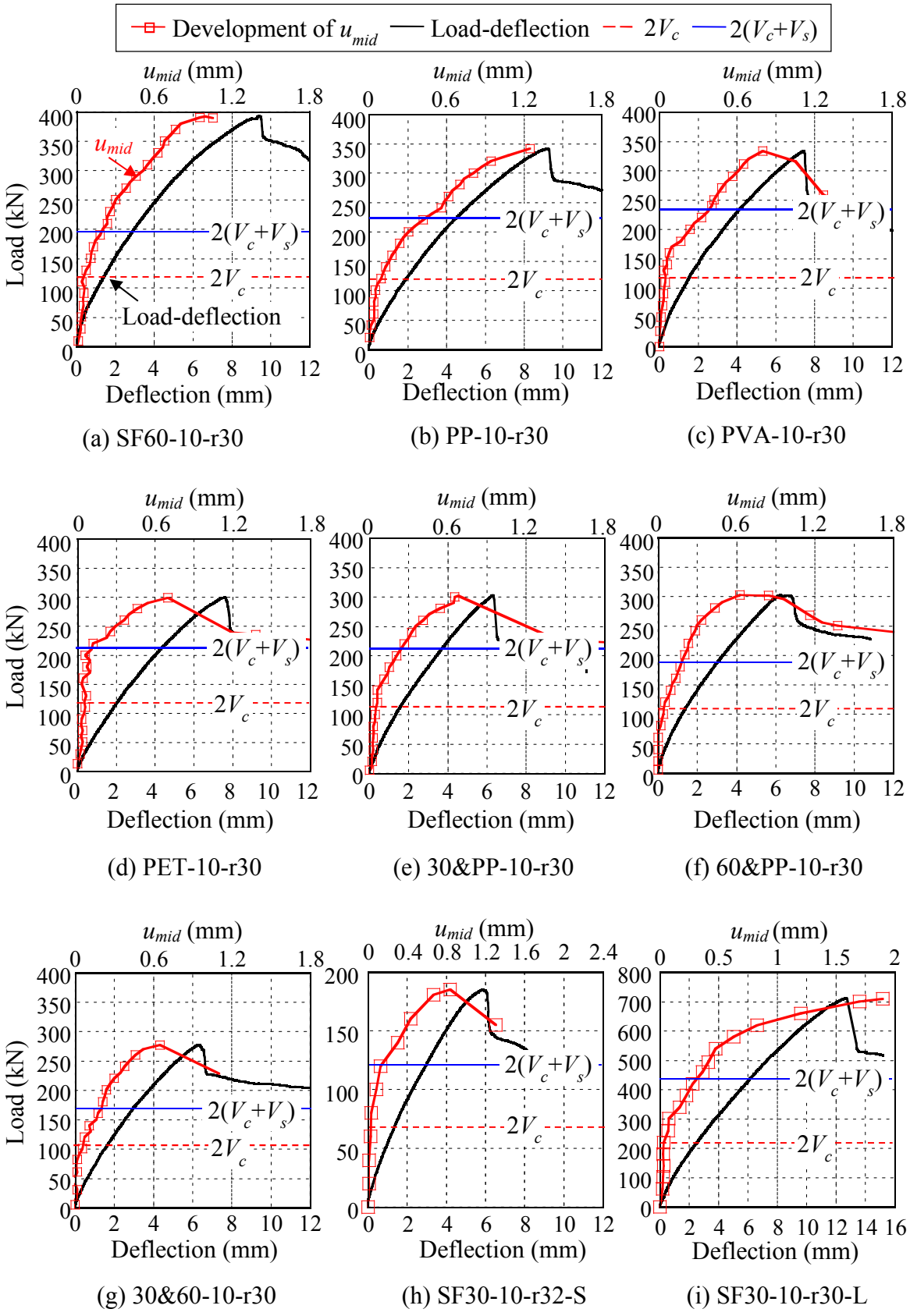

Figure 5.15 Development of crack surface displacement and deflection (Series III and IV)

5.6.2 Diagonal crack length

The crack length (L) is the summation of crack length of each layer (L_i) in the region of interest. L is listed in **Table 5.1.** The influences of fiber volume fractions, stirrup ratios, fiber types and effective depths on L are discussed. By varying fiber volume fractions, types and combinations of fibers, it was found that there was a relation between L and the fracture energy, G_F. The fracture energy is used because Bencardino et al. (2010) concluded that G_F included the effects of fiber types, fiber properties and volume fractions. Fracture energy of each specimen is listed in **Table 5.1**. **Figure 5.16(a)** plots the values of L of nine specimens from Series I and III that had the same r_w and d against the fracture energy. In addition, after excluding the effect of G_F, the values of L of 15 specimens having the same d were plotted against r_w in **Fig. 5.16(b)**. L decreased with the increase in G_F (**Fig. 5.16(a)**). In addition, L tended to decrease with the increase in r_w (**Fig. 5.16(b)**). It is because the angle of diagonal crack became steeper with the increase in G_F and r_w. As a result, the crack length reduced. The effect of G_F conforms to the effect of r_w on L. The formulation of the equations for the

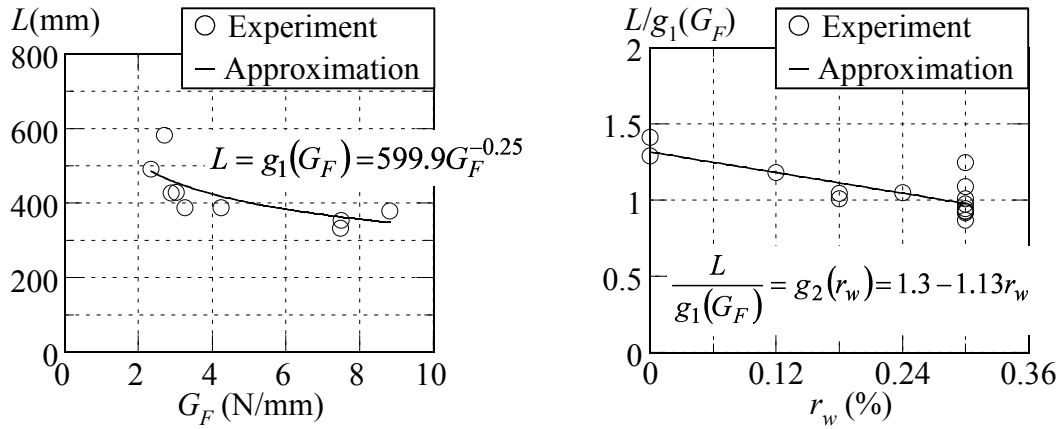

Figure 5.16 Effects of G_F and r_w on diagonal crack length

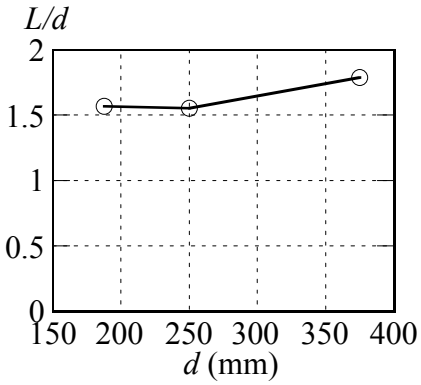

Figure 5.17 Relation between L/d and d

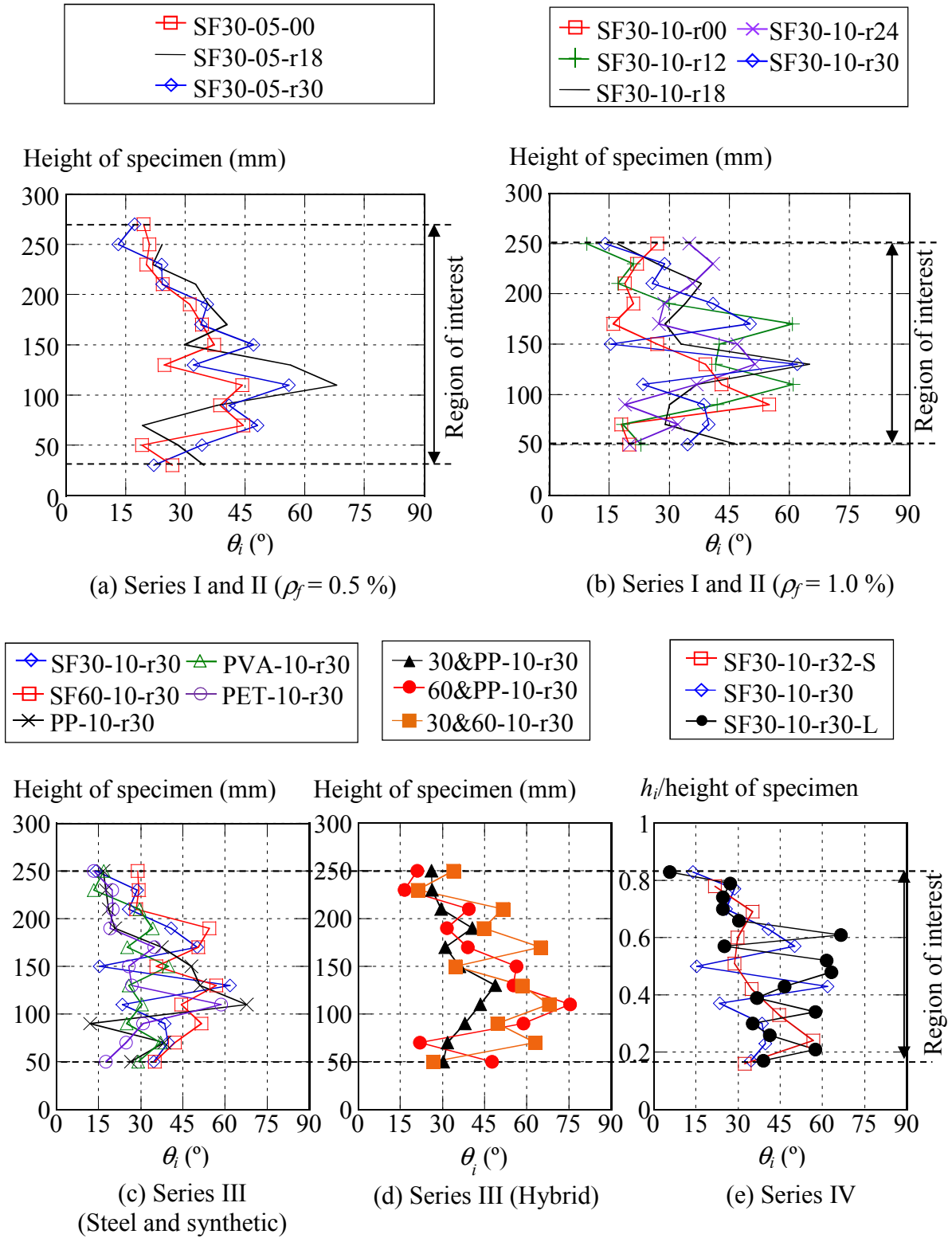

Figure 5.18 Distribution of the angle of diagonal crack along the height of specimens at the peak load

effects of each parameter will be discussed later in **Chapter 7**. Furthermore, the results of diagonal crack length of specimens with different size can be discussed by considering the values of *L/d*. *L/d* increased with the increase in the beam depth as presented in **Fig. 5.17**. This is because the shape of diagonal crack changed from straight line to bilinear shape when the specimen size became larger. This behavior can be seen in **Fig. 5.9(c)**.

5.6.3 Angle of diagonal crack

The angles of diagonal crack (θ_i) of each layer were measured and shown in **Fig. 5.18**. For SF30-10-r30-L, the values of θ_i became smaller near to top of specimens. The average values of θ_i in the region of interest ($=\theta$) are listed in **Table 5.1**. θ was varied from 26.5° to 46.9°. The effects of fiber volume fractions, stirrup ratios, fiber types and effective depths on θ are illustrated in **Fig. 5.19**. Using the same procedure as explained in **Fig. 5.16**, the values of θ were plotted in **Fig. 5.19**. The specimens showed steeper angle of diagonal crack (θ) with

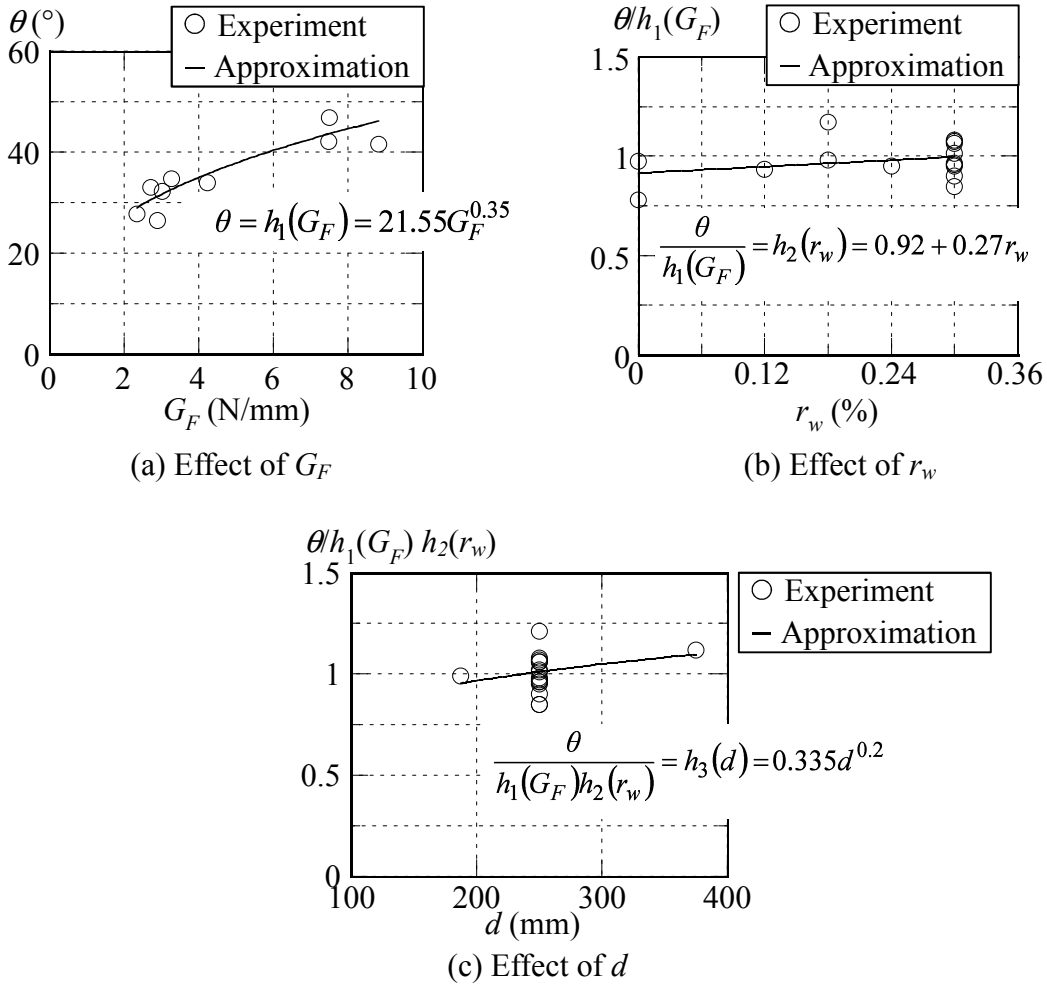

(a) Effect of G_F

(b) Effect of r_w

(c) Effect of d

Figure 5.19 Effects of G_F, r_w and d on angle of diagonal crack

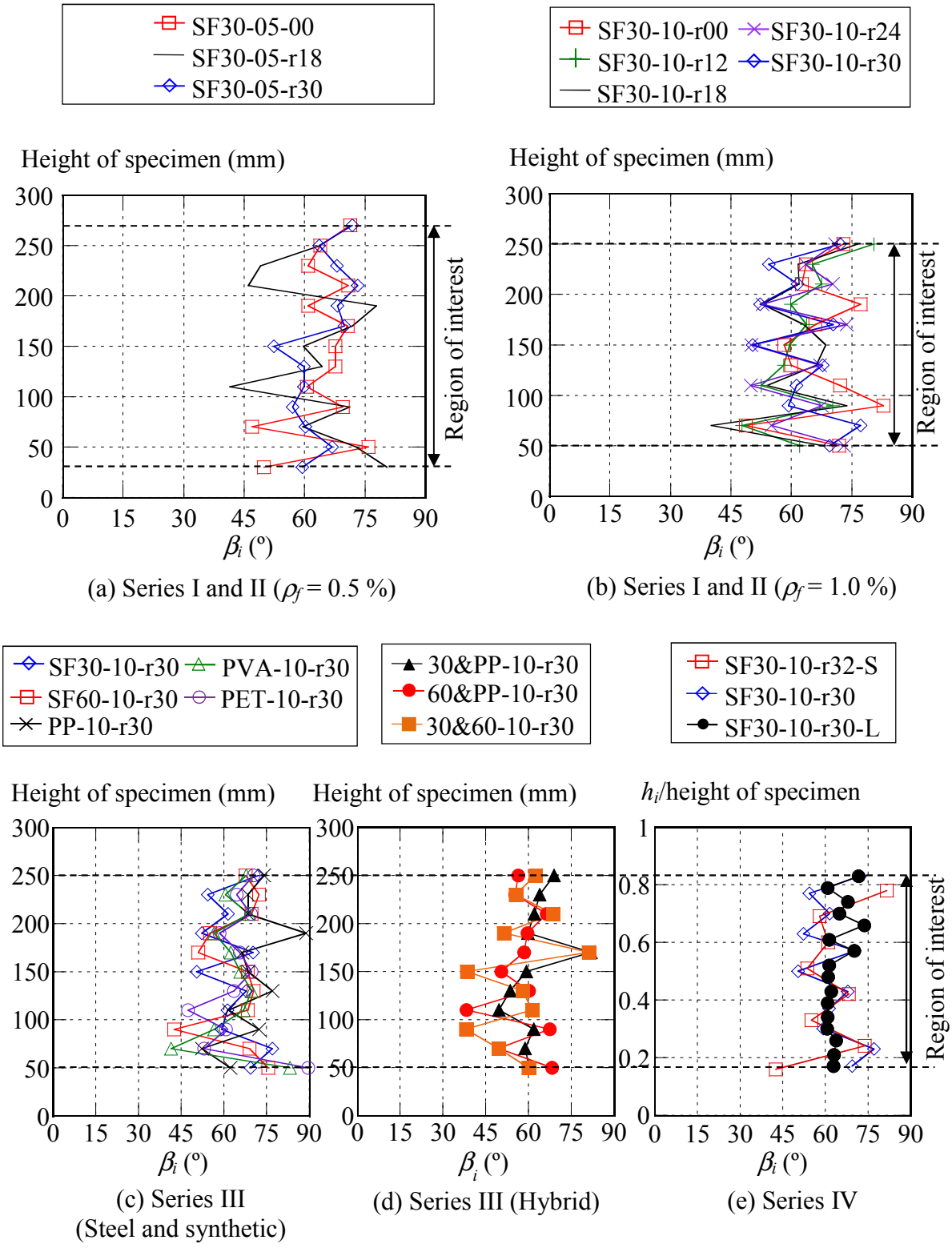

Figure 5.20 Distribution of the angle of principal tensile strain along the height of specimens at the peak load

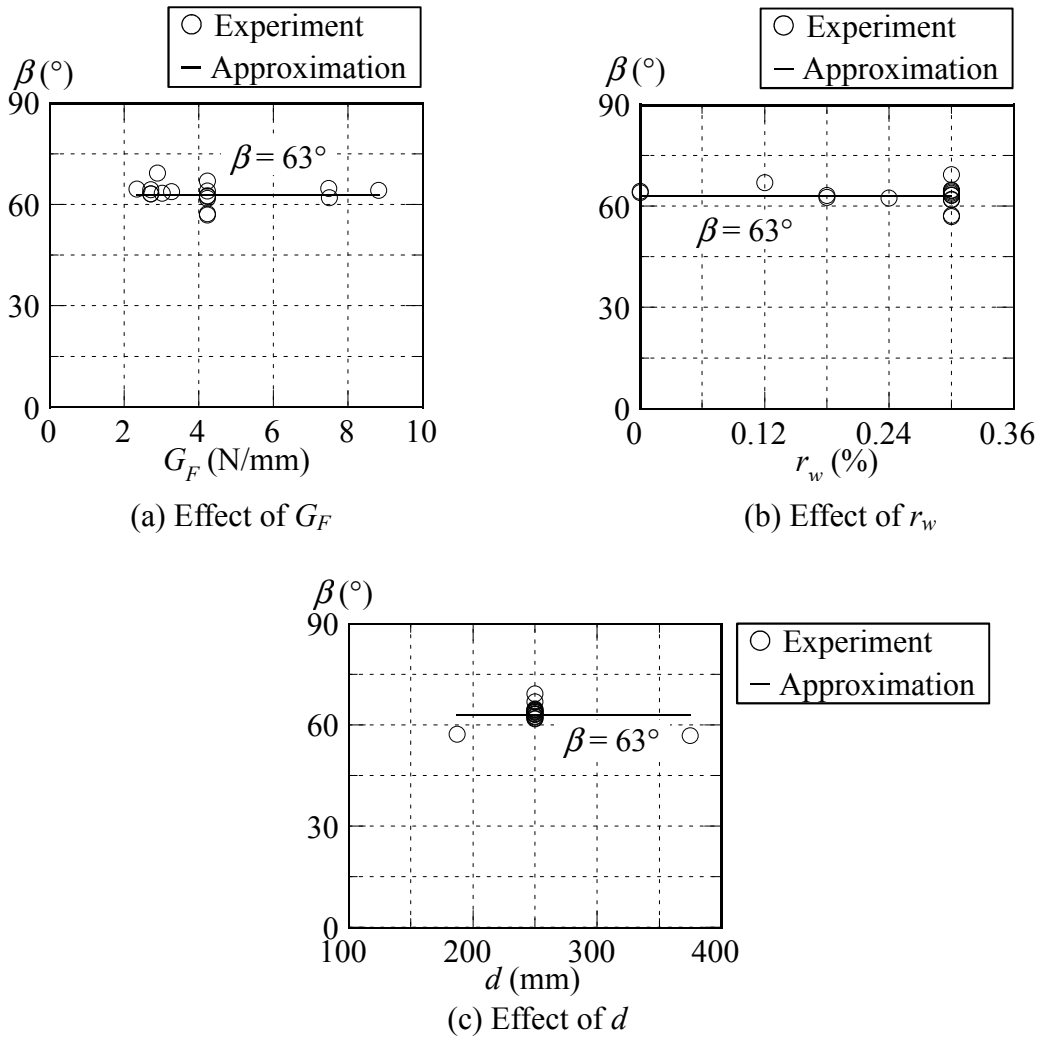

(a) Effect of G_F

(b) Effect of r_w

(c) Effect of d

Figure 5.21 Effects of G_F, r_w and d on angle of principal tensile strain

higher G_F and r_w (**Fig. 5.19(a)** and **(b)**). Moreover, the values of θ excluding the effects of G_F and r_w of 17 specimens were plotted with d in **Fig. 5.19(c)**. The angle of diagonal crack slightly increased when effective depth increased.

5.6.4 Angle of principal tensile strain

Using the image analysis, the angles of principal tensile strain (β_i) were calculated from the displacement of the nodal point of each layer. **Figure 5.20** presents the values of β_i. The tendency between β_i and height of specimen could not be observed. **Table 5.1** gives the average values of β_i in the region of interest (β). **Figure 5.21** plots the influences of fracture energy, stirrup ratio and effective depths on β. The angle of principal tensile strain did not change significantly among these specimens.

In addition, the values obtained from the summation between θ and β are almost 90 degree. This means that the sliding displacement is comparatively smaller than the opening displacement. Therefore, the utilization of tension softening curves for the shear problem is acceptable in this study.

5.7 Conclusions of Chapter 5

The experimental results of seventeen FRC beams were discussed in this chapter. The experimental parameters were fiber volume fractions, stirrup ratios, fiber types and effective depths. The influences of parameters on shear resisting mechanism and diagonal cracking behavior of FRC beams were reported. The influences of fiber volume fractions and fiber types on diagonal cracking behavior of FRC beams can be represented by the fracture energy of fiber reinforced concrete. Based on the experimental results in this chapter, the following conclusions were drawn.

(1) The addition of steel, synthetic and hybrid fibers to concrete beams significantly increased the shear capacity of the FRC beams. Steel fibers, especially 60-mm steel fibers, were the most effective to enhance the shear carried by fibers when there is enough fiber length and boding strength.

(2) There was an increase in shear capacity and shear carried by fibers of FRC beams when fiber volume fraction increased. However, the increment of shear capacity and shear carried by fibers due to the addition of fibers became less significant in specimens with higher stirrup ratio. The effect of fibers as shear reinforcement was dominant in case of low stirrup ratio.

(3) While the shear carried by stirrups increased with the increase in stirrup ratio, there was a reduction of the shear carried by fibers. This reduction was because length of the diagonal crack became shorter with the increase in stirrups. As a result, it led the smaller area that fibers can transfer stress. From these increase and decrease of shear contribution from stirrups and fibers, the shear capacity did not monotonically increased with the increase in stirrup ratio. This confirmed that there was an optimized combination of fiber volume fractions and stirrup ratio to increase the shear capacity of FRC beams.

(4) When the fiber volume fraction was 1.0%, the values of κ_{exp} of specimens having steel fibers were greater than 1.0, which is the value recommended in the JSCE design guidelines. On the other hand, κ_{exp} of synthetic fibers and hybrid fibers between 30-mm steel fibers and polypropylene were less than 1.0.

(5) The size effect on shear capacity of FRC beams was very slight in case that effective depth was varied from 187.5 to 375 mm. Moreover, there was no size effect in shear carried by fibers.

(6) The crack surface displacements of the diagonal crack around the middle height of FRC beams were larger than those at top and bottom of specimens because there was the compression zone at the top fiber and restraint by the longitudinal steel bars at the bottom of specimens.

(7) The crack surface displacement of diagonal crack increased drastically just before the peak load. At the same time, the shear force-deflection curve showed nonlinear behavior. This sudden increase led the failure of FRC beams.

(8) With the increase in fracture energy and stirrup ratio, the length of diagonal crack decreased. In addition, the ratio of diagonal crack length to effective depth was greater in the larger specimen. It is because the shape of diagonal crack changed from straight line to bilinear curve.

(9) The angle of diagonal crack was steeper with higher fracture energy, stirrup ratio and effective depth. On the other hand, the angel of principal tensile strain did not vary.

CHAPTER 6

EVALUATION METHOD FOR SHEAR CARRIED BY FIBERS OF FRC BEAMS USING TENSION SOFTENING CURVES

6.1 Introduction

The post-cracking behavior of fiber reinforced concrete is crucial in FRC beams. After cracking, the tensile stress (σ) can transfer along the length of the diagonal crack due to the bridging effect of fibers and this stress becomes the shear contribution from fibers. The values of stress transferred across the diagonal crack; however, relate to the crack surface displacement (u). The crack surface displacement is the displacement of crack in the principal tensile strain direction (β), which is the direction of crack's movement. The crack surface displacement consists of the displacements from crack opening and crack sliding. The relationship between crack surface displacement and stress is represented by the tension softening curve. As a result, the tension softening curve is an effective tool for evaluating stress.

In this chapter, the investigation procedures are explained. The stress was calculated from crack surface displacement and tension softening curves. The shear carried by fibers was evaluated and the calculated results were validated with the experimental results of shear carried by fibers.

6.2 Specimen Modeling

In order to evaluate the shear carried by fibers precisely, the specimens were modeled as many layers with a height of 20 mm (**Fig. 6.1**) corresponding to the interval of red targets for

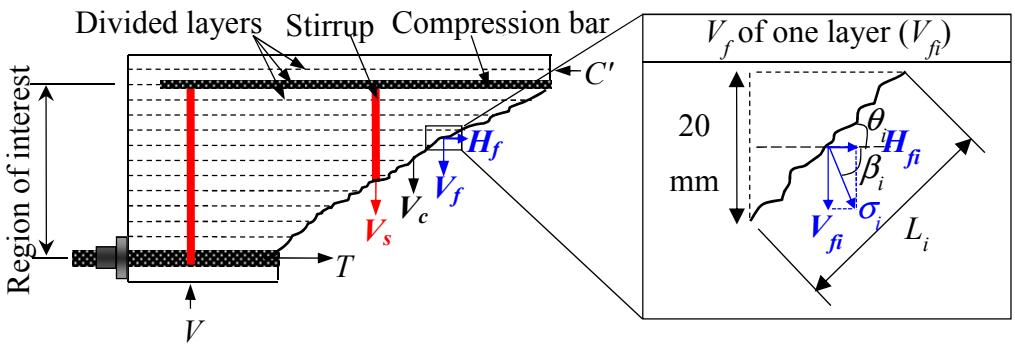

Figure 6.1 Specimen modeling and free body diagram

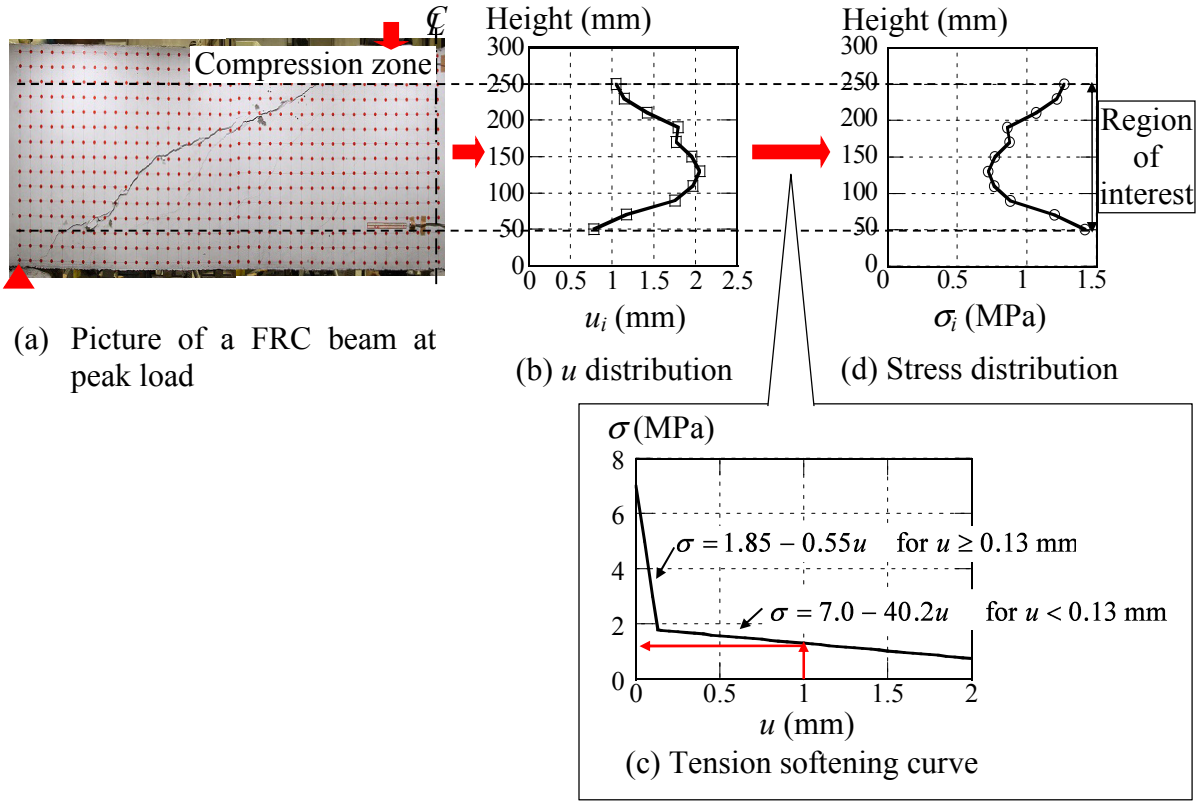

Figure 6.2 Investigation procedures of tensile stress transferred across the diagonal crack (Example of SF30-10-r00)

the image analysis. Crack surface displacement (u_i), diagonal crack length (L_i), angle of a diagonal crack (θ_i), and angle of principal tensile strain (β_i) of each layer at the peak load were investigated from the image processing. The total number of layers of the specimens in Series I, II and III was 15. In addition, there were 11 layers in SF30-10-r32-S and 21 layers in SF30-10-r30-L. The interested zone for investigating the shear carried by fibers; however, was only a part that the fibers showed the tensile performance. That was the diagonal crack from the part below compression zone to the tip of diagonal crack in tension zone as shown in

Table 6.1 Number of layers in the region of interest

Specimen	Number of layers
Series I and Series II (ρ_f=0.5%)	13 layers
Series I and Series II (ρ_f=1.0%)	11 layers
Series III	11 layers
SF30-10-r32-S (Series IV)	7 layers
SF30-10-r30-L (Series IV)	16 layers

Fig. 6.2(a). The compression zone is the height of specimens from the top of specimen to the location of neutral axis, which was calculated from the displacements of red targets obtained through the image analysis at the cross section of diagonal crack tip. Also, the crushing of concrete occurred in this portion. Therefore, it was considered as the compression dominant zone and the shear carried by the compression dominant zone is taken into account as a part of V_c. Furthermore, the tip of diagonal crack intension zone is treated as the edge of the region of interest.

The region of interest of the specimens is listed in **Table 6.1**. The region of interest of specimens having 1.0% of fibers was the part between the location of compression bars and tensile reinforcing bars. The number of layers in the region of interest was 11 for specimens with effective depth of 250 mm, 7 layers for SF30-10-r32-S and 16 layers for SF30-10-r30-L. However, in specimens with 0.5% of fibers, the diagonal crack propagated into the concrete cover zone and stopped at 30 mm from the bottom of specimens because of the less shear reinforcement. The number of layers in the region of interest was 13 for specimens with 0.5% of fibers.

6.3 Evaluation Method Using Tension Softening Curves

The stress across the diagonal crack and the shear carried by fibers were evaluated based on the fracture mechanics. Tensile stress transferred across the diagonal crack (σ_i) can be converted from crack surface displacement (u_i) by using the relationship between tensile stress and crack opening displacement of the tension softening curves. The calculation procedures of stress are shown in **Fig. 6.2**. The stress transferred across the diagonal crack (σ_i) (**Fig. 6.2(d)**)

was obtained by substituting the values of crack surface displacement of each layer (u_i) into the bilinear equation of tension softening curves (**Fig. 6.2(c)**). The bilinear equations of tension softening curves of each fiber reinforced concrete were explained in detail in **Chapter 3** and were presented in **Table 3.4**. The tension softening curve reflects the characteristic of each fiber. The tension softening response is dependent on the type, shape, content of fibers and properties of concrete. Since the values of crack surface displacement at the peak load were larger than 0.13 mm in all specimens, only the equation of the second linear line was used. The second linear equation of tension softening curves fitted well with the experimental data of the tension softening curve. Therefore, the variation due to curve fitting of tension softening curves did not affect the results. The direction of principal tensile stress of the layer has been assumed to be the same as the direction of principal tensile strain. Because of the nonlinear stage, both directions are not identical. However, the direction is almost the same. Therefore, the difference between them will not significantly affect the results.

After investigating the stress transferred across the diagonal crack, the shear carried by fibers was investigated. The shear force carried by fibers is equal to the stress multiplied by the area of crack surface normal to direction of stress. The area of crack surface of each layer was computed from the diagonal crack length (L_i) and web width (b_w). The area of crack that perpendicular to the direction of stress is equal to $b_w \cdot L_i \cdot \cos(\beta_i + \theta_i - 90)$. The vertical component of the force with consideration of the angle β is the shear carried by fibers (see **Fig. 6.1**). The stress, area of crack surface and shear forces were calculated layer by layer.

By considering the force acting at the diagonal crack in a FRC beam due to the effect of fibers (**Fig. 6.1**), the shear carried by fibers (V_{fcal}) is the summation of the forces in the region of interest and can be calculated from Eq. (6.1).

$$V_{fcal} = \sum_{i=1}^{n} (\sigma_i \cdot b_w \cdot L_i \cdot \cos(\beta_i + \theta_i - 90) \cdot \sin\beta_i) \tag{6.1}$$

where n is the number of layers in the region of interest (**Table 6.1**), σ_i is the tensile stress of the layer i (MPa), L_i is the length of the diagonal crack of the layer i (mm), β_i is the angle of the principal tensile strain of layer i (degree) and θ_i is the angle of the diagonal crack of the layer i (degree).

6.4 Stress Transferred Across the Diagonal Crack in FRC Beams

The distribution of σ_i is shown in **Fig. 6.3**. The larger stress can be resisted at the top and bottom parts of specimens due to the smaller crack surface displacement. The difference in tensile stress among specimens having ρ_f = 0.5% was slight even though stirrup ratio was varied (**Fig. 6.3(a)**). This is because the slope of tension softening curve, which ρ_f = 0.5%, is almost flat when the crack surface displacement is larger than 0.06 mm. Therefore, σ_i converted from u_i did not change significantly. The result was expected that SF30-05-r30 would provide the smallest crack surface displacement; however, SF30-05-r30 showed the variation that may be caused by the orientation of fibers in the specimen. Therefore, SF30-05-r30 revealed the relatively large crack surface displacement. As a result, instead of SF30-05-r30, SF30-05-r18 showed the largest stress due to the smallest crack surface displacement. With the increase in fiber volume fraction from 0.5 to 1.0%, the values of stress across diagonal crack increased. This result can be observed by comparing between **Figs. 6.3(a)** and **(b)**. It is because, comparing with 0.5% of fibers, the tension softening curves of ρ_f = 1.0% can resist more stress at the same crack surface displacement and the slope of the curve when crack surface displacement is greater than 0.13 mm is steeper than the slope of ρ_f = 0.5% resulting in the significant stress converted from u_i.

Although u_i of the specimens with different types of fibers (Series III) was varied without the clear tendency as discussed in **Chapter 5**, the value of σ_i of Series III was significantly different and a tendency was observed as shown in **Fig. 6.3(c)**. It is because each fiber reinforced concrete transferred the different stress at the identical crack surface displacement as observed in tension softening curves. SF60-10-r30 resisted the highest σ_i (**Fig. 6.3(c)**). Synthetic fibers resisted relatively low and uniform σ_i at the peak load due to their flat slope of the second branch of tension softening curves (i.e. when $u \geq$ 0.12, 0.16 and 0.10 mm for PP, PVA and PET, respectively). Hybrid fibers containing SF60 provided high σ_i at the peak load because of the influence of the long fibers. Besides, the stress transferred across crack decreased in a larger specimen as shown in **Fig. 6.3(d)** because u_i increased when the specimen became larger.

The average values of stress in the region of interest (σ) are summarized in **Table 6.2**. The influences of fracture energy (G_F), stirrup ratio (r_w) and effective depth (d) on stress (σ) are

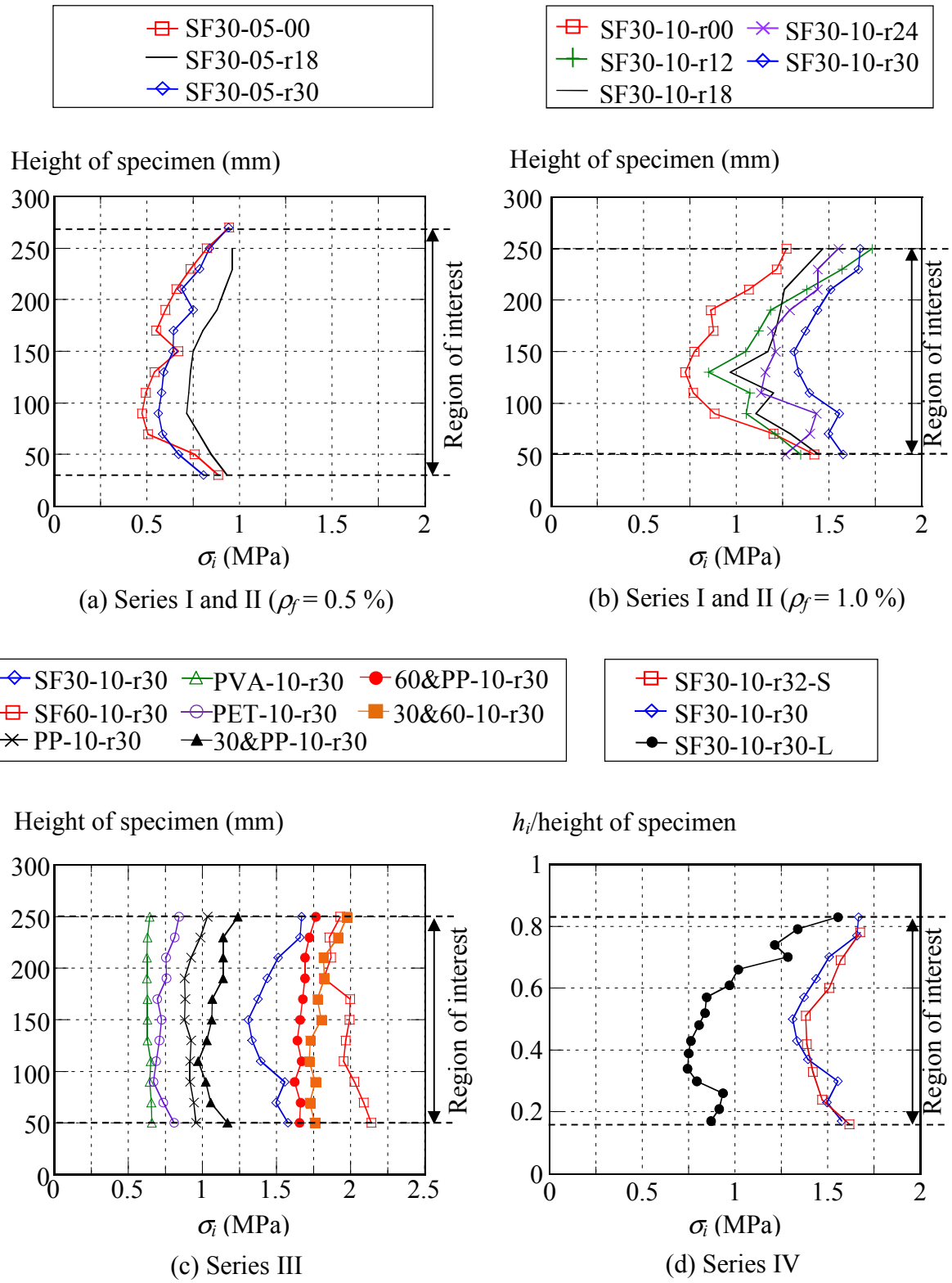

Figure 6.3 Distribution of stress along the height of specimens at the peak load

Table 6.2 Calculated results from the evaluation method based on tension softening curves

Series	Specimen	Type of fibers	ρ_f (%)	G_F (N/mm)	r_w (%)	d (mm)	σ (MPa)	V_{fexp} (kN)	V_{fcal} (kN)	V_{fexp}/V_{fcal}
I and II	SF30-05-r00	Steel (30 mm)	0.5	2.71	0.00	250	0.66	66.5	60.2	1.11
	SF30-05-r18			2.71	0.18		0.83	50.4	51.2	0.98
	SF30-05-r30			2.71	0.30		0.70	56.2	56.1	1.00
	SF30-10-r00		1.0	4.24	0.00		1.00	81.7	73.5	1.11
	SF30-10-r12			4.24	0.12		1.23	79.1	83.5	0.95
	SF30-10-r18			4.24	0.18		1.25	57.0	63.4	0.90
	SF30-10-r24			4.24	0.24		1.33	57.6	71.6	0.80
I-IV	SF30-10-r30			4.24	0.30		1.48	59.5	72.6	0.82
III	SF60-10-r30	Steel (60 mm)		8.82			1.97	98.3	96.2	1.02
	PP-10-r30	PP		3.02			0.93	54.1	53.6	1.01
	PVA-10-r30	PVA		2.34			0.64	46.1	40.4	1.14
	PET-10-r30	PET		2.89			0.75	43.0	43.0	1.00
	30&PP-10-r30	Hybrid		3.27			1.09	46.1	55.0	0.84
	60&PP-10-r30			7.49			1.68	57.2	66.1	0.86
	30&60-10-r30			7.50			1.80	56.4	70.6	0.80
IV	SF30-10-r32-S	Steel (30 mm)		4.24	0.32	187.5	1.51	34.1	42.4	0.80
	SF30-10-r30-L			4.24	0.30	375	0.99	137.6	136.6	1.01

ρ_f: fiber volume fraction, G_F: fracture energy, r_w: stirrup ratio, d: effective depth, σ: average stress in the region of interest, V_{fexp}: the experimental value of shear carried by fibers and V_{fcal}: calculated shear carried by fibers from Eq. (6.1).

presented in **Fig. 6.4**. The influence of G_F on σ of nine specimens which had the same r_w and d is plotted in **Fig. 6.4(a)**. After excluding the effect of G_F on stress, the values of $\sigma/f_1(G_F)$ of 15 specimens, which had the same d, are plotted with r_w (**Fig. 6.4(b)**). And the values of σ excluding the effects of G_F and r_w of 17 specimens are plotted against the effective depth (**Fig. 6.4(c)**). Stress transferred across the diagonal crack increased with the increase in G_F as observed in **Fig. 6.4(a)**. Moreover, stirrup ratio enhanced the stress across the crack as presented in **Fig. 6.4(b)**. The stress transferred across the diagonal crack increased with the increase in G_F and r_w because fibers having better fracture properties G_F can resist higher stress in post-cracking behavior, whereas stirrups help to restrain the growth of crack surface displacements. However, as shown in **Fig. 6.4(c)**, the stress transferred across crack decreased

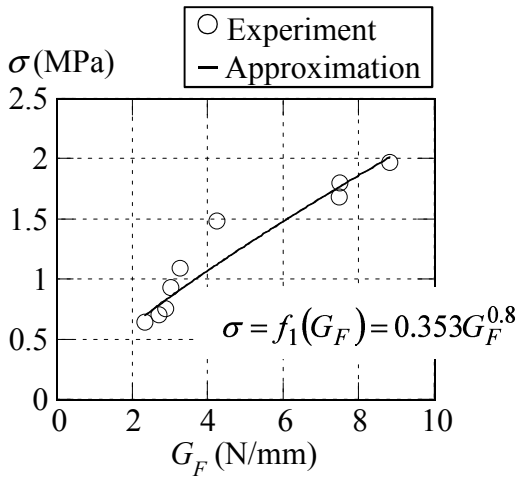

(a) Effect of G_F

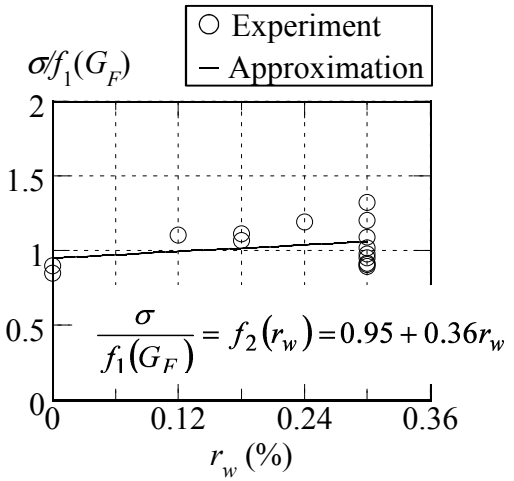

(b) Effect of r_w

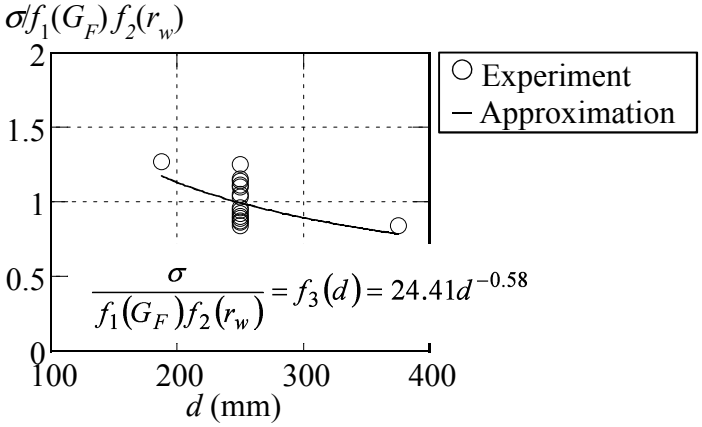

(c) Effect of d

Figure 6.4 Effects of G_F, r_w and d on stress transferred across the diagonal crack

in a larger specimen because of the increase in crack surface displacement when the specimen became larger.

6.5 Calculated Shear Carried by Fibers

The shear carried by the fibers (V_{fcal}) was calculated using Eq. (6.1) and was summarized in **Table 6.2**. As described before, the shear carried by fibers is calculated from the stress and area of crack surface, which is the area that stress transferred. It is not only the stress that affects the shear carried by fibers but also the area of crack surface. Although the stress of hybrid fibers was high, the area of crack surface was short due to the short L_i and steep θ_i as discussed in **Chapter 5**. Thus, the shear carried by fibers did not increase significantly.

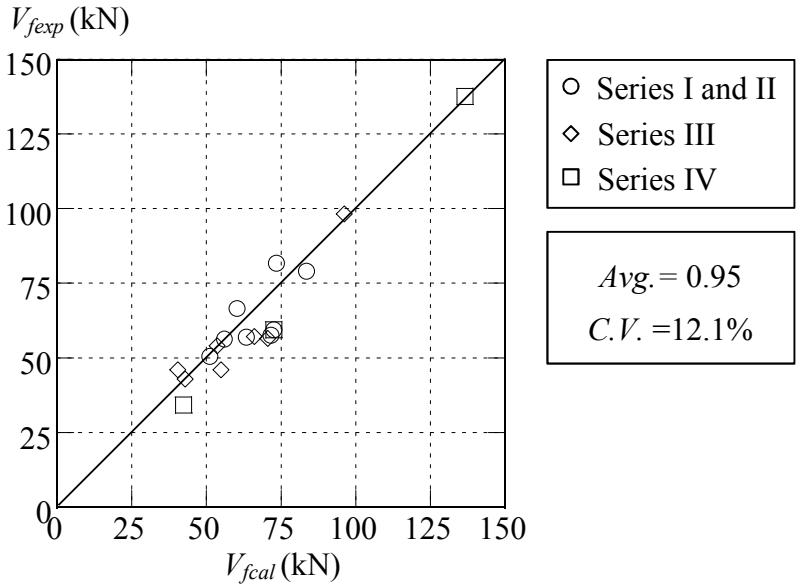

Figure 6.5 Comparison between experimental and calculated shear carried by fibers

The results of the experimental value (V_{fexp}) given by Eq. (6.2).

$$V_{fexp} = V_{exp} - V_c - V_s \tag{6.2}$$

where, V_{exp} is the shear capacity from the experiment, V_c is the shear capacity of members without shear reinforcement and V_s is the shear carried by stirrups.

The comparison between V_{fexp} and V_{fcal} is shown in **Table 6.2**. **Figure 6.5** shows the variation of V_{fexp}/V_{fcal}. A total of seventeen FRC beams were used to confirm the applicability of the evaluation method. The average (*avg*.) and the coefficient of variation (*C.V*.) of the ratio of the experimental to the calculated value (V_{fexp}/V_{fcal}) are 0.95 and 12.1%, respectively. The comparison demonstrates that V_{fcal} shows a good agreement with V_{fexp}. Therefore, this method can examine the shear carried by fibers of FRC beams though fiber volume fractions, stirrup ratios, effective depths are varied and can be applied in FRC beams without stirrups. Furthermore, this method can be used in the FRC beams with various material types, lengths and combinations of fibers because the tension softening curves can reflect the characteristic of each fiber.

6.6 Conclusions of Chapter 6

The stress transferred across the diagonal crack was investigated using tension softening curves (explained in **Chapter 3**) and the crack surface displacement (discussed in **Chapter 5**). The shear carried by fibers was calculated from the stress and area of crack surface. Based on the calculation in this chapter, the conclusions are as follows:

(1) The larger stress can be transferred at top and bottom of specimens due to the smaller crack surface displacement.

(2) The stress transferred across the diagonal crack increased with the increase in fracture energy and stirrup ratio. It is because fibers having higher fracture energy showed better post-peak behavior in tension. Moreover, with higher stirrup ratio, crack surface displacement became smaller because stirrups helped to prevent the crack growth. Nonetheless, stress reduced with the increase in specimen size.

(3) Good correlation between experimental results and calculated results was observed. The method to investigate the shear carried by fibers based on the tension softening curves can be used even for various fiber volume fractions, stirrup ratios, effective depths, fiber types and combinations of fibers.

CHAPTER 7

PROPOSAL OF PREDICTIVE EQUATION FOR SHEAR CAPACITY OF FRC BEAMS

7.1 Introduction

The evaluation method of the shear carried by fibers (**Chapter 6**) can investigate the shear carried by fibers accurately. However, the image analysis must be performed in order to measure the diagonal cracking behavior. In addition, the shear carried by fibers has to be calculated layer by layer. Therefore, more simplified equation is developed for the practical design purpose. The predictive equation for the shear carried by fibers is formulated based on concept of using tension softening curves together with the experimental results of 17 FRC beams. The equation for shear capacity is proposed for the fiber reinforced concrete beams that can be applied for various kinds of fibers.

7.2 Proposal of Predictive Equations for Shear Carried by Fibers

In this study, the experimental results cover several factors. The compressive strength of concrete was from 45 MPa to 60 MPa. Fiber volume fractions were 0.5 and 1.0% to full volume of concrete. Stirrup ratio was varied from 0.0% to 0.30%. Effective depth was from 187.5 mm to 375 mm. Eight types of fibers were tested. There were steel fibers with 30 mm length (SF30), steel fibers with 60 mm length (SF60), polypropylene (PP), polyvinyl alcohol (PVA), polyethylene terephthalate (PET), hybrid fibers between SF30 and PP, SF60 and PP and SF30 and SF60. Based on the method proposed in the **Chapter 6**, the predictive equation is developed.

Table 7.1 Detail of specimens

Specimen	b_w (mm)	d (mm)	a/d	p_w (%)	r_w (%)	Type of fibers	L_f (mm)	D_f (mm)	ρ_f (%)	f'_c (MPa)	f_t (MPa)	G_F (N/mm)
SF30-05-r00	150	250.0	2.8	2.7	0.00	Steel	30	0.62	0.5	54.1	2.8	2.71
SF30-05-r18					0.18					45.0	2.6	2.71
SF30-05-r30					0.30					59.3	3.2	2.71
SF30-10-r00					0.00				1.0	64.9	3.9	4.24
SF30-10-r12					0.12					53.0	3.9	4.24
SF30-10-r18					0.18					46.6	3.5	4.24
SF30-10-r24					0.24					48.3	3.3	4.24
SF30-10-r30					0.30					55.3	3.0	4.24
SF60-10-r30						Steel	60	0.90		61.9	3.7	8.82
PP-10-r30						PP	30	1.6×0.6		57.0	3.1	3.02
PVA-10-r30						PVA	30	0.66		65.4	3.0	2.34
PET-10-r30						PET	30	0.70		51.8	3.0	2.89
30&PP-10-r30						Hybrid	-	-		52.2	2.7	3.27
60&PP-10-r30							-	-		49.2	3.4	7.49
30&60-10-r30							-	-		40.2	2.3	7.50
SF30-10-r32-S	113	187.5			0.32	Steel	30	0.62		52.0	3.4	4.24
SF30-10-r30-L	225	375.0		2.4	0.30					55.9	3.0	4.24

b_w: web thickness, d: effective depth, a/d: shear span to effective depth ratio, p_w: longitudinal reinforcement ratio ($=A_s/b_w d$), r_w: stirrup ratio, L_f: fiber length, D_f: diameter of fibers, ρ_f: fiber volume fraction, f'_c: the compressive strength of the concrete, f_t: tensile strength from split tensile test and G_F: fracture energy.

The simplified predictive equation for shear carried by fibers is formulated based on Eq. (6.1) and the average concept is used. The average values of stress (σ_i), angle of diagonal crack (θ_i) and angle of principal tensile strain (β_i) in the region of interest (denoted as σ, θ and β, respectively) are used for expressing the relation. On the other hand, the total diagonal crack length in the region of interest (L) is used.

The simplified equation is shown in Eq. (7.1).

Table 7.2 Variables and representing parameter of the experimental cases

Variables	Range	Representing parameter
Fiber types	8 types	Fracture energy (G_F)
Fiber volume fraction (ρ_f)	0.5-1.0%	
Stirrup ratio (r_w)	0.0-0.3%	r_w
Effective depth (d)	187.5-375 mm	d

$$V_f = \sigma \cdot b_w \cdot L \cdot \cos(\beta + \theta - 90°) \cdot \sin\beta \tag{7.1}$$

where, V_f is the predictive shear carried by fibers, σ is the average tensile stress along a diagonal crack, b_w is the web thickness, L is the crack length in the region of interest, β is the average angle of principal tensile strain (degree) and θ is the average angle of diagonal crack (degree).

The equations for each variable in Eq. (7.1), which are σ, θ, β and L, were formulated from the experimental results of 17 FRC beams as listed in **Table 7.1**. **Table 7.2** presents variables, range of variables and representing parameter for each variable of the experimental cases. The effects of fiber types and fiber volume fractions are represented by the fracture energy (G_F) because G_F is the parameter already including the effects of fiber types, fiber properties and fiber volume fraction (Bencardino, 2010). Furthermore, the effect of compressive strength of concrete (f'_c) on shear carried by fibers is assumed to be represented by G_F in this study. The influence of shear reinforcement is presented by stirrup ratio (r_w). Besides, the effect of specimen size is represented by effective depth, d.

The influences of G_F, r_w and d on σ, L, θ and β were already discussed in **Chapter 5** and **Chapter 6**. The formulation of each factor is explained in this section. **Figures 7.1** to **7.4** show the effects of G_F, r_w and d on σ, L, θ, β and the formulation of equations. The values of σ, L and θ of nine specimens having the same r_w and d were plotted against G_F as presented in **Figs. 7.1(a)**, **7.2(a)** and **7.3(a)**. After excluding the effect of G_F, the values of σ, L and θ of 15 specimens having the same d were plotted against r_w in **Figs. 7.1(b)**, **7.2(b)** and **7.3(b)**. Moreover, the values of σ, L and θ excluding the effects of G_F and r_w of 17 specimens were plotted with d in **Figs. 7.1(c)**, **7.2(c)** and **7.3(c)**.

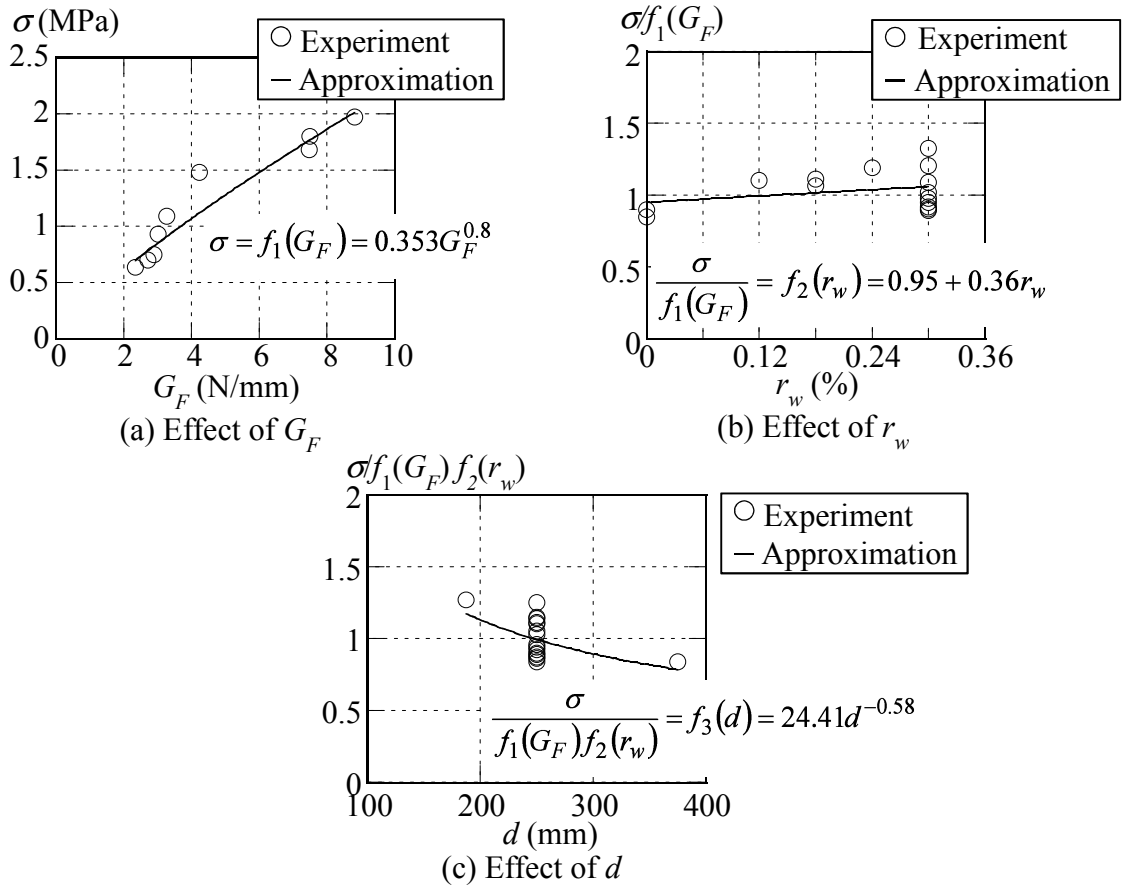

Figure 7.1 Formulation of the equation for stress transferred across the diagonal crack

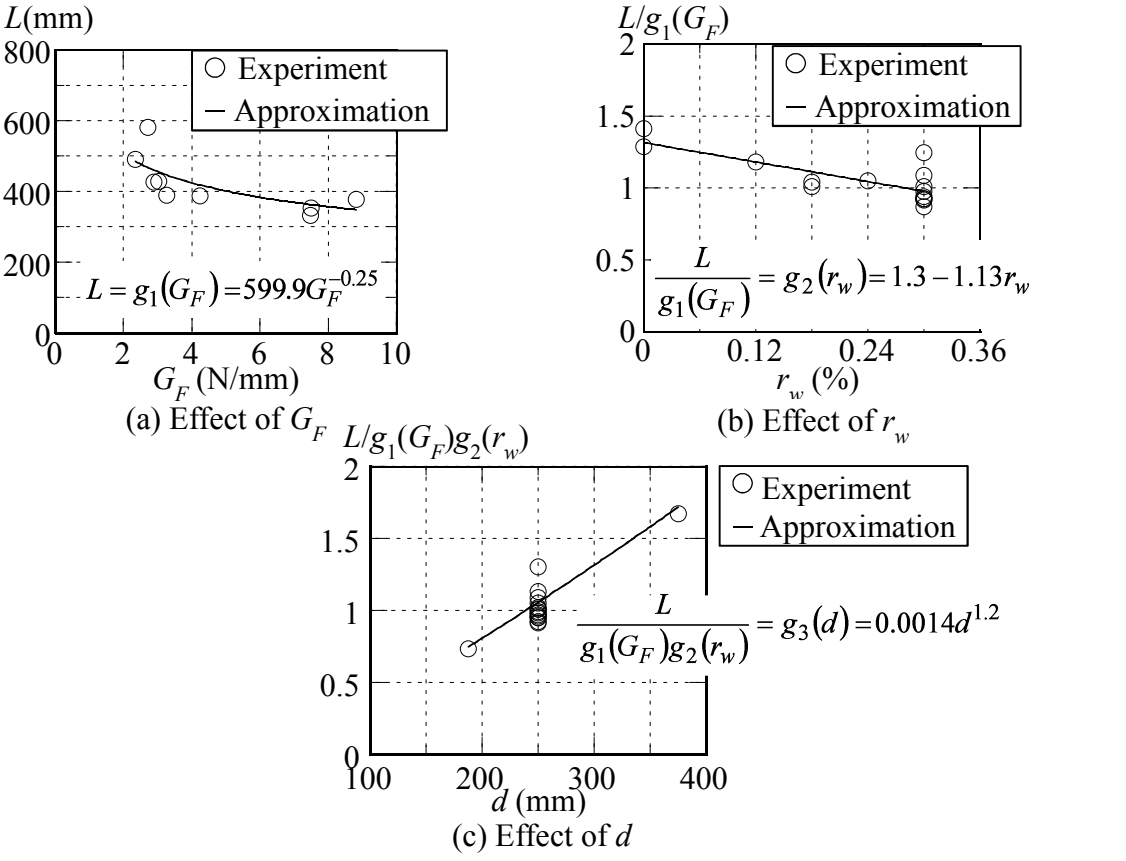

Figure 7.2 Formulation of the equation for diagonal crack length

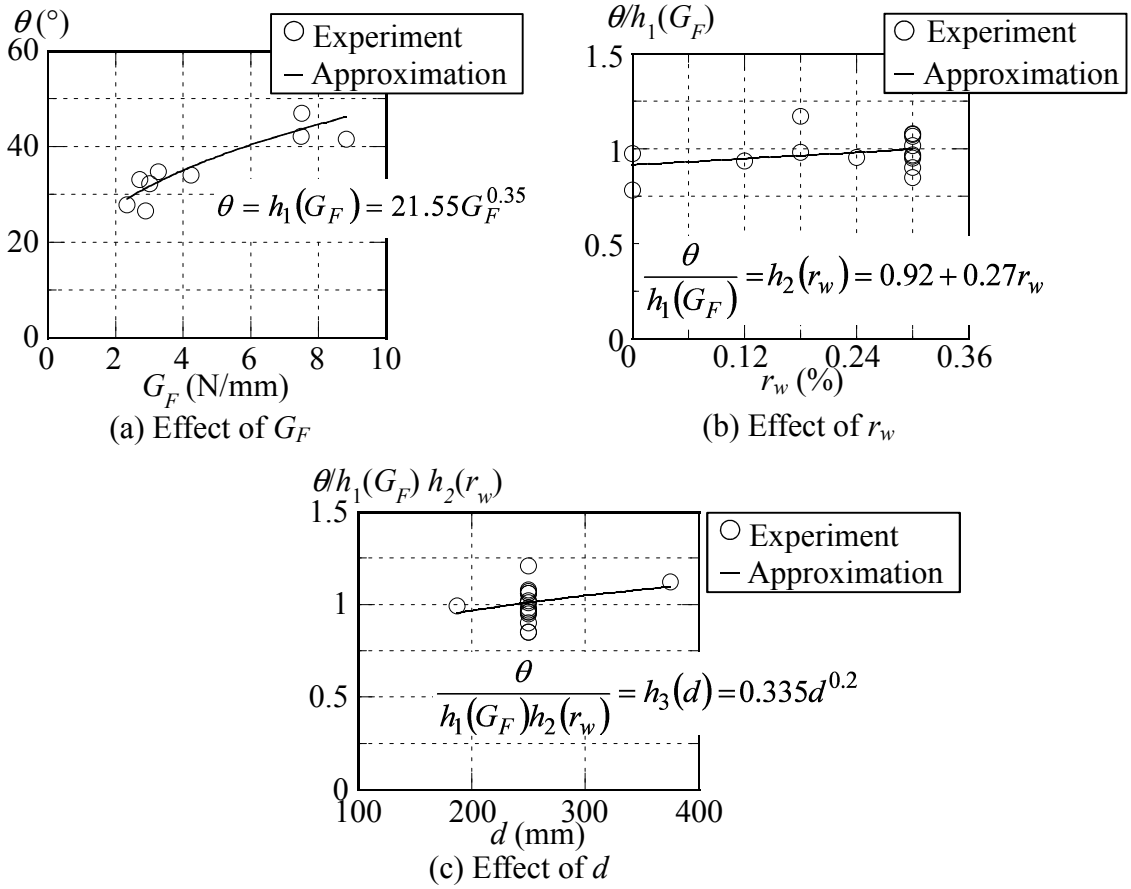

(a) Effect of G_F (b) Effect of r_w

(c) Effect of d

Figure 7.3 Formulation of the equation for angle of diagonal crack

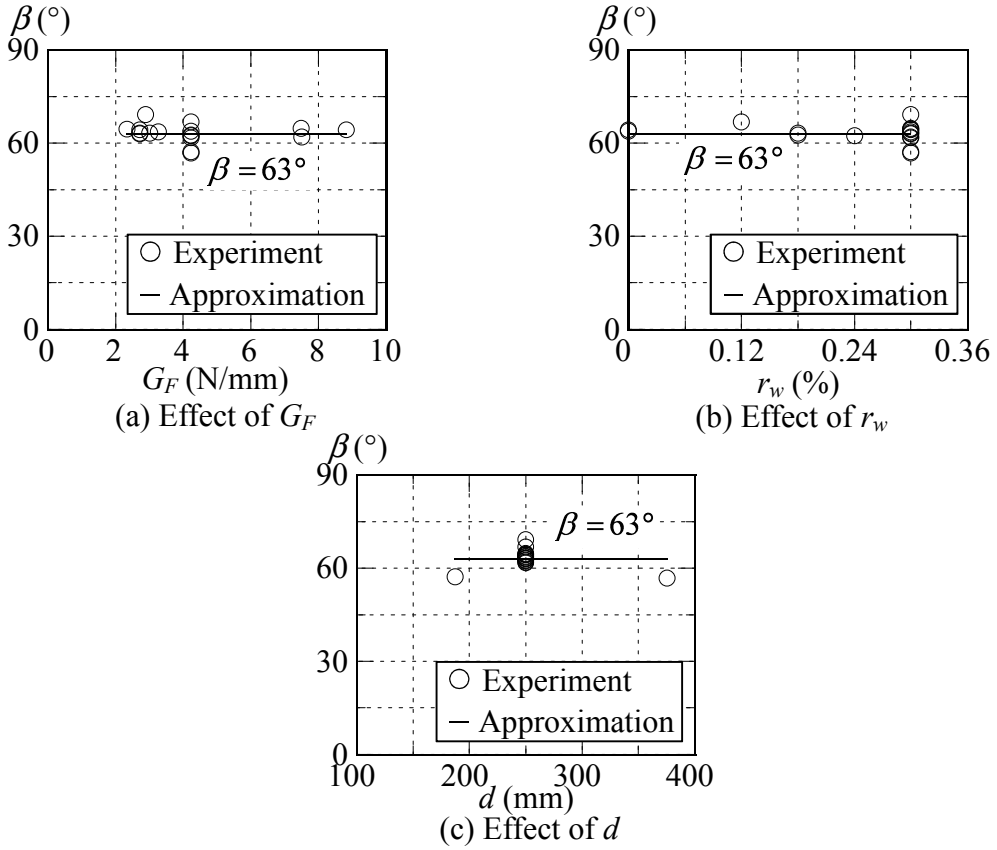

(a) Effect of G_F (b) Effect of r_w

(c) Effect of d

Figure 7.4 Formulation of the equation for angle of principal tensile strain

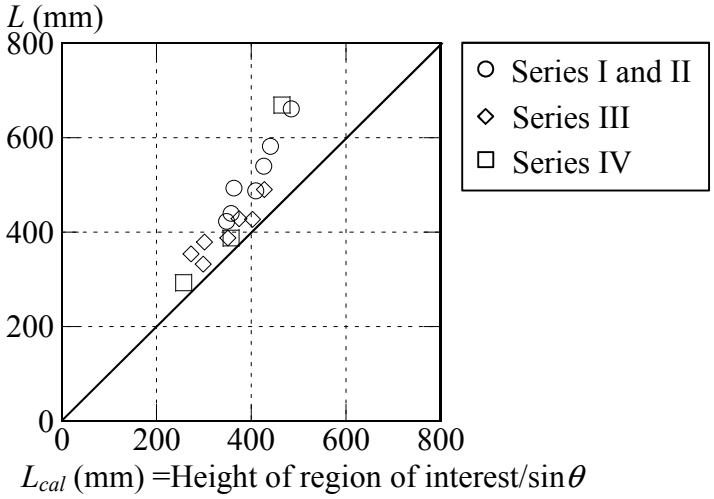

Figure 7.5 Comparison of the values of diagonal crack length

The formulation is explained step by step. Firstly, the effect of G_F on σ was demonstrated by the function $f_1(G_F)$ as shown in **Fig. 7.1(a)**. Secondly, the effect of G_F was excluded by dividing σ by $f_1(G_F)$ and the effect of r_w on $\sigma/f_1(G_F)$ was represented by the function $f_2(r_w)$ as shown in **Fig. 7.1(b)**. Lastly, the effects of both G_F and r_w were excluded by dividing σ by $f_1(G_F)f_2(r_w)$ and the effect of d on $\sigma/f_1(G_F)f_2(r_w)$ was formulated by the function $f_3(d)$ as presented in **Fig. 7.3(c)**. The formula of σ was obtained from these steps. The formulas for the effects of G_F, r_w and d on σ are written in the figures and can be expressed as Eq. (7.2).

$$\sigma = f_1(G_F) f_2(r_w) f_3(d) = G_F^{0.8}\left(8.2 + 3.1 r_w\right) \cdot d^{-0.58} \tag{7.2}$$

Focusing on the values of L and θ, it was found that value of the actual diagonal crack length (L) in the region of interest is more than the value of crack length that is computed from θ (L_{cal}=Height of region of interest/sinθ) as shown in **Fig. 7.5**. It is because the diagonal crack of FRC beams was not a perfectly straight line. The shape of crack in each layer was sometimes curved. In addition, as presented in **Chapter 5** (Section 5.6.2), the value of L/d increased with the increase in d. Therefore, in order to present the actual behavior and investigate precisely, the value of diagonal crack should not be calculated from the angle of diagonal crack. As a result, the formulas of L and θ were separately formulated in this study. By using the same procedures, the formulas of L and θ were formulated as shown in **Figs. 7.2** and **7.3**. The results revealed that the value of L decreased with the increase in G_F and r_w as illustrated in **Figs. 7.2(a)** and **(b).** Equations of diagonal crack length (L) and angle of diagonal crack (θ) of FRC beams were proposed as Eqs. (7.3) and (7.4), respectively.

$$L = g_1(G_F)g_2(r_w)g_3(d) = G_F^{-0.25}(1.0 - 0.9r_w)\cdot d^{1.2} \tag{7.3}$$

$$\theta = h_1(G_F)h_2(r_w)h_3(d) = G_F^{0.35}(6.6 + 1.95r_w)\cdot d^{0.2} \tag{7.4}$$

The equations are basically empirical based on the experimental results. However, the behavior of diagonal crack is also taken into account in the selection of function. The power function was used to express the effects of G_F and d on σ, L and θ. It is because the increment of σ, L and θ due to the effects of G_F and d became less when the values of G_F and d became higher. The reverse tendency was observed for the effect of d on L. The use of linear function will lead the misestimating of these values. As a result, power function was selected.

Figure 7.4 presents the relation between angle of principal tensile strain (β) and G_F, r_w and d. β did not significantly change among all specimens. Thus, β is proposed to be constant and equal to 63 degree.

$$\beta = 63° \tag{7.5}$$

By substituting β = 63 degree in Eq. (7.1), Eq. (7.6) is obtained. Besides, from the relationships obtained from **Figs. 7.1** to **7.4**, the equations for each variable can be expressed as Eq. (7.2), Eq. (7.3) and Eq. (7.4).

Therefore, the shear carried by fibers can be formulated by Eq. (7.6).

$$V_f = 0.89\ \sigma \cdot b_w \cdot L \cdot \cos(\theta - 27°) \tag{7.6}$$

where,

$$\sigma = G_F^{0.8}(8.2 + 3.1r_w)\cdot d^{-0.58}$$

$$L = G_F^{-0.25}(1.0 - 0.9r_w)\cdot d^{1.2}$$

$$\theta = G_F^{0.35}(6.6 + 1.95r_w)\cdot d^{0.2}$$

G_F , r_w and d are in N/mm, % and mm, respectively.

It is noted that these equations were derived based on the authors' experimental data. In order to clarify the applicability of the proposed equations and to confirm the range of application, the equations are validated with specimens of other researchers. The validation is explained in Sections 7.4 and 7.5.

7.3 Equations for the Shear Capacity of FRC Beams

The shear capacity of FRC beams with stirrups and various fiber types and combinations can be predicted by using the following equations. The shear capacity of FRC beams consisted of three components that are the shear capacity of members without shear reinforcement (V_c), the shear carried by stirrups (V_s) and the shear carried by fibers (V_f) as shown in Eq. (7.7).

$$V = V_c + V_s + V_f \tag{7.7}$$

$$V_c = 0.2 \cdot \sqrt[3]{f'_c} \cdot \sqrt[4]{1000/d} \cdot \sqrt[3]{100 p_w} \cdot b_w \cdot d \tag{7.8}$$

$$V_s = A_w f_{wy} \left(z \cot \theta / s\right) \tag{7.9}$$

V_c can be calculated from Eq. (7.8) following the JSCE design guidelines (1999). V_s is Eq. (7.9). The angle of diagonal crack for calculating V_s is obtained from Eq. (7.4). Moreover, the shear carried by fibers is Eq. (7.6). It is noted that the equations of V_c and V_s are the same equations that are used in the calculation of shear forces in **Chapter 5** (Section 5.2). Only V_f is proposed and added in Eq. (7.7). Therefore, as long as this set of equations is used together, the shear capacity can be predicted.

7.4 Accuracy of the Existing Equations

The experimental results of the total of 43 beams including specimens from this study (**Table 7.1**) and specimens of other researchers, which are Watanabe et al. (2010b), Kodama et al. (2004), Kodama et al. (2005), Dinh et al. (2011) and Sharma (1986), were collected. All of the papers that tested the FRC beams and reported the values of the fracture energy have been used for the validation already. The specimens from other studies were fiber reinforced concrete beams with different types of fibers and dimensions. The details of specimens from other investigators are shown in **Table 7.3**. Steel fibers had round cross section and polypropylene fibers (PP) were rectangular. The experimental results of all specimens were validated with the calculated shear capacity from the existing equations listed in **Table 7.4**. The equations were explained in **Chapter 2**. Equations (7.12)-(7.16) were proposed based on the FRC beams without stirrups. Therefore, in order to calculate the shear capacity of FRC beams with stirrups, the shear carried by stirrups was calculated following the equation

Table 7.3 Details of specimens from other researchers

Reference	Specimen	b_w (mm)	d (mm)	a/d	p_w (%)	r_w (%)	Type of fibers	L_f (mm)	D_f (mm)	ρ_f (%)	f'_c (MPa)	f_t (MPa)	G_F (N/mm)
Watanabe et al. (2010b)	SF03-r18-B	150	250	2.8	2.7	0.18	Steel	30	0.6	0.3	51.5	3.5	1.48[a)]
	SF05-r24-B					0.24	Steel			0.5	79.9	4.2	2.42[a)]
	SF05-r30-B					0.30	Steel			0.5	79.9	4.2	2.42[a)]
	SF08-r12-B					0.12	Steel			0.75	83.7	4.9	3.78[a)]
	SF08-r18-B					0.18	Steel			0.75	83.7	4.9	3.78[a)]
	SF10-r12-B					0.12	Steel			1.0	85.5	4.4	2.95[a)]
	SF10-r18-B					0.18	Steel			1.0	85.5	4.4	2.95[a)]
	SF10-r24-B					0.24	Steel			1.0	57.5	3.3	2.66[a)]
	SF10-r30-B					0.30	Steel			1.0	57.5	3.3	2.66[a)]
Kodama et al. (2004)	ST05	100	200	3.5	1.29	0.0	Steel	30	0.6	0.5	34.4	2.8	2.17
	ST10						Steel			1.0	31.2	2.0	5.13
	ST15						Steel			1.5	31.4	2.0	4.99
	ST30						Steel			3.0	30.0	2.5	6.01
	ST+PP15						Steel+ PP	-	-	3.0	36.0	2.5	7.17
Kodama et al. (2005)	25-200-A	100	200	2.5	1.94	0.0	Steel	30	0.6	1.0	24.7	2.0	4.04
	35-200-A			3.5			Steel			1.0	40.7	3.0	5.19
	45-200-A			4.5			Steel			1.0	31.6	2.5	4.54
	35-200-B			3.5	3.97		Steel			1.0	29.9	2.3	4.50
	35-400-A	200	400	3.5	1.99		Steel			1.0	29.9	2.4	4.38
Dinh et al. (2011)	B18-2a	152	381	3.5	2.0	0.0	Steel	30	0.55	1.0	38.1	3.3[b)]	2.81[c)]
	B18-2b						Steel			1.0	38.1	3.3[b)]	2.81[c)]
	B18-2c				2.7		Steel			1.0	38.1	3.3[b)]	2.81[c)]
	B18-2d						Steel			1.0	38.1	3.3[b)]	2.81[c)]
Sharma (1986)	S3F	150	271	1.9	2.45	0.0	Steel	50	0.6	1.0	48.6	6.5	7.98[d)]
	D3F					0.21	Steel			1.0	47.7	5.8	8.11[d)]
	D4F						Steel			1.0	43.2	6.5	8.81[d)]

b_w: web thickness, d: effective depth, a/d: shear span to effective depth ratio, p_w: longitudinal reinforcement ratio ($=A_s/b_w d$), r_w: stirrup ratio, L_f: fiber length, D_f: diameter of fibers, ρ_f: fiber volume fraction, f'_c: the compressive strength of the concrete, G_F: fracture energy, [a)] Kimura (2008), [b)] calculated from equation proposed by Narayanan and Darwish (1987) ($f_t = f'_c/(20-\sqrt{F})+0.7+\sqrt{F}$), [c)] referred G_F from Kurihara et al. (2000) and [d)] referred G_F from Bencardino et al. (2010).

Table 7.4 Existing equations for the shear capacity of FRC beams

Reference	Equations for the shear capacity of FRC beams	
JSCE (1999)	$V_{JSCE} = 0.2 \cdot (1+\kappa) \cdot \sqrt[3]{f'_c} \cdot \sqrt[4]{1000/d} \cdot \sqrt[3]{100\,p_w} \cdot b_w \cdot d + V_s$ $V_s = (A_w f_{wy} z)/s$ and κ=1	(7.10)
ACI (1999)	$V_{ACI} = \frac{2}{3} f_t \left(\frac{d}{a}\right)^{0.25} b_w d + \frac{A_w f_{wy} d}{s}$	(7.11)
Narayanan and Darwish (1987)	$V_{Nar} = \left[e\left(0.24 f_t + 80 p_w \frac{d}{a}\right) + 0.41\tau F \right] b_w d$ e=1 for a/d >2.8 or e=2.8d/a for other cases	(7.12)
Ashour et al. (1992)	$V_{Ash} = \left[\left(0.7\sqrt{f'_c} + 7F\right)\frac{d}{a} + 17.2 p_w \frac{d}{a} \right] b_w d$	(7.13)
Khuntia et al. (1999)	$V_{Khu} = \left[(0.167 + 0.25F)\sqrt{f'_c} \right] b_w d$	(7.14)
Kwak et al. (2002)	$V_{Kwak} = \left[2.1 e f_t^{0.7} \left(p_w \frac{d}{a} \right)^{0.22} + 0.8(0.41\tau F)^{0.97} \right] b_w d$ e=1 for a/d >3.5 or e=3.5d/a for other cases	(7.15)
Greenough and Nehdi (2008)	$V_{Gre} = \left[0.167\sqrt{f'_c} + \frac{L_f}{D_f} \rho_f p_w \frac{d}{a} + 0.369\tau \frac{L_f}{D_f} \rho_f \right] b_w d$	(7.16)

f'_c: compressive strength of concrete (MPa), f_t: split cylinder strength of fiber concrete (MPa), b_w: web thickness (mm), d: effective depth (mm), a: shear span (mm), p_w: the amount of tensile reinforcement ($p_w = A_s/bd$), τ: fiber-matrix interfacial bond stress between the fiber and corresponding concrete (τ= 4.15 MPa), F: fiber factor ($F=(L_f/D_f)\rho_f d_f$), L_f: fiber length (mm), D_f: fiber diameter (mm), ρ_f: volume percentage of fibers (%), d_f: bond factor, A_w: the total cross-sectional area of stirrups provided in the range of s (mm^2), f_{wy}: the yield strength of stirrups (MPa) and z = 7d/8.

proposed by JSCE (1999). The ratio between the shear capacity from the experiments and the calculated results of the shear capacity obtained by the existing equations in **Table 7.4** were calculated and summarized in **Table 7.5** and **Table 7.6**. **Figure 7.6** presents the accuracy of the JSCE and ACI equations while **Fig. 7.7** shows accuracy of the existing equations proposed by other researchers. The average of the ratio (*Avg.*) and a coefficient of variation (*C.V.*) are also presented in these figures.

The JSCE equation underestimates the capacities of FRC beams in all specimens, especially the specimens without stirrups. The average value is 1.22. The coefficient of variation (*C.V.*)

Table 7.5 Comparison of the shear capacity from the experiments and calculation (Author's specimens)

Specimen	V_{exp} (kN)	V_{exp}/V_{JSCE}	V_{exp}/V_{ACI}	V_{exp}/V_{Nar}	V_{exp}/V_{Ash}	V_{exp}/V_{Khu}	V_{exp}/V_{Kwak}	V_{exp}/V_{Gre}	V_{exp}/V_{pre}
SF30-05-r00	122.4	1.10	2.26	1.86	1.33	1.95	1.48	2.04	1.07
SF30-05-r18	126.9	1.01	1.74	1.52	1.20	1.64	1.29	1.67	0.91
SF30-05-r30	156.5	1.05	1.58	1.53	1.22	1.58	1.28	1.64	0.97
SF30-10-r00	141.1	1.19	1.87	1.62	1.22	1.62	1.27	1.80	1.06
SF30-10-r12	155.5	1.26	1.72	1.55	1.28	1.70	1.26	1.80	1.09
SF30-10-r18	136.8	1.09	1.54	1.34	1.11	1.47	1.12	1.52	0.93
SF30-10-r24	143.1	1.07	1.55	1.34	1.09	1.42	1.14	1.47	0.94
SF30-10-r30	158.8	1.10	1.66	1.42	1.12	1.41	1.24	1.49	0.99
SF60-10-r30	196.3	1.33	1.84	1.57	1.24	1.52	1.35	1.65	1.13
PP-10-r30	170.8	1.18	1.78	1.69	1.34	1.75	1.41	1.81	1.09
PVA-10-r30	166.8	1.11	1.77	1.64	1.24	1.59	1.39	1.54	1.05
PET-10-r30	149.9	1.06	1.61	1.49	1.20	1.57	1.27	1.48	0.97
30&PP-10-r30	151.2	1.06	1.71	1.46	1.14	1.46	1.29	1.52	0.96
60&PP-10-r30	151.3	1.08	1.47	1.32	1.10	1.41	1.13	1.46	0.91
30&60-10-r30	138.7	1.04	1.72	1.27	1.00	1.30	1.18	1.32	0.85
SF30-10-r32-S	92.4	1.07	1.54	1.39	1.15	1.45	1.19	1.51	0.92
SF30-10-r30-L	356.0	1.16	1.54	1.38	1.07	1.33	1.20	1.40	1.07

V_{exp}: the shear capacity from the experiments.

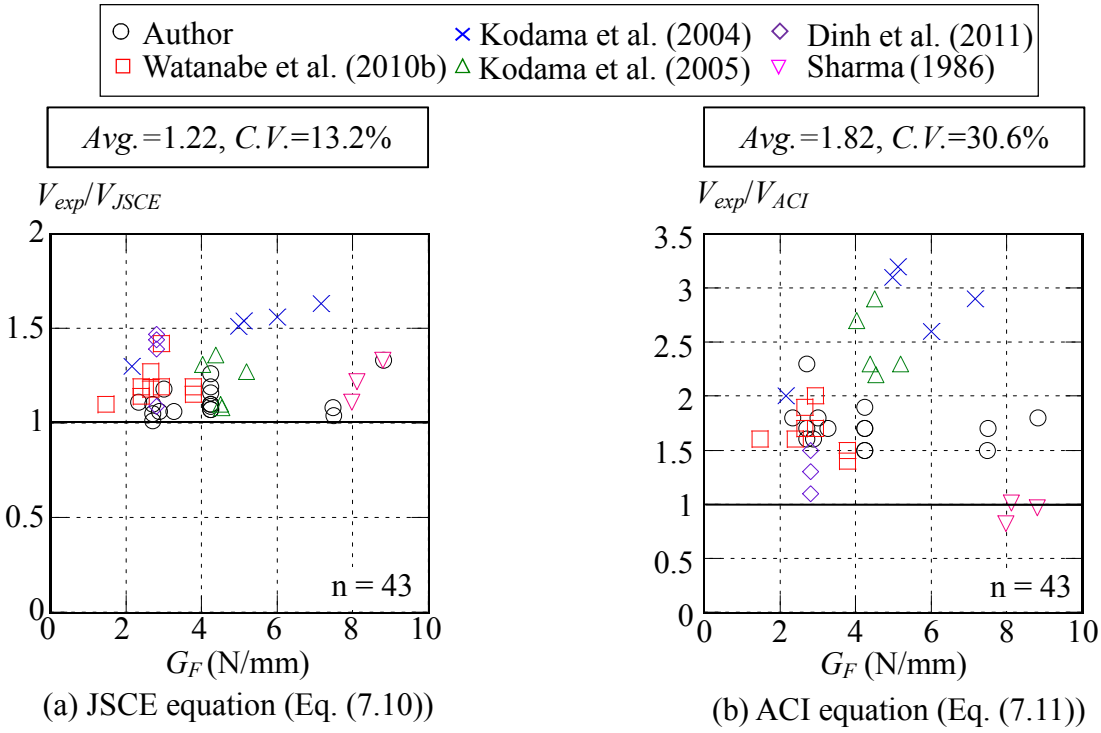

(a) JSCE equation (Eq. (7.10)) (b) ACI equation (Eq. (7.11))

Figure 7.6 Accuracy of existing equations in the design guidelines

Table 7.6 Comparison of the shear capacity from the experiments and calculation (Specimens from other researchers)

Reference	Specimen	V_{exp} (kN)	V_{exp}/V_{JSCE}	V_{exp}/V_{ACI}	V_{exp}/V_{Nar}	V_{exp}/V_{Ash}	V_{exp}/V_{Khu}	V_{exp}/V_{Kwak}	V_{exp}/V_{Gre}	V_{exp}/V_{pre}
Watanabe et al. (2010b)	SF03-r18-B	145.0	1.10	1.58	1.63	1.37	1.89	1.29	1.93	1.03
	SF05-r24-B	177.9	1.14	1.57	1.66	1.30	1.68	1.32	1.79	1.10
	SF05-r30-B	193.7	1.19	1.60	1.70	1.35	1.72	1.36	1.82	1.13
	SF08-r12-B	171.2	1.19	1.53	1.62	1.29	1.65	1.25	1.83	1.13
	SF08-r18-B	173.0	1.15	1.44	1.53	1.24	1.56	1.20	1.72	1.08
	SF10-r12-B	172.4	1.19	1.71	1.62	1.21	1.49	1.30	1.70	1.18
	SF10-r18-B	215.6	1.42	1.98	1.90	1.44	1.75	1.54	1.99	1.38
	SF10-r24-B	181.2	1.27	1.89	1.63	1.28	1.62	1.40	1.72	1.16
	SF10-r30-B	176.5	1.18	1.69	1.49	1.19	1.48	1.29	1.57	1.07
Kodama et al. (2004)	ST05	55.0	1.30	2.02	2.14	1.71	2.04	1.81	2.02	1.08
	ST10	63.0	1.54	3.22	2.23	1.63	1.93	2.08	1.85	0.93
	ST15	61.9	1.51	3.13	1.78	1.34	1.56	1.75	1.48	0.92
	ST30	63.2	1.56	2.65	1.13	0.93	1.06	1.19	0.98	0.88
	ST+PP15	70.1	1.63	2.93	1.48	1.17	1.28	1.51	1.26	0.90
Kodama et al. (2005)	25-200-A	57.1	1.31	2.65	1.52	1.11	1.97	1.31	1.78	0.90
	35-200-A	65.4	1.27	2.27	1.82	1.54	1.76	1.68	1.78	0.89
	45-200-A	50.9	1.08	2.20	1.60	1.66	1.55	1.47	1.49	0.75
	35-200-B	64.9	1.10	2.92	1.55	1.59	2.03	1.70	1.93	0.88
	35-400-A	214.4	1.36	2.31	1.61	1.38	1.68	1.53	1.59	1.01
Dinh et al. (2011)	B18-2a	173.7	1.39	1.26	1.54	1.39	1.60	1.41	1.60	1.24
	B18-2b	179.5	1.44	1.30	1.59	1.44	1.66	1.46	1.66	1.28
	B18-2c	202.7	1.47	1.47	1.66	1.60	1.87	1.57	1.87	1.38
	B18-2d	150.6	1.09	1.09	1.23	1.19	1.39	1.17	1.39	1.02
Sharma (1986)	S3F	122.6	1.11	0.82	0.62	0.59	1.15	0.47	1.23	0.76
	D3F	154.5	1.22	1.01	0.75	0.69	1.27	0.60	1.33	0.94
	D4F	163.8	1.33	0.97	0.76	0.75	1.40	0.60	1.44	0.99

V_{exp}: the shear capacity from the experiments.

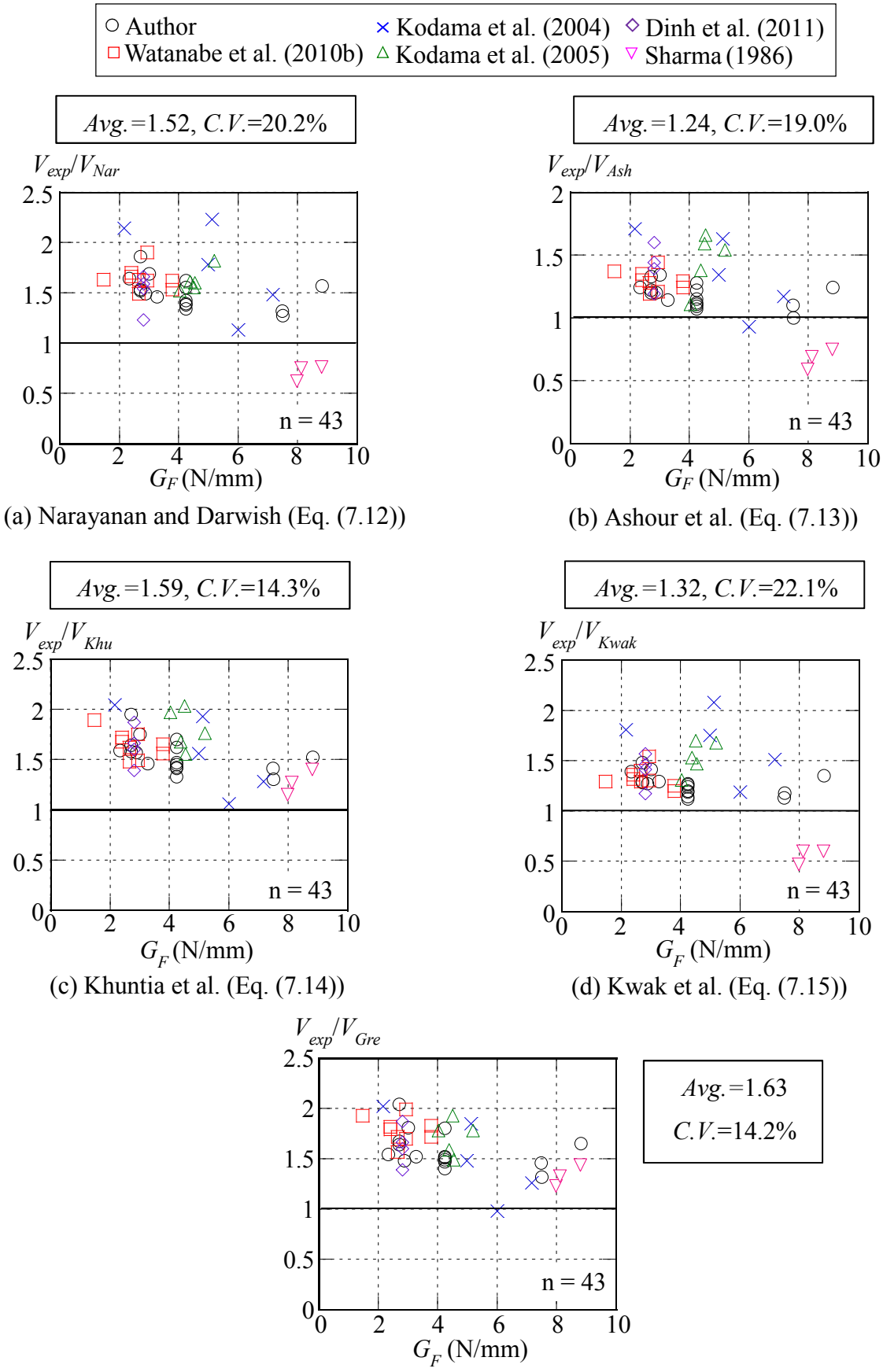

(a) Narayanan and Darwish (Eq. (7.12))

(b) Ashour et al. (Eq. (7.13))

(c) Khuntia et al. (Eq. (7.14))

(d) Kwak et al. (Eq. (7.15))

(e) Greenough and Nehdi (Eq. (7.16))

Figure 7.7 Accuracy of the equations proposed by other researchers

is 13.2%. Even though the specimens whose the experimental values of κ_{exp} are less than 1.0 (This means that the shear carried by fibers (V_f) is overestimated), JSCE equation underestimates the total shear capacity. It is because the shear carried by stirrups (V_s) is underestimated by assuming 45 degree for angle of diagonal crack (θ). Nevertheless, in this study, the value of θ is not constant at 45 degree and θ is recommended based on the experimental results, which is more physically correct concept. Furthermore, V_f is precisely investigated based on the post-cracking behavior of fiber reinforced concrete. As a result, V_s and V_f are accurately considered in this study.

The accuracy of ACI equation (Eq. (7.11)) is shown in **Fig. 7.6(b)**. ACI equation considerably underestimates the shear capacity of FRC beams as observed in the *Avg.*=1.82 and *C.V.*=30.6%. The accurate prediction is obtained only for the specimens of Sharma (1986) as the ACI equation was originally formulated by Sharma (1986). ACI equation considered only the effects of f_t and *a/d* for evaluating the shear carried by concrete and fibers. As a result, the equation is inaccurate and gives large scattering.

All equations proposed by other researchers (Eqs. (7.12)-(7.16)) underestimate the shear capacity of FRC beams as presented in **Fig. 7.7**. It is because Eqs. (7.12)-(7.16) developed based on the test results of FRC beams without stirrups. In addition, considering only the effects of f_t or fiber factor (F) are not enough to predict the shear carried by fibers precisely. Among the equations, Eq. (7.13) that proposed by Ashour (1992) gives the best average value (*Avg.*=1.24) but the equation shows large variation as *C.V.*=19.0%. On the other hand, the variation is relatively small for the equations proposed by Khuntia et al. (1999) ((Eq. (7.14)) and Greenough and Nehdi (2008) (Eq. (7.16)) but the accuracy is low since the averages of V_{exp}/V_{Khu} and V_{exp}/V_{Gre} are 1.59 and 1.63, respectively. Nevertheless, Eqs. (7.12), (7.13) and (7.14), which required the fiber factor (F), overestimate the shear capacity of Sharma's specimens. This imply that the fiber factor (F) proposed in their studies and used in the equations may not appropriate for all fiber types. Based on these evaluations, the existing equations are not accurate enough to evaluate the shear capacity of FRC beams.

7.5 Accuracy of the Proposed Equations

The proposed equations (Eqs. (7.7), (7.8), (7.9) and (7.6)) was validated by the total of 43 FRC beams. The same database used in Section 7.4 is utilized for the verification. The

predicted shear capacity (V_{pre}) was calculated from the proposed equations (Eqs. (7.7), (7.8), (7.9) and (7.6)).

Dinh et al. (2011) and Sharma (1986) did not report the values of fracture energy of their specimens. Consequently, G_F were referred from Kurihara et al. (2000) and Bencardino et al. (2010), which are the papers testing G_F of the steel fibers having the same length, aspect ratio, end type and volume fraction with the steel fibers used in Dinh et al. (2011) and Sharma (1986), respectively. **Table 7.7** lists the detail of fibers, concrete properties and fracture energy of Kurihara et al. (2000) and Bencardino et al. (2010).

The effect of difference in compressive strength of concrete (f'_c) on G_F was adjusted following the JSCE design guidelines (1999). According to the JSCE design guidelines (1999), the tension softening curves of steel fiber reinforced concrete can be drawn as shown in **Fig. 7.8**. Based on **Fig. 7.8**, G_F, which is the area under the tension softening curve, can be computed from Eq. (7.17). It is noted that G_F is size-independent material property. The influence of the specimen size on the fracture energy could not be observed (Kurihara et al., 2000).

$$G_F = \frac{1}{2}\mu f_t\left(1.4 + 100/f'_c\right) \tag{7.17}$$

By focusing on tensile strength (f_t) of fiber reinforced concrete, Wafa and Ashour (1992) reported that f_t of FRC consisted of the effect of f'_c and the effect of fibers, which depended on the volume fraction of fibers (ρ_f) only, as shown in Eq. (7.18).

$$f_{t,FRC} = g\left(f'_c\right) + h\left(\rho_f\right) \tag{7.18}$$

Table 7.7 Referred fracture energy

Reference	Type of fibers	L_f (mm)	Aspect ratio	End types	ρ_f (%)	f'_c (MPa)	f_t (MPa)	G_F (N/mm)
Kurihara et al. (2000)	Steel	30	50	Hooked	1.0	48.6	4.0	2.2
Bencardino et al. (2010)	Steel	50	80	Hooked	1.0	80.5	7.1	5.2

L_f: fiber length, ρ_f: fiber volume fraction, f'_c: the compressive strength of the concrete, f_t: tensile strength from split tensile test and G_F: fracture energy.

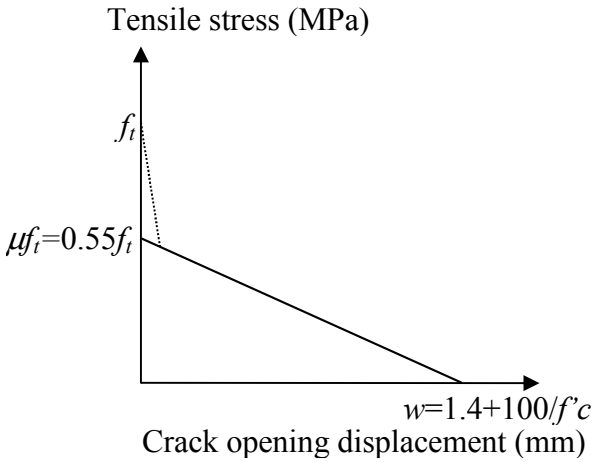

Figure 7.8 Tension softening curve proposed by JSCE design guidelines (1999)

As there was no change in ρ_f when compared specimens of Dinh et al. (2011) with Kurihara et al. (2000) and Sharma (1986) with Bencardino et al. (2010), the effect of fibers on f_t was the same. As a result, only the influence of change in f'_c on f_t is needed to be calibrated. From the JSCE standard specifications for plain concrete (2010), the effect of f'_c on f_t for plain concrete can be calculated from Eq. (7.19).

$$f_t = 0.23 f'^{\,2/3}_c \tag{7.19}$$

If f'_c changes from f'_{c1} to f'_{c2}, the value of f_{t1} will become f_{t2} as shown in Eq. (7.20).

$$f_{t2} = f_{t1} + 0.23\left(f'^{\,2/3}_{c2} - f'^{\,2/3}_{c1}\right) \tag{7.20}$$

Based on Eq. (7.17), the equation for adjust the fracture energy was derived. The ratio between two values of G_F can be expressed by Eq. (7.21).

$$\frac{G_{F2}}{G_{F1}} = \frac{\frac{1}{2}\mu f_{t2}\left(1.4 + 100/f'_{c2}\right)}{\frac{1}{2}\mu f_{t1}\left(1.4 + 100/f'_{c1}\right)} \tag{7.21}$$

In addition, Eq. (7.22) was derived from Eq. (7.21). Finally, the values of G_{F1}, which were reported by Kurihara et al. (2000) and Bencardino et al. (2010), were used to adjust the difference of f'_c by Eq. (7.22) and became G_{F2}. The referred G_F (=G_{F2}) of those specimens are listed in **Table 7.3**.

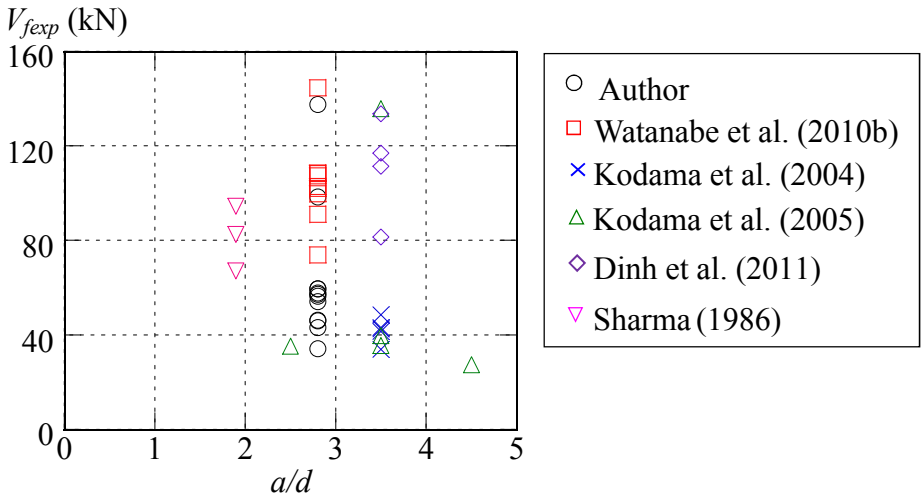

Figure 7.9 Effect of *a/d* on shear carried by fibers

$$G_{F2} = \frac{f_{t2}\left(1.4+100/f'_{c2}\right)}{f_{t1}\left(1.4+100/f'_{c1}\right)} G_{F1} \tag{7.22}$$

where f'_{c1}, f_{t1} and G_{F1} are the values of the f'_c, f_t and G_F reported by Kurihara et al. (2000) or Bencardino et al. (2010), f'_{c2} is f'_c of Dinh et al. (2011) or Sharma (1986), f_{t2} is Eq. (7.20) and G_{F2} is the adjusted fracture energy.

The comparison between the experimental results and calculated results obtained from the proposed equations is listed in **Table 7.5** and **Table 7.6**. In the proposed equation, the shear carried by fibers can be calculated from fracture energy, stirrup ratio and the effective depth of beams. The effect of *a*/*d* was not included because there was no clear pattern of the effect of *a*/*d* on shear carried by fibers of 43 FRC beams ($1.9 \le a/d \le 4.5$) as shown in **Fig. 7.9**. In addition, the proposed equation was confirmed its applicability with 43 FRC beams with various *a*/*d* from 1.9 to 4.5. Good correlation between the experimental results and calculated results can be obtained. Therefore, the proposed equation can be used in the range of $1.9 \le a/d \le 4.5$, which are the beams that failed in the diagonal tension.

The accuracy of the proposed equation validated by the total of 43 FRC beams is shown in **Fig. 7.10**. The average of the ratio of experimental values to predicted values (V_{exp}/V_{pre}) is 1.02 with *C.V.* of 13.7%. The proposed equation demonstrates the best mean ratio among all existing equations listed in **Table 7.4** and gives the same level of the coefficient of variation with JSCE equation. Although the JSCE equation reveals low variation, the JSCE equation predicts the shear carried by fibers directly from the shear carried by concrete (V_c) and κ;

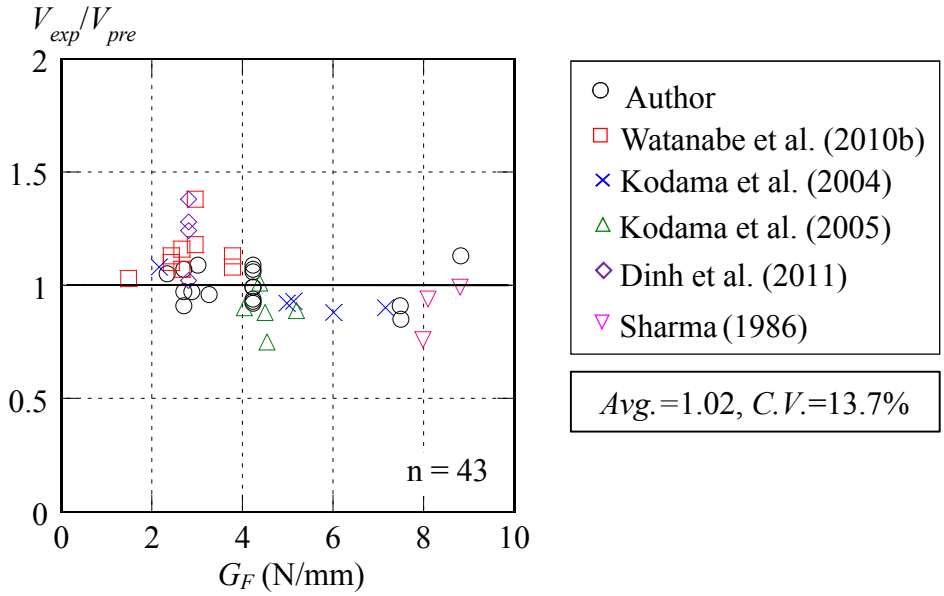

Figure 7.10 Accuracy of the proposed equation

which has no theoretical background. Using V_c to represent V_f does not agree with the actual behavior of shear carried by fibers. It is because the shear carried by fibers does not depend on p_w and f'_c but it depends on G_F, r_w and d. The proposed equation will provide a better *C.V.* if the parameters that have not been thoroughly focused are considered such as the effect of compressive strength of concrete on the shear carried by fibers, which is assumed to be perfectly represented by the fracture energy in this study. However, the proposed equation offers precise mean ratio with the acceptable coefficient of variation. In addition, by using the fracture energy, the fibers types, fiber properties and fiber volume fraction can be represented. Therefore, the proposed equation can generally cover all types of fibers.

In conclusion, the proposed equation can predict the shear capacity of FRC beams more accurately than the existing equations such as JSCE equation, ACI equation and equations proposed by other researchers. The proposed equation can be applied in not only steel but also synthetic and hybrid fiber reinforced concrete beams both with and without stirrups. This equation can be utilized in the FRC beams with following values: 1.5 N/mm ≤ G_F ≤ 8.8 N/mm, 0.0% ≤ r_w ≤ 0.3% and 187.5 mm ≤ d ≤ 400 mm. The proposed equation was confirmed the applicability with the beams having 1.9 ≤ a/d ≤ 4.5. For FRC beams which the effective depth exceeds 400 mm, more experimental data are required to confirm the applicability of the equation. This range of G_F covers concrete strength for 24.7 ≤ f'_c ≤ 85.5 MPa, 0.3% ≤ ρ_f ≤ 3.0% and fibers having length between 0.3-0.6 mm. Both round fibers (diameter between

0.55-0.9 mm) and rectangular fibers are also in the range. In general, the proposed equation can be employed in more cases when compared with the existing JSCE equation because it can be applied for various fiber types, fiber geometry and volume fractions.

7.6 Conclusions of Chapter 7

The equation for the shear capacity of fiber reinforced concrete beams was proposed. The shear capacity consists of shear carried by members without shear reinforcement, the shear carried by stirrups and shear carried by fibers. The shear carried by members without shear reinforcement can be calculated using the equation proposed by JSCE (1999). The shear carried by stirrups was computed based on the truss model. The angle of diagonal crack of the FRC beams can be calculated from the proposed equation. The predictive equation for shear carried by fibers was formulated. The average value of stress, angle of diagonal crack, angle of principal tensile strain in the region of interest were used for the formulations. The total diagonal crack length in the region of interest was considered in the equation. By using the proposed simplified equation, the image analysis is no longer needed to predict the shear carried by fibers. The predictive equation for shear capacity of FRC beams was verified by comparisons with existing test results of 43 FRC beams from the author and other investigators. The proposed equation gave higher accuracy (*Avg.*=1.02) with low variation (*C.V.*=13.7%) when compared with other existing equations. In contrast with the JSCE equation, the equation for shear capacity proposed in this study considered the post-cracking behavior of fiber reinforce concrete in detail and can be applied for various fiber reinforced concrete beams. In summary, the proposed equation was found to be able to accurately predict the shear capacity of fiber reinforced concrete beams with and without stirrups. In addition, the equation can be used for various types and combinations of fibers.

CHAPTER 8

CONCLUSIONS

8.1 General Conclusions

Shear behavior of fiber reinforced concrete (FRC) beams is explained by the knowledge of fracture mechanics in this study. The stress transferred across the diagonal crack at the peak load was investigated using the crack surface displacements, which were measured from the image analysis, and tension softening curves, which were obtained from the notched beam tests. Seventeen FRC beams were prepared and tested under four-point bending. The specimens were varied in fiber volume fractions (0.5 and 1.0% of fiber volume to concrete volume), stirrup ratios (0.0, 0.12, 0.18, 0.24 and 0.30%), types and combinations of fibers (30-mm steel fibers, 60-mm steel fibers, polypropylene fibers, polyvinyl alcohol fibers, PET fibers, hybrids fibers between 30-mm steel and polypropylene, 60-mm steel and polypropylene and 30-mm steel and 60-mm steel) and effective depths (187.5, 250 and 375 mm). The influences of these parameters on shear capacity of FRC beams were investigated. The tensile stress transferred across the diagonal crack was calculated. The diagonal crack length, angle of diagonal crack and angle of principal tensile strain were measured.

The shear failure occurred in all specimens. The shear capacity of FRC beams increased with the increase in fiber volume fraction from 0.5% to 1.0%. It is because the value of shear carried by fibers increased. Nevertheless, the shear capacity did not monotonically increase with the increase in stirrup ratio. Although stirrup ratio enhanced the shear carried by stirrups, the reduction of shear carried by fibers was observed when stirrup ratio increased. The addition of fibers was more beneficial for specimens with less stirrup ratio. Due to these positive and negative effects, the shear capacity, which is the summation of shear carried by a member without shear reinforcement, shear carried by stirrups and shear carried by fibers, did not necessarily improve with the increase in stirrup ratio. There were optimum values between

fiber volume fractions and stirrup ratios to increase the shear capacity. Furthermore, there was no size effect on shear strength of FRC beams within the effective depth between 187.5 to 375 mm.

Steel, synthetic and hybrid fibers significantly enhanced the shear capacity of FRC beams. Among all fiber types, the steel fibers with 60 mm length were the best to enhance the shear capacity of the specimens since the fibers had long length resulting in better bonding between fibers and matrix. Moreover, the steel fibers were the most effective to improve the shear carried by fibers due to their high tensile strength and bonding strength.

Crack surface displacement, which is the total displacement of crack surface on the direction of crack's movement, was measured using the image analysis. The crack surface displacement of diagonal crack of FRC beams was narrower in the top and bottom of specimens because there were compression zone on the top of specimens and tensile reinforcing bar in the bottom of specimens. The crack surface displacement along the height of FRC beams revealed the parabolic shape. In addition, the crack surface displacement was drastically wider just before the peak load. The sudden increase in crack surface displacement may relate to the failure of FRC beams.

Tension softening curves and the fracture energy of various fiber types were investigated from the notched beam tests. Stress transferred across the diagonal crack was computed. More stress was transferred around the top and bottom of specimens because of the smaller crack surface displacement.

Considering the diagonal cracking behavior, the stress, length and angle of diagonal crack were affected by fracture energy of fiber reinforced concrete, stirrup ratio and effective depth of beams. Fracture energy can be one of the indicators to represent the shear strengthening effect on FRC members. Fracture energy and stirrup ratio led the same tendency on the diagonal cracking behavior. The increase in fracture energy or stirrup ratio made the stress and angle of diagonal crack increase but reduced the diagonal crack length. With the increase in specimen size, the stress decreased while the diagonal crack length was longer and the angle of diagonal crack increased.

The shear force carried by fibers was calculated by multiplying tensile stress with the area of crack surface. The calculated shear carried by fibers was verified with the experimental results of 17 FRC beams. Although fiber volume fractions, stirrup ratios, types and combinations of

fibers and effective depths were varied, the evaluation of shear carried by fibers based on fracture mechanics offered a good correlation with the experimental results. This implied that the tension softening curves are applicable for the evaluation of shear carried by fibers.

The predictive equation for shear carried by fibers was formulated. The equation for shear capacity of FRC beams was proposed. The equation was validated with the 43 specimens from author and other researchers. The proposed equation provided the best mean ratio among other existing equations such as the JSCE equation, the ACI equation and the equations proposed by other researchers. The proposed equation can predict the shear capacity of FRC beams accurately. The post-cracking of fiber reinforced concrete was taken into account in the proposed equation. Moreover, the equation can be applied in not only steel but also synthetic and hybrid fiber reinforced concrete beams both with and without stirrups. This equation can be implemented in the FRC beams having the properties as follows: a) fracture energy between 1.5 N/mm to 8.8 N/mm, b) stirrup ratio between 0.0% to 0.30% and c) effective depth between 187.5 mm to 400 mm. This range of fracture energy included concrete strength from 24.7 MPa to 85.5 MPa, fiber volume fraction from 0.3% to 3.0% and fibers having length between 0.3-0.6 mm. Both round fibers (diameter between 0.55-0.9 mm) and rectangular fibers are also in the range. In addition, the proposed equation was confirmed its applicability with the beams having a/d from 1.9 to 4.5.

From these findings, this research provides the understanding of the effects of fiber volume fractions, stirrup ratios, fiber types and effective depths on the shear behavior of FRC beams. In addition, the method to evaluate the shear carried by fibers and predictive equation proposed in this study shall help to improve the rational procedure for predicting the shear capacity of FRC members in the future.

8.2 Recommendations for the Further Study

The shear carried by fibers of FRC beams was evaluated using the tension softening curves. In this study, the effects of fiber types and concrete strength were represented by fracture energy even though different failure modes of fibers were observed. In case of fiber rupture, tensile strength of fibers is dominant. On contrary, for the pull-out failure, the shape of fibers and concrete strength may affect the failure. The effect of concrete strength may be different for

different failure modes. However, it was expressed by the same parameter that was fracture energy in this study. Thus, further consideration on this issue is encouraged.

The equation for predicting the shear capacity of FRC beams was proposed based on the experimental results. The applicability of the equation was confirmed in a limit range of each parameter in FRC beams used in this study. In the practical application, some large size of FRC beams is designed. Consequently, in order to apply this equation to the large size of FRC beams, the further study should be carried out to broaden the application rage of the equation.

Moreover, if the predictive equation is applied to columns and piers in the future, the effect of side longitudinal bars should be taken into account. The tested results in this study revealed that the width of diagonal crack became narrower at the position of the tensile bars. Therefore, the effect of side longitudinal bars in columns or piers is not negligible.

In addition, this study covered the fiber reinforced concrete (FRC) beams with various fiber types, fiber volume fractions, specimen sizes and both FRC beams with or without stirrups. However, the shear capacity of fiber reinforced concrete members improves not only by concrete, stirrups and fibers but also by the effectiveness of tensile force in longitudinal tendon. In the JSCE design guidelines, the shear carried by the longitudinal tendons is considered for calculating the shear capacity of FRC members. Since this study focused on the shear capacity of fiber reinforced concrete beams with stirrups, the shear carried by the prestressed force nor the axial load has not been considered yet. In order to promote the wide use of fiber reinforced concrete in many types of members, the further studies on fiber reinforced concrete beams with axial force or prestressed force are suggested. The effect of prestressed force or the stimulation of axial load from the super structures (low prestressed level) on the shear resisting mechanism of FRC beams can be the parameter in the further studies.

REFERENCES

ACI Committee 318 (2008): Building code requirement for structural concrete and commentary, ACI 318-08.

ACI Committee 554 (1999): Design considerations for steel fibers reinforced concrete, ACI 554.4R-88.

ACI Committee 554 (2002): State-of-the-art report on fibers reinforced concrete, ACI 554.1R-96.

Altoubat, S., Yazdanbakhsh, A. and Rieder, K. A. (2009): Shear behavior of macro-synthetic fiber-reinforced concrete beams without stirrups, *ACI Materials Journal*, Vol. 106, No. 4, pp. 381-389.

Ashour, S. A., Hasanain, G. S. and Wafa, F. F. (1992): Shear behavior of high-strength fiber reinforced concrete beams, *ACI Structural Journal*, Vol. 89, No. 2, pp. 176-184.

Balaguru, P., Narahari, R. and Patel, M. (1992): Flexural toughness of steel fiber reinforced concrete, *ACI Material Journal*, Vol. 89, No. 6, pp. 541-546.

Bencardino, F., Rizzuti, L., Spadea, G. and Swamy, R. N. (2008): Stress-strain behavior of steel fiber-reinforced concrete in compression, *Journal of Materials in Civil Engineering*, Vol. 20, No. 3, pp. 255-263.

Bencardino, F., Rizzuti, L., Spadea, G. and Swamy, R.N. (2010): Experimental evaluation of fiber reinforced concrete fracture properties, *Composite Part B: Engineering*, Vol. 41, pp. 17-24.

Bischoff, P. H. (2003): Tension stiffening and cracking of steel fiber-reinforced concrete, *Journal of Materials in Civil Engineering*, Vol. 15, No. 2, pp. 174-182.

Cucchiara, C., Mendola, L. L. and Papia, M. (2004): Effectiveness of stirrups and steel fibers as shear reinforcement, *Cement Concrete and Composites*, Vol. 26, No. 7, pp. 777-786.

Dinh, H. H., Parra-Montesinos, G. J. and Wight, J. K. (2011): Shear strength model for steel fiber reinforced concrete beams without stirrup reinforcement, *Journal of Structural Engineering*, ASCE, Vol. 137, No. 10, pp. 1039-1051.

El-Niema, E. I. (1991): Reinforced concrete beams with steel fibers under shear, *ACI Structural Journal*, Vol. 88, No. 2, pp. 178-183.

Greenough, T. and Nehdi, M. (2008): Shear behavior of fiber-reinforced self-consolidating concrete slender beams, *ACI Materials Journal*, Vol. 105, No. 5, pp. 468-477.

Higashi, H., Watanabe, K. and Niwa, J. (2009): Image analysis for failure mode of RC beams with fractured longitudinal reinforcement, *Proceedings of the JCI*, Vol. 31, No. 2, pp. 727-732. (in Japanese)

Japan Concrete Institute (JCI) (2003a): Method of test for fracture energy of concrete by use of notched beams, JCI-S-001-2003.

Japan Concrete Institute (JCI) (2003b): Method of test for load-displacement curve of fiber reinforced concrete by use of notched beams, JCI-S-002-2003.

Japan Society of Civil Engineers (JSCE) (1999): Guidelines of design for steel fiber reinforced concrete (SFRC) piers, *Concrete Library 97*. (in Japanese)

Japan Society of Civil Engineers (JSCE) (2010): Standard specifications for concrete structures-2007 [Design].

Kimura, T. (2008): Shear reinforcement for RC members by combination of stirrups and steel fibers, Master's thesis, Department of Civil Engineering, Tokyo Institute of Technology, Tokyo, Japan. (in Japanese)

Kitsutaka, Y. (1997): Fracture parameters by poly-linear tension softening analysis, *Journal of Engineering Mechanics*, ASCE, Vol. 123, No. 5, pp. 444-450.

Khuntia, M., Stojadinavic, B. and Goel, S. C. (1999): Shear strength of normal and high-strength fiber reinforced concrete beams without stirrups, *ACI Structural Journal*, Vol. 96, No. 2, pp. 282-289.

Kodama, T., Odera, I. and Niwa, J. (2004): Study on shear carrying capacity of RC beams with short fiber, *Proceeding of the JCI*, Vol. 26, No. 2, pp. 1501-1506. (in Japanese)

Kodama, T., Odera, I. and Niwa, J. (2005): Study on properties of diagonal crack of RC beams with short fiber, *Proceeding of the JCI*, Vol. 27, No. 2, pp. 1327-1332. (in Japanese)

Kurihara, N., Ando, T., Kunieda, M., Uchida, Y. and Rokugo, K. (1996): Determination of tension softening diagram of concrete by poly-linear approximation analysis and failure behavior of fiber reinforced concrete, *Journal of Material, Concrete Structure and Pavements*, JSCE, No. 532, Vol. 30, pp. 119-129. (in Japanese)

Kurihara, N., Kunieda, M., Kamada, T., Uchida, Y. and Rokugo, K. (2000): Tension softening diagrams and evaluation of properties of steel fiber reinforced concrete, *Engineering Fracture Mechanics*, Vol. 65, pp. 235-245.

Kwak, Y.-K., Eberhard, M. O., Kim, W.-S. and Kim, J. (2002): Shear strength of steel fiber-reinforced concrete beams without stirrups, *ACI Structural Journal*, Vol. 96, No. 4, pp. 530-538.

Li, V. C., Ward, R. and Hamaza, A. M. (1992): Steel and synthetic fibers as shear reinforcement, *ACI Materials Journal*, Vol. 89, No. 5, pp. 499-508.

Lim, D. H. and Oh, B. H. (1999): Experimental and theoretical investigation on the shear of steel fiber reinforced concrete beams, *Engineering Structures*, Vol. 21 pp. 937-944.

Mansur, M., Ong, K. and Paramasivam, P. (1986): Shear strength of fibrous concrete beams without stirrups, *Journal of Structural Engineering*, ASCE, Vol. 112, No. 9, pp. 2066-2079.

Nanakorn, P. and Horii, H. (1996): Back analysis of tension-softening relationship of concrete, *Journal of Material, Concrete Structure and Pavements*, JSCE, No. 544, Vol. 32, pp. 265-275.

Narayanan, R. and Darwish, I. Y. S. (1987): Use of steel fibers as shear reinforcements, *ACI Structural Journal*, Vol. 84, No. 3, pp. 216-227.

Niyogi, S. C. and Dwarakanath, G. I. (1985): Fiber reinforced beams under moment and shear, *Journal of Structural Engineering*, ASCE, Vol. 111, No. 3, pp. 35-40.

Nonghabai, K. (2000): Beams of fibrous concrete in shear and bending: experiment and model, *Journal of Structural Engineering*, Vol. 126, No. 2, pp. 243-251.

Sharma, A. K. (1986): Shear strength of steel fiber reinforced concrete beams, *ACI Journal*, Vol. 83, No. 4, pp. 624-628.

Suwatnodom, P. (2008): Three-dimensional micromechanical damage models, fiber pullout models and fracture toughness of discontinuous steel fiber reinforced cementitious composites, PhD thesis, Department of Civil Engineering, University of California, Los Angeles, USA.

Swamy, R. N. and Bahia, H. M. (1985): The effectiveness of steel fibers as shear reinforcement, *Concrete International*, Vol. 7, No. 3, pp. 35-40.

Tan, K. H., Muragappan, K. and Paramasivam, P. (1992): Shear behavior of steel fiber reinforced concrete beams, *ACI Structural Journal*, Vol. 89, No. 6, pp. 3-11.

Thomas, J. and Ramaswamy, A. (2007): Mechanical properties of steel fiber-reinforced concrete, *Journal of Materials in Civil Engineering*, Vol. 19, No. 5, pp. 285-392.

Wafa, F.F. and Ashour, S.A. (1992): Mechanical properties of high-strength fiber reinforced Concrete, *ACI Material Journal*, Vol. 89, No. 5, pp. 449-455.

Watanabe, K., Higashi, H., Miki, T. and Niwa, J. (2010a): Real-time image analyzing system for loading tests of structural concrete, *Journal of Materials, Concrete Structures and Pavements,* JSCE, Vol. 66, No. 1, pp. 94-106. (in Japanese)

Watanabe, K., Kimura, T. and Niwa J. (2010b): Synergetic effect of steel fibers and shear-reinforcing bars on the shear-resistance mechanisms of RC linear members, *Construction and Building Materials*, Vol. 24, pp. 2369-2375.

Zhou, B. and Uchida, Y. (2013): Fiber orientation in ultra high performance fiber reinforced concrete and its visualization, *Proceeding of the 8th International Conference on Fracture Mechanics of Concrete and Concrete Structures (FraMCoS-8)*, pp. 217-224.

APPENDIX

PICTURES OF THE SPECIMENS AFTER LOADING TESTS

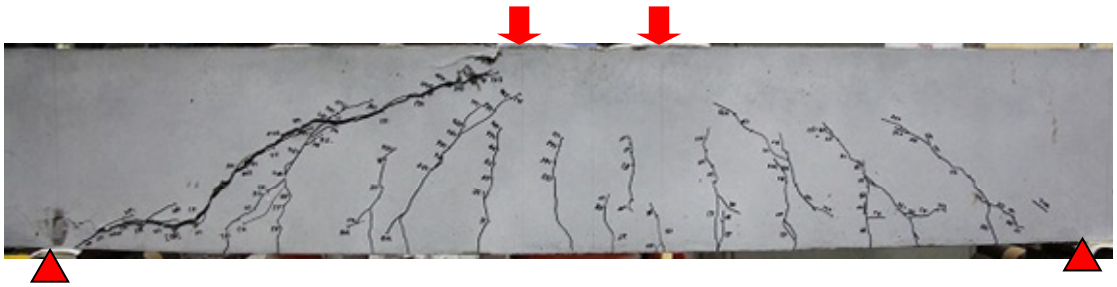

(a) SF30-05-r00

(b) SF30-05-r18

(c) SF30-05-r30

Figure A.1 Specimens in Series I and II (Fiber volume fraction = 0.5%)

(a) SF30-10-r00

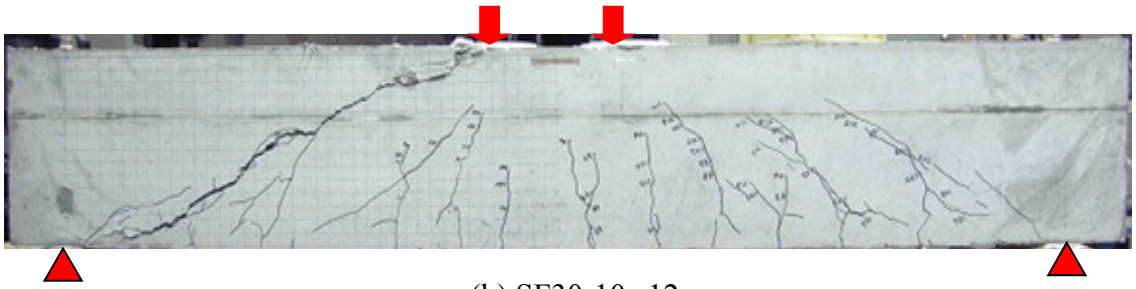

(b) SF30-10-r12

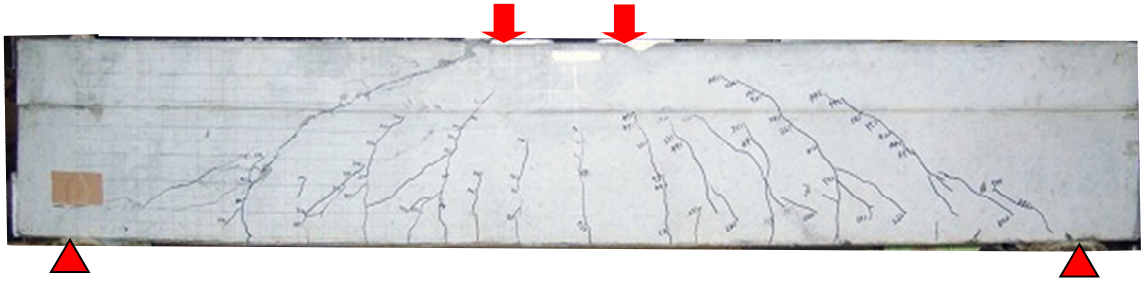

(c) SF30-10-r18

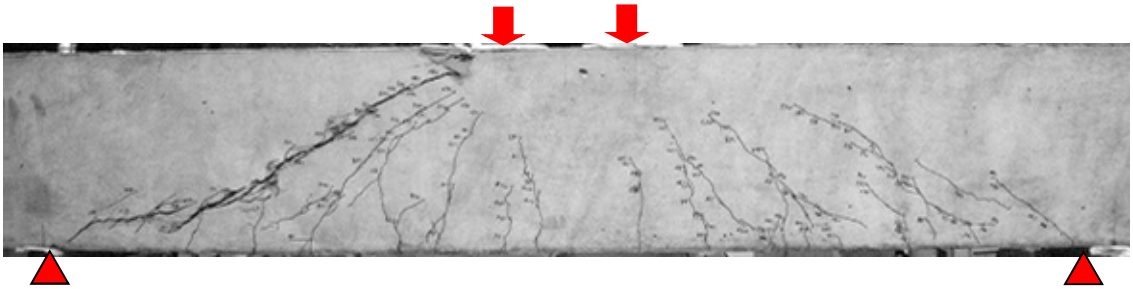

(d) SF30-10-r24

(e) SF30-10-r30

Figure A.2 Specimens in Series I and II (Fiber volume fraction = 1.0%)

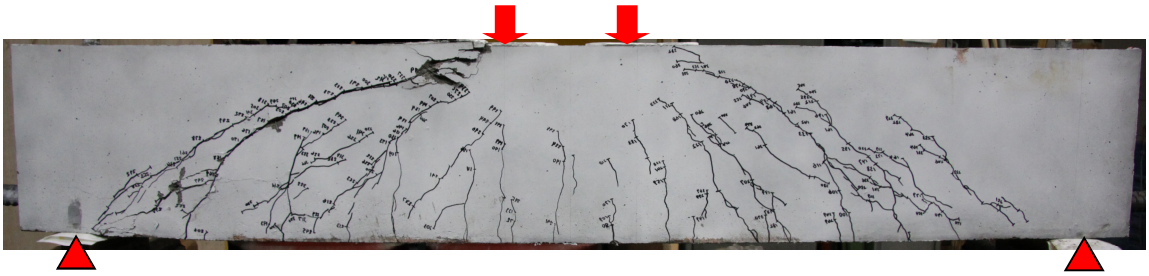

(a) SF60-10-r30

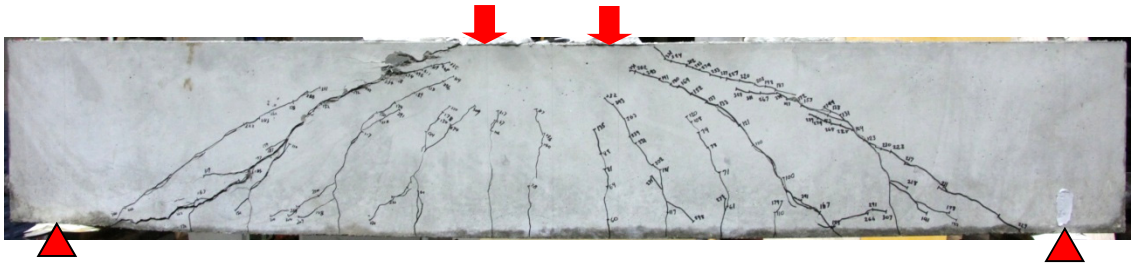

(b) PP-10-r30

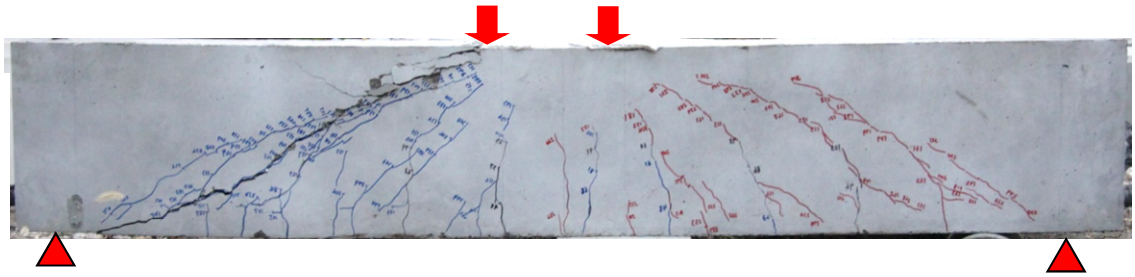

(c) PVA-10-r30

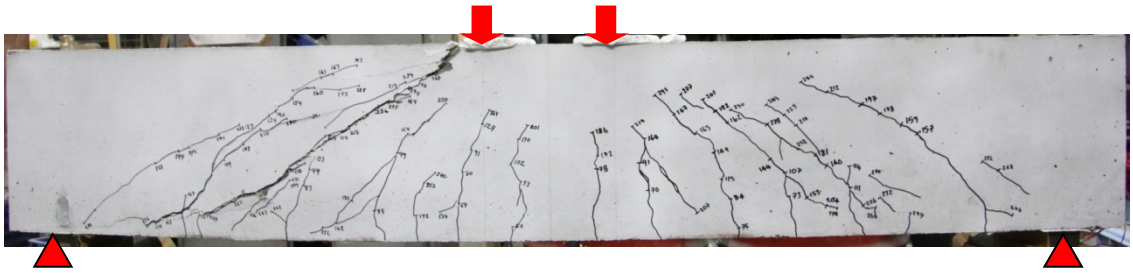

(d) PET-10-r30

Figure A.3 Specimens in Series III (Steel and synthetic fibers)

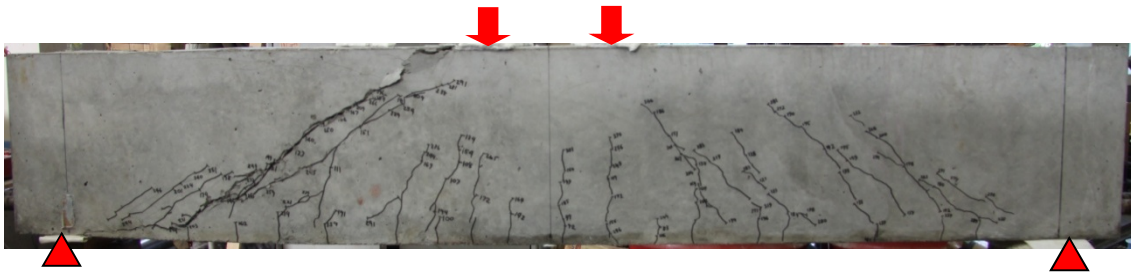

(a) 30&PP-10-r30

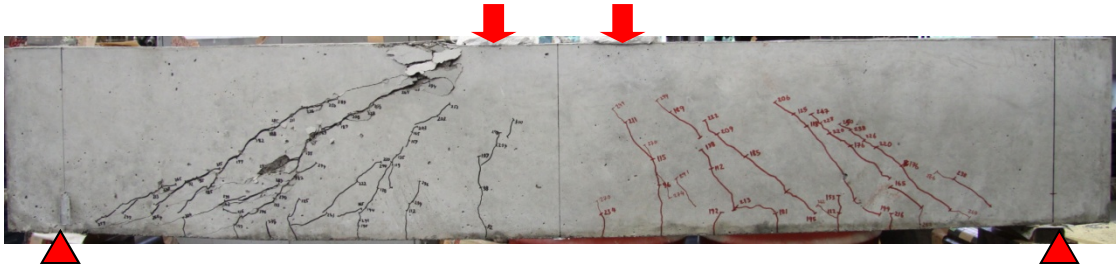

(b) 60&PP-10-r30

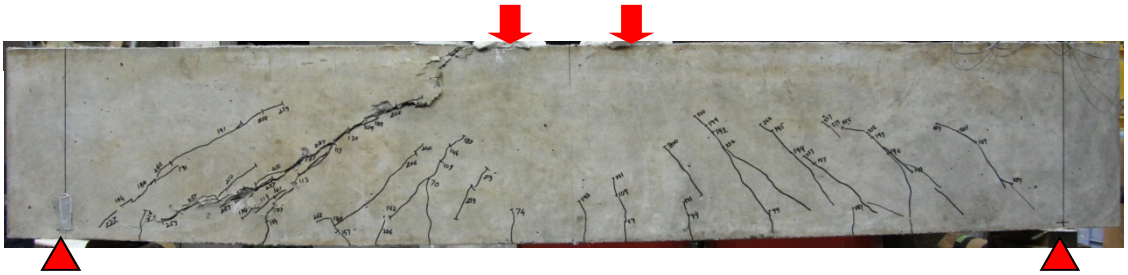

(c) 30&60-10-r30

Figure A.4 Specimens in Series III (Hybrid fibers)

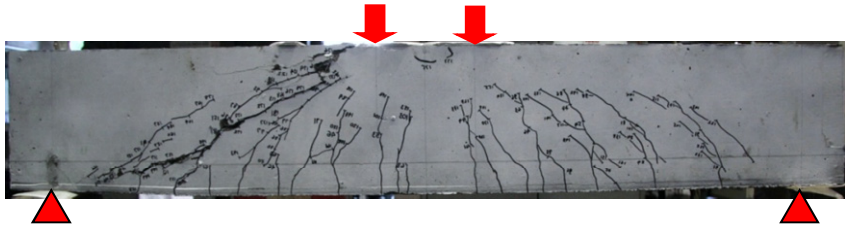

(a) SF30-10-r32-S

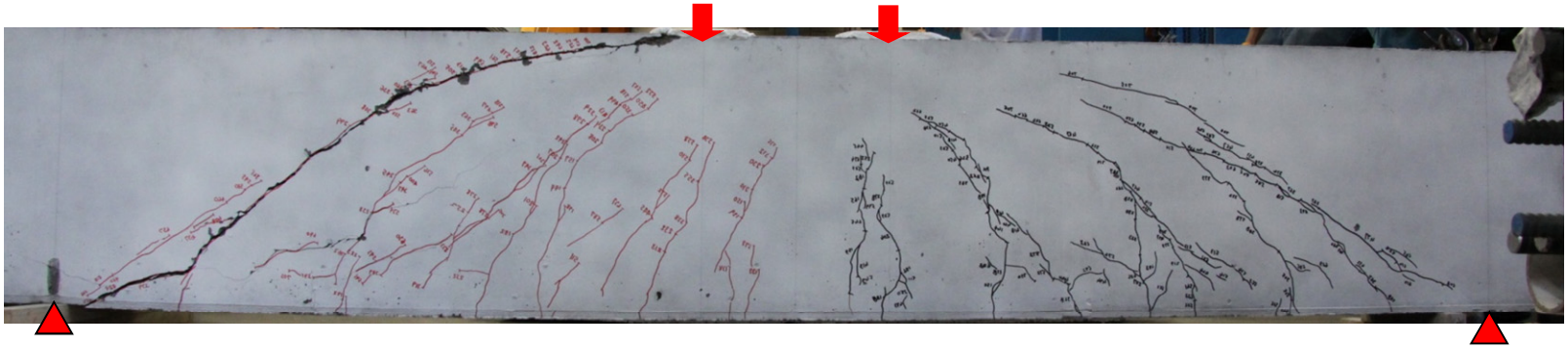

(b) SF30-10-r30-L

Figure A.5 Specimens in Series IV